UNIVERSIDAD DE CÓRDOBA

FACULTAD DE MEDICINA

DEPARTAMENTO DE BIOLOGÍA CELULAR, FISIOLOGÍA E INMUNOLOGÍA

TESIS DOCTORAL

Programa de Doctorado en Biomedicina

NON PSYCHOTROPIC CANNABINOIDS FOR THE TREATMENT OF INFLAMMATORY DISEASES

Memoria presentada para optar al grado de Doctor en Biomedicina por

Belén Palomares Cañero

Directores

Eduardo Muñoz Blanco

Marco Antonio Calzado Canale

Córdoba, Enero de 2010

TITULO: *NON PSYCHOTROPIC CANNABINOIDS FOR THE TREATMENT OF INFLAMMATORY DISEASES*

AUTOR: *Belén Palomares Cañero*

TÍTULO DE LA TESIS: NON-PSYCHOTROPIC CANNABINOIDS FOR THE TREATMENT OF INFLAMMATORY DISEASES

DOCTORANDO/A: Belén Palomares Cañero

INFORME RAZONADO DE LOS DIRECTORES DE LA TESIS
(se hará mención a la evolución y desarrollo de la tesis, así como a trabajos y publicaciones derivados de la misma).

La Tesis Doctoral presentada por la estudiante de doctorado Belén Palomares ha estudiado el mecanismo de acción y los efectos *in vitro* e *in vivo* de dos cannabinoides no-psicotrópicos como son el VCE-004.8 y el Δ^9-THCA-A.

VCE-004.8 es un derivado semisintético del CBD que es un agonista dual de PPARγ/ CB$_2$R y que está en fase II clínica para el tratamiento de la Esclerodermia. La candidata a doctora ha demostrado los efectos antiinflamatorios y anti-obesidad del VCE-004.8 en un modelo murino de obesidad inducida por una dieta alta en grasas. La doctoranda también ha investigado el efecto de Δ^9-THCA-A, el precursor no psicotrópico de Δ^9-THC, en modelos *in vitro* e *in vivo*. Ha demostrado que el Δ^9-THCA-A es un potente agonista de PPARγ y también modula CB$_1$R. La actividad ortostérica y alostérica de Δ^9-THCA-A sobre CB$_1$R se ha demostrado mediante métodos *in vitro* e *in silico*. Además, se ha estudiado la eficacia de Δ9-THCA en modelos murinos de obesidad y artritis.

Es evidente que la Doctoranda ha aprendido y utilizado numerosas técnicas durante el período de tesis y ha publicado 10 artículos relacionados en mayor o menor medida con la Tesis. De esos 10 artículos, dos lo son de primera autora y además tiene en revisión otro artículo de primera autora directamente relacionado con la Tesis. Por otra parte, la Doctoranda ha realizado una estancia de 3 meses en la Universidad de Dundee (Escocia, UK) y ha presentado sus resultados en 3 congresos internacionales, así como en otros congresos nacionales.

Por todas estas razones, consideramos que la tesis tiene suficientes méritos para ser defendida en un comité de tesis internacional.

Por todo ello, se autoriza la presentación de la tesis doctoral.

Córdoba, 18 de diciembre de 2019
Firma de los directores

Fdo: Eduardo Muñoz Blanco   Fdo.: Marco A. Calzado Canale

La verdadera ciencia enseña,
sobre todo, a dudar y a ser ignorante.

Miguel de Unamuno.

Acknowledgements

Y casi sin darme cuenta llegué hasta el final del camino. Un largo viaje con múltiples destinos siempre compartido al lado de maravillosas personas que de un modo u otro han participado y hecho posible la realización de esta tesis.

El primer agradecimiento es para mis directores de tesis Eduardo y Marco, ya que tras un aterrizaje casual en vuestro grupo, me disteis la oportunidad de crecer y aprender a vuestro lado. Muchas gracias Marco por todos tus consejos tanto a nivel científico como a nivel personal. Y en especial a Eduardo "mi padre de la ciencia". Sin ninguna duda, tu profesionalidad, experiencia, conocimiento y apoyo me han ayudado y convertido en lo que soy, además de haberme inculcado la pasión por la ciencia.

Gracias Laure, por acogerme en tu laboratorio durante mi estancia en Dundee (desde donde estoy escribiendo estas palabras), y a todos mis compañeros. Gracias por vuestra amabilidad, disponibilidad y paciencia. En especial a Angus, por todas esas conversaciones para intentar mejorar mi inglés. Fran, gracias por todo lo que aprendimos juntos.

Agradecer también a todas las personas que en algún momento del recorrido han formado parte del grupo Inflamación y Cáncer. Irene, Carla, Paloma, Maribel, Carmen, Estrella y Víctor muchísimas gracias por todos esos momentos que hemos compartido de conocimientos, consejos, experiencias y mucho más, tanto dentro como fuera del trabajo.

Y como no, gracias a todos los que actualmente siguen formando parte del grupo:

A Rosario y Alex, una pareja especial, inteligente y divertida, dispuestos siempre a aportarte algo nuevo.

A Juan Antonio, el responsable de que esto haya ocurrido. Gracias por todo lo que me has enseñado desde el primer día, por tu paciencia (o no) para que el laboratorio funcione, por tu disponibilidad y por todo lo que haces.

Carmen N., las dos tan iguales y tan diferentes a la vez, creo que nos hemos complementado perfectamente hasta llegar a ser grandes compañeras y amigas en todo tipo de ambientes. Muchas gracias por estar siempre presente haciendo más fácil el camino.

Adela, rápidamente te convertiste en alguien imprescindible, que siempre necesitaba tener al lado y que siempre estaba disponible para cualquier duda y consejo. Gracias.

Mi pinche Marujita, gracias por ser como eres y darme tanto cariño cada día. Por poner orden en mi vida, por tu ayuda y apoyo en todo momento. Un trocito de esta tesis es tuya.

Gracias Anita por estar siempre dispuesta a escuchar los análisis de todos los experimentos de esta tesis, además de ser un gran auxilio ante ciertas dudas.

Martín, parte de esta tesis también es tuya. Muchos resultados no hubiesen salido a la luz sin ti. Muchas gracias por hacerme entender lo incomprensible!

A Rafa, Jon y Bea, de las últimas incorporaciones al grupo. Muchas gracias por querer formar parte de esta familia y aportar cosas positivas para que todo siga funcionando.

No me podría olvidar de todo lo que tengo que agradecer al grupo de fisiología, especialmente a Manuel Tena y Curro por su papel clave en la realización de los experimentos *in vivo* de esta tesis. Muchas gracias a todos por vuestra ayuda, disponibilidad y profesionalidad.

Gracias también al grupo del Dr. Javier Fernández Ruiz por su participación en la realización de los ensayos de afinidad y por hacer fácil la comunicación a pesar de la distancia, a Innohealth Group y Nostrum Biodiscovery por la cesión de líneas celulares y por colaborar en los ensayos de docking respectivamente, a Phytoplant por facilitarnos cannabinoides naturales para la realización de los ensayos, a Emerald Health Biotechnology, en especial a Juandi, por la colaboración y el apoyo en todo momento y a Carmen Cabrero Doncel por la revisión de los manuscritos.

Gracias a toda **mi familia**, tíos/as, primos/as, abuela por apoyarme y creer en mí durante todos estos años. Gracias a mis padres, Rafa y Paqui, y a hermanos, Rafa y María, las personas más importantes de mi vida, por cuidarme y estar conmigo en el día a día. Nunca os podré agradecer lo suficiente todo lo que me habéis transmitido y lo que habéis confiado en mí. Os quiero.

Y por último darte las gracias a ti, a esa persona que aun estando ausente siempre ha estado presente. Muchas gracias equipo.

Resumen

El cannabis medicinal y los cannabinoides purificados han captado la atención mundial, ya que millones de pacientes pueden beneficiarse de sus propiedades terapéuticas. En los últimos años, el sistema endocannabinoide (SEC) ha presentado un papel crucial en la regulación de mecanismos fisiológicos relacionados con procesos inflamatorios e inmunomoduladores, así como con la ingesta de alimentos y el metabolismo energético. Por lo tanto, su manipulación farmacológica representa una nueva estrategia para el tratamiento de enfermedades inflamatorias como son síndrome metabólico y artritis reumatoide (AR).

Para investigar el verdadero potencial medicinal de la marihuana, se han realizado estudios preclínicos y clínicos con resultados positivos en determinadas condiciones neurológicas como la esclerosis múltiple y ciertas formas genéticas de epilepsia juvenil. Todos estos estudios han utilizado cannabinoides neutros, especialmente Δ^9-THC y CBD, sin prestar atención a los auténticos fitocannabinoides de la planta, sus formas ácidas, como es el precursor nativo del Δ^9-THC, el Δ^9-THC ácido (Δ^9-THCA-A), un fitocannabinoide no psicoactivo que permanece en gran medida inexplorado. Además, se ha realizado una modificación de la estructura química del CBD con el fin de aumentar su aplicación en el tratamiento de diferentes enfermedades.

En el presente trabajo, el derivado aminoquinona del CBD, VCE-004.8, un agonista dual de los receptores PPARγ y CB$_2$, que también activa la ruta de HIF, y Δ^9-THCA-A, un modulador selectivo y parcial de PPARγ, mostraron una menor actividad adipogénica que rosiglitazona (RGZ), un agonista completo de PPARγ, y además, no presentaron efectos adversos asociados a los agonistas completos de PPARγ, como por ejemplo inhibición de osteoblastogénesis. En un modelo murino i*n vivo* de obesidad inducida por una dieta alta en grasa (HFD), el tratamiento con VCE-004.8 y Δ^9-THCA-A indujo una reducción significativa del peso corporal, masa grasa total, volumen de adipocitos, niveles plasmáticos de triglicéridos y esteatosis en ratones obesos. Además, también mejoraron la sensibilidad a la insulina y regularon la expresión de otros biomarcadores metabólicos.

Por otro lado, el análisis posterior *in vitro* e *in silico* también demostró que Δ^9-THCA-A puede actuar como un agonista ortostérico de CB$_1$ y también como un modulador alostérico positivo en presencia de CP-55,940. Además, se muestra que Δ^9-THCA-A es un agonista inverso de CB$_2$. Experimentos *in vivo* en un modelo murino de artritis inducida por colágeno (CIA) demostraron que el tratamiento con Δ^9-THCA-A previno la

inflamación y el daño del cartílago en las articulaciones de la rodilla. El efecto antiartrítico de Δ^9-THCA-A fue evitado en gran medida por SR141716 o T0070907. El análisis de biomarcadores plasmáticos, así como la determinación de citoquinas y anticuerpos anti-colágeno confirmaron que Δ^9-THCA-A actúa principalmente a través de las vías PPARγ y CB$_1$.

Nuestros hallazgos establecen que VCE-004.8 a través de PPARγ, CB$_2$ y HIF, y Δ^9-THCA-A a través de PPARγ, tienen un potencial terapéutico para el tratamiento de la obesidad y síndrome metabólico, sin presentar los efectos nocivos en adipogénesis y osteoblastogénesis asociados a los agonistas completos de PPARγ.

Además, Δ^9-THCA-A modula al receptor CB$_1$ tanto a través del sitio de unión ortostérico como alostérico. Es más, Δ^9-THCA-A también previene el desarrollo de artritis, principalmente a través de las vías CB$_1$/PPARγ, destacando su potencial para el tratamiento de enfermedades inflamatorias crónicas como es la artritis reumatoide.

Table of contents

TABLE OF CONTENTS

2

Abstract

Medicinal cannabis and purified cannabinoids have garnered worldwide attention since millions of patients can benefit from their medical properties. Over the past few years, the endocannabinoid system (ECS) has emerged as a crucial player for the regulation of physiological mechanisms related to inflammatory and immunomodulatory processes as well as food intake and energy metabolism. Hence, its pharmacological manipulation represents a novel strategy for the management of inflammatory diseases such as metabolic syndrome (MetS) and rheumatoid arthritis (RA)

To investigate the real potential of medicinal marijuana, pre-clinical and clinical studies have been launched, with positive results for some neurological conditions like multiple sclerosis and some genetic juvenile forms of epilepsy. All these studies have used neutral cannabinoids, especially Δ^9-THC and CBD, with little attention to the genuine phytocannabinoids of the plant, namely their acidic forms, such as the native precursor of Δ^9-THC, the Δ^9-THC acid A (Δ^9-THCA-A), a non-psychoactive phytocannabinoid that remains largely unexplored. In addition, the modification of CBD scaffold was carried out in order to increase its application in different diseases. Δ^9-THCA has two isomers, Δ^9-THCA-A, in which the carboxylic acid group is in the 1 position, between the hydroxy group and the carbon chain, and Δ^9-THCA -B, in which the carboxylic acid group is in the 3 position. Δ^9-THCA-A is the most abundant isomer.

In the present work, the CBD aminoquinone derivative VCE-004.8, a dual PPARγ and CB$_2$ receptor agonist that also activates the HIF pathway, and Δ^9-THCA-A, a partial and selective PPARγ modulator, showed lower adipogenic activity than the full PPARγ agonist rosiglitazone (RGZ) and did not affect osteoblastogenesis in hMSC. In an *in vivo* murine model of high fat diet (HFD)-induced obesity, both VCE-004.8 and Δ^9-THCA-A treatments induced a significant reduction in body weight gain, total fat mass, adipocyte volume, plasma triglyceride levels, and liver steatosis in HFD mice. In addition, the treatments improved sensitivity to insulin and regulated the expression of other metabolic biomarkers in obese mice. Thus, VCE-004.8 and Δ^9-THCA-A were qualified as novel therapeutic candidates for the management and improvement of the symptoms of obesity-associated metabolic syndrome and inflammation.

In addition, subsequent *in vitro* and *in silico* analyses also showed that Δ^9-THCA-A can act as an orthosteric CB$_1$ agonist and also as a positive allosteric modulator in the presence of CP-55,940. Moreover, Δ^9-THCA-A seemed to be an inverse agonist for CB$_2$.

In vivo experiments in a murine model of collagen-induced arthritis (CIA) demonstrated that Δ^9-THCA-A prevented the inflammation and cartilage damage on knee joints. The anti-arthritic effect of Δ^9-THCA-A was greatly prevented by either SR141716 or T0070907. Analysis of plasmatic biomarkers as well as determination of cytokines and anti-collagen antibodies confirmed that Δ^9-THCA-A is mediating its activity mainly through PPARγ and CB_1 pathways. Thus, our studies document that Δ^9-THCA-A exerted anti-arthritis activity through CB_1/PPARγ pathways highlighting its potential for the treatment of chronic inflammatory diseases such as RA.

Abbreviations

2-AG: 2-arachidonoylglycerol

ABHD12: Alpha/beta domain hydrolases 12

ABHD6: Alpha/beta domain hydrolases 6

AD: Adipogenic differentiation

AEA: Anandamide or *N*-arachidonoyl-ethanolamine

AF-1: Activation function 1

ANM: anisotropic network model

AM: Adipogenic medium

Ambp: Alpha-1-microglobulin/bikunin precursor

AP-1: Activator protein-1

Apcs: Serum amyloid P component

Apoa1: Apolipoprotein a1

Apoa3: Apolipoprotein a3

ARNT: Aryl hydrocarbon receptor nuclear translocator

AUC: Area-under-the-curve

BAT: Brown adipose tissue

BW: Body weight

CB$_1$R: CB$_1$ receptor

CB$_2$R: CB$_2$ receptor

CBCA: Cannabichromenic acid

CBCVA: Cannabichromevarinic acid

CBD: Cannabidiol

CBDA: Cannabidiolic acid

CBDVA: Cannabidivarin acid

Abbreviations

CBG: Cannabigerol

CBGA: Cannabigerolic acid

CBGVA: Cannabigerovaric acid

CBP: Creb Binding Protein

CCL2: Chemokine ligand 2

CD: Control or standard diet

CIA: Collagen type II-induced arthritis

CLS: Crown-like structures

COX-2: Cyclooxygenase-2

DAGs: Diacylglycerols

DBD: DNA-binding domain

DDA: Data-dependent acquisition

DIO: Diet-induced obesity

ECS: Endocannabinoid system

FAAH: Fatty acid amino hydrolase

FABP1: Fatty acid binding protein 1

FABP3: Fatty acid binding protein 3

FDR: False discovery rate

GI: Gastrointestinal

GIP: Gastric inhibitory peptide

GLP-1: Glucagon-like peptide-1

GlyR: Glycine Receptors

GPCRs: G protein-coupled receptors

H&E: Hematoxylin and eosin

HFD: High fat diet

HIF: Hypoxia-inducible factor

Hp: Haptoglobin

Hpx: Hemopexin

HREs: Hypoxia-response elements

IL: Interleukin

I.p: Intraperitoneal injection

Itih: Inter-alpha-trypsin inhibitor heavy chain

iWAT: Inguinal white adipose tissue

LBD: Ligand-binding domain

LBP: Ligand-binding pocket

MAGL: Monoacylglycerol lipase

MAPK: Mitogen-activated protein kinase

MEP: 2-C-methyl-D-erythritol 4-phosphate

MetS: Metabolic syndrome

MMPs: Metalloproteinases

MSCs: Mesenchymal stem cells

NAAA: *N*-acylethanolamine-hydrolyzing acid amidase

NAM: Negative allosteric modulator

NF-κB: Nuclear Factor of *kappa* B

NTD: Amino-terminal domain

OD: Osteoblast differentiation

OLA: Olivetolic acid

OM: Osteoblastogenic medium

ORO: Oil Red O

PAI-1: Plasminogen-activator inhibitor-1

PAM: Positive allosteric modulator

pBAT: Primary brown adipocytes

PCA: Principal component analysis

PDB: Protein Data Bank

PELE: Protein Energy Landscape Exploration

PGZ: Pioglitazone

PHDs: Prolyl-hydroxylases domain proteins

Pmbs2: Proteasome subunit beta type-2

POMC: Proopiomelanocortin

PPARγ: Peroxisome proliferator-activated receptor-γ

QMR: Quantitative magnetic resonance

RA: Rheumatoid arthritis

RGZ: Rosiglitazone

SNC: Central nervous system

SNS: Sympathetic nervous system

T2D: Type-2 diabetes

TGZ: Troglitazone

TNF-α: Tumor necrosis factor alpha

TR-FRET: Time-resolved fluorescence resonance energy transfer

TRP: Transient Receptor Potential

TZDs: Thiazolidinediones

UCP-1: Uncoupling protein-1

WAT: White adipose tissue

Δ⁹-THC: Δ^9-tetrahydrocannabinol

Δ⁹-THCA: Tetrahydrocannabinolic acid

Δ⁹-THCVA: Δ^9-tetrahydrocannabivarin carboxylic acid

Introduction

1. Discovering cannabis

Cannabis sativa L. (*C. sativa*), an annual plant of the Cannabaceae family, has been cultivated since ancient times in Asia and Europe. *C. sativa* has traditionally been used for multiples purposes such as a source of fibres, food, oil, recreational and religious rituals and medicine.

1.1. History of medicinal cannabis

C. sativa has a very long history of medicinal use. It is perfectly well known the advanced medical practice in ancient Egypt. One of the oldest mention of cannabis has been dated to 1.700 B.C., when a series of medical papyri, written in ancient Egypt and Mesopotamia, demonstrated the use of *C. sativa* in glaucoma and anti-inflammatory diseases [1]. Then, there was a movement of medical knowledge from Alexandria to Greece and Rome. In the first century B.C., the Greek Diodorus Siculus reported the use of the plant to cure anger and sorrow. In addition, the use of medical cannabis in China was also very wide. The legendary Chinese emperor Shen-Nung tested the curative powers of the plant in himself as a guinea-pig and after finishing all the experiments, wrote the *Pen Ts'ao*, a medicinal herbs text that later became well-known. Although the original text does not exist, the oldest *Pen Ts'ao* (first century A.C.) reports that *C. sativa* was given as treatment for menstrual fatigue, gout, rheumatism, malaria, beri-beri, constipation, and absentmindedness. In the second century A.C., the famous Chinese surgeon Hua T'o used *C. sativa* to carry out difficult surgical procedures without pain, that is, it showed anaesthetic properties [2]. Moreover, it was also described that *C. sativa* seed oils decreased the chronic pain knee associated to arthritis and improved blood circulation. The beneficial effects were attributed, at least in part, to the abundant content of the essential fatty acids, proteins, fibers, vitamins and minerals in the seeds [3]. The literature documents how the knowledge of medicinal power of *C. sativa* was extended to the rest of the world until nowadays [4]. During this period, the therapeutic properties of the plant in different types of diseases have become clear. However, it is important to understand the potential efficacy of cannabis in the broad range of medical conditions.

1.2. Natural cannabinoids (phytocannabinoids)

C. sativa is constituted by around 480 compounds of different chemical classes which may be divided into either compounds belonging to primary metabolism (amino acids, fatty acids and steroids) or to secondary metabolism (cannabinoids, flavonoids,

stilbenoids, terpenoids, lignans and alkaloids). The cannabinoid group is the most studied and is represented by terpenophenolic compounds with C22 (carboxylated/acid form) or C21 (decarboxylated/neutral form). There are almost 150 known cannabinoids and they can be classified into 10 subclasses depending on the structure. The most investigated cannabinoids are the neutral compounds, such as Δ^9-tetrahydrocannabinol (Δ^9-THC) and cannabidiol (CBD), possibly related to their medical efficacy. However, the most abundant phytocannabinoids in the plant are the carboxylated or acid forms, which include tetrahydrocannabinolic acid (Δ^9-THCA), cannabidiolic acid (CBDA), cannabigerolic acid (CBGA) and cannabichromenic acid (CBCA) [5, 6].

The central precursor for cannabinoid biosynthesis is the CBGA or its analogue, the cannabigerovaric acid (CBGVA), which are created from two pathways: the polyketide pathway, leading olivetolic acid (OLA) or divarinic acid (DA) and the plastidal 2-C-methyl-D-erythritol 4-phosphate (MEP) pathway, producing geranyl pyrophosphate (GPP). A catalytic reaction of OLA or DA with GPP finishes in the formation of CBGA or CBGVA, respectively [6, 7]. Both precursors CBGA and CBGVA are used as substrates by three different oxydocyclases such as cannabidiolic acid synthase, Δ^9-tetrahydrocannabinolic acid synthase and cannabichromenic acid synthase, originating CBDA or cannabidivarin acid (CBDVA), Δ^9-THCA or Δ^9-tetrahydrocannabivarin carboxylic acid (Δ^9-THCVA) and CBCA or cannabichromevarinic acid (CBCVA), respectively [8] (Figure 1).

The unstable acidic phytocannabinoids can be converted to the neutral form through a decarboxylation process. This process takes place slowly in the living plant. However, it increases after harvesting as a result of storing or being exposed to light, heat (via smoking/baking) or auto-oxidation [9]. The phytocannabinoid acids do not suffer this process *in vivo*, which is really interesting to distinguish between a recreational or medical use of cannabis [10, 11].
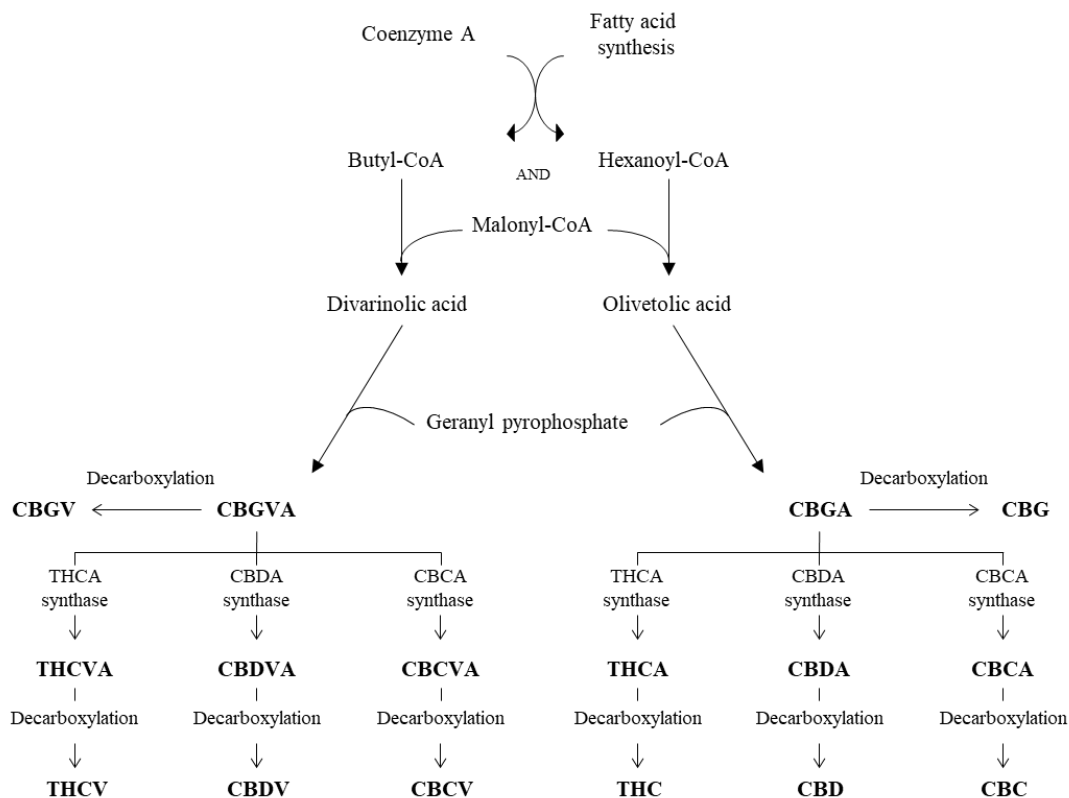
Figure 1. Biosynthesis of phytocannabinoids. CBGVA-Cannabigerovaric acid; CBGV-Cannabigerivarin; THCVA-Tetrahydrocannabivarinic acid; THCV-Tetrahydrocannabivarin; CBDVA-Cannabidivarinic Acid; CBDV-Cannabidivarin; CBCVA-Cannabichromevarinic-Acid; CBCV-Cannabichromevarin; CBGA-Cannabigerolic acid; CBG-Cannabigerol; THCA-Tetrahydrocannabinolic acid; THC-Tetrahydrocannabinol; CBDA-Cannabidiolic acid; CBD-Cannabidiol; CBCA-Cannabichromenic acid; CBC-Cannabicromene.

1.2.1. Phytocannabinoid acids

In spite of being the cannabinoids with the largest presence in the plant, our knowledge of their biological activities is very limited. Depending on the cannabis variety and other characteristics (i.e., age, sex), phytocannabinoid acids can be found with different proportions in all cannabis plant tissues such as leaves, stems, roots and buds [12]. Interestingly, our group has recently described that phytocannabinoid acids activate the peroxisome proliferator-activated receptor-γ (PPARγ) with a higher potency than their decarboxylated analogues, making them more interesting to explore future therapeutic strategies for metabolic, inflammatory and neurodegenerative diseases [13]

Preliminary studies and anecdotal evidence suggest that Δ^9-THCA displays a potential therapeutic profile showing anti-inflammatory, neuroprotective, anti-proliferative and anti-emetic properties which result in beneficial effects in the treatment of arthritis, lupus, neurodegenerative diseases, cancer, nausea and appetite loss [13-17].

However, further research is required to provide a functional validation and preclinical confirmation of its action mechanism.

Remarkably, the phytocannabinoid Δ^9-THCA, unlike Δ^9-THC, is not psychotropic, and controversy exists regarding its binding affinity for the main cannabinoid receptors (CB_1 and CB_2). According to the results, it has been speculated that Δ^9-THCA has a peripheral binding affinity for CB_1 receptor but its ability to enter into the central nervous system (CNS) is limited [10]. It has been shown that Δ^9-THCA is antiemetic in shrews and this activity was reversed by co-treatment with SR141716, a selective CB_1 antagonist [18]. *In vitro* studies have demonstrated that Δ^9-THCA is a TRPA1 agonist and TRPM8 antagonist [19] and inhibits both cyclooxygenase enzymes (COX-1 and COX-2) in a high concentration range (mM) [14]. In addition, we have showed that Δ^9-THCA, contrary to Δ^9-THC, is a potent agonist of PPARγ. We provided first evidence that Δ^9-THCA is neuroprotective in establishing *in vitro* and *in vivo* models of Huntington's disease [13].

CBDA is a selective inhibitor of COX-2 and a weak TRPA1 agonist and TRPM8 antagonist, similar to Δ^9-THCA [8]. Some authors have shown CBDA (per se or combined with Δ^9-THC) to be effective in reducing acute and anticipatory nausea. [20, 21]. Prior biological research about CBCA is also very limited. However, evidence suggests that CBCA exhibits anti-inflammatory and antibacterial properties.

1.2.2. Neutral phytocannabinoids

Theoretically, the levels of neutral cannabinoids in the fresh plant is low since most phytocannabinoids are present in their acidic form. After a decarboxylation process, the phytocannabinoid acids are converted in their analogues. In the last decades, research has been focused on the neutral forms because they were thought to be the major cannabinoids of therapeutic interest.

Δ^9-THC is the main psychoactive phytocannabinoid. It is a partial agonist with the highest affinity at CB_1 and CB_2 receptors of all phytocannabinoids. Although most of its effects are associated to CB_1 receptor, which include locomotor activity suppression, decrease in body temperature, catalepsy and analgesic properties, other Δ^9-THC targets such as GPR55, GPR18, TRPV2, TRPA1 and glycine receptors have been identified [8, 19]. Currently, there are three medications based on Δ^9-THC available: Dronabinol (Marinol; pure synthetic Δ^9-THC) is used in HIV/AIDS-induced anorexia and chemotherapy-induced nausea and vomiting, Nabilone (Cesamet; synthetic form of Δ^9-

THC) is also used for the treatment of nausea and vomiting in cancer patients and Nabiximols (Sativex; combination of Δ^9-THC/CBD, 50/50%) is used to treat neuropathic pain and spasticity related to multiple sclerosis and cancer.

In contrast to Δ^9-THC, CBD is the major non-psychoactive component of *C. sativa*, exhibiting low affinity for cannabinoid receptors, CB_1 (allosteric inhibitor) and CB_2 (weak inverse agonist). On the other hand, a wide range of different molecular targets has been described, which explains the biological potential of this molecule in a variety of pathological conditions. Briefly, CBD acts as a GPR18 partial agonist and GPR55 antagonist, activates TRPV1, TRPV2 and TRPA1, antagonizes TRPM8, is a positive allosteric modulator of glycine receptors and activates PPARγ receptors, among others. [19] Although the action mechanism of CBD is not fully understood, there is substantial evidence that CBD is an effective treatment for psychosis, epilepsy, anxiety, ischemia, neurodegenerative diseases, pain, inflammation, autoimmunity, bone formation or cancer [19]. Currently, in addition to the previously mentioned Sativex, Epidiolex, an oral CBD pharmaceutical formulation, is used for the treatment of seizures associated with epilepsy that begin in childhood called Lennox-Gastaut syndrome or Dravet syndrome.

Although there has been a lower interest in CBG rather than in Δ^9-THC or CBD, nowadays the attention to CBG products is growing quickly. CBG is a non-psychotropic cannabinoid, showing low affinity for cannabinoid receptors (CB_1 and CB_2) but it has been reported to be a TRPV1 and TRPA1 agonist and a potent TRPM8 antagonist. Moreover, CBG is also a α2-adrenoceptor agonist and a 5-HT1A receptor antagonist [19]. Different authors have suggested CBG to be used for the treatment of Huntington's disease, inflammatory bowel disease, psoriasis, acne and colorectal cancer [19, 22, 23].

2. The endocannabinoid system

The endocannabinoid system (ECS) is a complex and essential biological system in the body identified in the early 1990s when scientists were studying Δ^9-THC in depth. This system is presented in mammals, birds, reptiles, and fish and maintains homeostasis by controlling and regulating vital physiologic functions such as sleep, appetite, pain, inflammation, memory or reproduction.

The ECS is comprised by three main components: the natural cannabinoids produced inside the body named endocannabinoids, the cannabinoid receptors through which they act, and the enzymes that synthesize and degrade them (Figure 2).
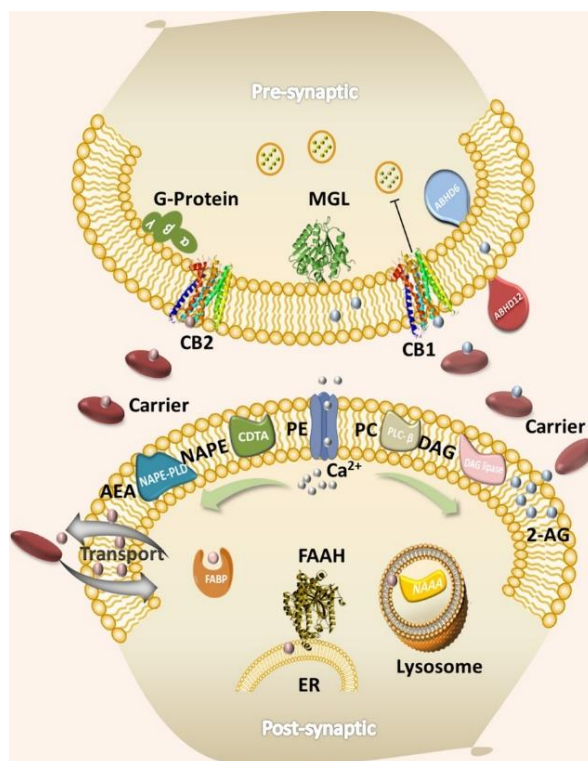
Figure 2. Schematic representation of the endocannabinoid signalling system. CB1, cannabinoid receptor 1; CB2, cannabinoid receptor 2; MGL, monoacylglycerol lipase; FAAH, fatty acid amide hydrolase; ABHD6, α-β hydrolase domain-containing protein 6; ABHD12, α-β hydrolase domain-containing protein 12; NAPE, N-arachidonoyl phosphatidylethanolamine; PE, phosphatidylethanolamine; PC, phospholipase C; PD, phospholipase D; DGL, diacylglycerol lipase; FABP, fatty-acid-binding protein; AEA, arachidonoylethanolamide; 2-AG, 2-arachidonoylglycerol; ER, endoplasmic reticulum. *Source: Adapted from [24].*

2.1. Cannabinoid receptors

After Δ^9-THC was first isolated from *C. sativa* in Mechoulam's laboratory in 1964, researchers focused on understanding the pharmacological effect of cannabis [25]. At first, it was thought that cannabinoids acted non-specifically through the cell membrane. However, in 1990, the first cannabinoid receptor (CB$_1$) was discovered by Tom Bonner's laboratory at NIH and three years later Sean Munro's laboratory in Cambridge found the second canonical cannabinoid receptor (CB$_2$) [26]. Both receptor types are mainly couple to G proteins of the Gα_i, Gα_q, Gα_s or Gα_o class, depending on cell types. Generally, the activation of these receptors inhibits adenylyl cyclases, induces arrestin recruitment and activates mitogen-activated protein kinase (MAPK), leading diverse cellular processes

[27]. Recently, it has appeared the concept of "biased signaling", in which the activation of receptors is ligand and tissue specific, leading to specific receptors conformations and, as a consequence, activating different intracellular pathways [27]. This approach has a good translational sight due to the increasing possibility of focusing on the desired pathway and reducing potential side effects (especially for CB_1).

CB_1 receptor (CB_1R or CB_1), encoded by the CNR1 gene, has a sequence relatively well conserved among species (around 98% the amino acid sequence homology between human and rodents) [28]. CB_1 receptor is expressed not only in the brain but also in numerous peripheral tissues, although at lower levels than those found in the brain [29]. The highest density of CB_1R in the brain is localized in olfactory bulb, hippocampus, basal ganglia and cerebellum, whereas a lower expression is found in the cerebral cortex, septum, amygdala, hypothalamus, thalamus, and parts of the brainstem and the dorsal/ventral horn of spinal cord [30]. This receptor is usually on presynaptic terminals of central and peripheral neurons, where it performs neurotransmitter release inhibition. Moreover, CB_1R is present in astrocytes, oligodendrocytes and microglia, regulating synaptic transmission [28]. On the other hand, it has been described that CB_1R is also expressed in other tissues such as gastrointestinal (GI) tract, modulating the GI tract mobility, the intestinal epithelium permeability and the secretion of gastric acids, fluids, neurotransmitter and hormones. In addition, CB_1R takes part in control appetite from the hypothalamus and energy balance and food intake from the GI tract [28]. Under pathological conditions, CB_1R increases in the liver, leading to hepatic insulin resistance, fibrosis and lipogenesis [31], and in the cardiovascular system, worsening the prognosis because of enhancing oxidative stress, inflammation and fibrosis [32]. CB_1R expression has also been identified in various tissues including adipose tissue, skeletal muscle, bone, skin, eye, reproductive system and different cancer cells [31]. Regarding CB_1R localization, a lot of evidence has suggested that CB_1R is mainly localized in the cell membrane. However, it is also found in mitochondria and intracellular endo/lysosomes originated by internalization of plasma membrane [28].

CB_2 receptor (CB_2R or CB_2) is encoded by the CNR2 gene and its sequence is a little lower conserved than the CNR1 (the amino acid sequence homology is about 80% between human and rodents) [28]. CB_2R is primarily expressed in the immune system, although it is also presented in other peripheral tissues, such as adrenal gland, heart, lung, prostate, uterus, pancreas, testis, GI tract, liver, adipose tissue, bone, reproductive system,

and at a much lower density compared to CB$_1$R, in the central nervous system, particularly in activated microglial cells [19, 29]. Generally, CB$_2$R activation is associated with antiinflammatory and cytoprotective effects [29].

2.2. Endocannabinoids

After discovering cannabinoid receptors, it was assumed that there had to exist some endogenous molecules functioning as specific ligands. Thus, follow-up studies revealed the presence of these molecules in specific tissues that were named endocannabinoids.

Endocannabinoids are endogenous lipids derived from arachidonic acid. The firsts and best studied endocannabinoids identified are *N*-arachidonoyl-ethanolamine (AEA; anandamide) and 2-arachidonoylglycerol (2-AG) [33, 34]. Nevertheless, next studies led to the identification of other fatty acid derivatives that belong to the group of endocannabinoids, i.e., 2-arachidonyl-glyceryl-ether (noladin ether), *N*-arachidonoyl-dopamine (NADA), and *O*-arachidonoyl-ethanolamine (virodhamine) [19].

Endocannabinoids are synthesized by neurons when and where they are necessary and their actions are mainly presynaptic, in some cases, acting as retrograde synaptic messengers [26]. Then, after their release, endocannabinoids are quickly removed from extracellular space by a process of transport carried out in the cellular membrane. Finally, once inside the cell, they are degraded mainly by two enzymes, the fatty acid amino hydrolase (FAAH) and the monoacylglycerol lipase (MAGL). In addition, endocannabinoids are also produced by non-neuronal cells, which explains how the ECS also works beyond the CNS.

2.3. Enzymes

Despite similarities between AEA and 2-AG in their chemical structure, they are synthetized and degraded by completely different enzymes. AEA and 2-AG are originated from *N*-arachidonoyl phosphatidyl ethanol (NAPE) and diacylglycerols (DAGs), respectively [28]. Regarding endocannabinoid degradation process, it is carried out by hydrolysis and/or oxidation. AEA is mainly degraded by the hydrolase enzyme FAAH, whereas 2-AG is degraded by MAGL. However, some other pathways may be involved in this process. For example, AEA is also degraded via *N*-acylethanolamine-hydrolysing acid amidase (NAAA) and 2-AG by alpha/beta domain hydrolases 6 and 12 (ABHD6 and 12). Moreover, both EAE and 2-AG can be oxidized by cyclooxygenase-2 (COX-2) [35].

26

3. Other targets for phytocannabinoids and endocannabinoids

CB$_1$ and CB$_2$ receptors were the first targets identified for endogenous as well as some exogenous cannabinoids, but subsequent research led to the discovery of other receptors able to respond to both endocannabinoids and phytocannabinoids.

3.1. G-protein-coupled receptors (GPCRs)

In the past few years it has been suggested that some cannabinoids display activity on several members of the family GPCR, such as GPR3, GPR6, GPR12, GPR18 and GPR55. However, this possibility has only been demonstrated for GPR18 and GPR55. Interestingly, the sequence homology between them and the canonical CB receptors is only around 10% [36].

GPR55 is highly expressed in the brain as well as in other peripheral tissues like gastrointestinal tract, bone marrow and immune system. GPR55 plays an important role in some pathologies, including inflammation, neuropathic pain, bone physiology, motor coordination, metabolic disorders and cancer [36]. On the contrary, GPR18 is mainly expressed in the lymphoid tissues, but it can also be found in lung, brain, testis and ovary. These receptors have been involved in different diseases, for example, cancer or metabolic disorders [36].

3.2. Glycine Receptors (GlyR)

Glycine receptors mediate synaptic inhibition of neurotransmitters in several regions of the CNS and some reports indicate that they may be modulated by cannabinoids [37-39]. Beneficial effects have been associated to GlyR ligands used in *in vitro* and *in vivo* models of inflammatory and neuropathic pain [38, 40].

3.3. Transient Receptor Potential (TRP) Channels

This family of ionotropic receptors is involved in many mammalian senses, including temperature sensation, smell, taste, vision, pressure or pain perception [36]. It was suggested that cannabinoid ligands targeting TRP channels could have a therapeutic benefit in the treatment of sensory and dermatological diseases [41]. Cannabinoids interact with three subfamilies of TRP channels: TRPV (Vanilloid), TRPA (Ankyrin) and TRPM (Melastatin), being TRPV1 one of the best studied TRP receptors for its response to cannabinoids.

TRPV1 is widely expressed in brain and sensory neurons, co-localizing with CB_2 and CB_1, respectively. It has been reported that CBD, CBG, CBC, Δ^9-THCV and CBDV are ligands of TRPV1 channel, and CBD, CBG, Δ^9-THCV, CBDV, Δ^9-THC and Δ^9-THCA, activate TRPV2 [42, 43]. In fact, it was concluded that some analgesic and antiproliferative properties associated to CBD could be explained by the interaction with this receptor [44, 45]. Other cannabinoids have been also shown to induce effects mediated by TRPV3 and TRPV4, suggesting that these receptors could be pharmacological targets in gastrointestinal inflammation [46].

On the other hand, TRPA1 and TRPM8 are also targets of different cannabinoids and may play a role in inflammation and neuropathic pain [36].

3.4. Peroxisome proliferator-activated receptors (PPARs)

Since 2002 consistent evidence has been accumulated indicating that cannabinoids bind to and activate PPARs [47]. Some analgesic, neuroprotective, neuronal function modulation, anti-inflammatory, metabolic, anti-tumour, gastrointestinal and cardiovascular properties of cannabinoids are associated to their interaction with PPARs, mainly with the PPARα and PPARγ isoforms [47]. However, PPARγ has always been the most interesting isoform among researchers because of its wide tissue distribution (heart, muscles, colon, kidney, pancreas, and spleen) as well as its role in the control of fatty acid storage, glucose metabolism, cell growth and cell differentiation.

4. Biological effects of non-psychotropic phytocannabinoids: CBD, CBG and semi-synthetic analogues

The best characterized non-psychoactive components of *C. sativa* are CBD and CBG. As mentioned previously, both of them exhibit a low affinity for CB_1 receptor compared to Δ^9-THC and are endowed with numerous pharmacological effects. CBD is suggested to have beneficial effects in the treatment of inflammatory lung, degenerative and bowel diseases among others, as well as, in the immunological antitumor response [48]. Other evidence highlights that CBD can be involved in brain signalling systems, showing it as a possible therapy for nervous system pathologies, for example, ischaemic stroke [49], schizophrenia [50], anxiety disorders [51], depression [52] or insomnia [53]. In addition, analgesic effects have been reported by non-malignant neuropathic pain patients [54]. Moreover, the use of CBD has been also validated in the cardiovascular

28

system, where it is demonstrated that CBD induces a vasodilator effect endothelium dependent [48] and also prevents pathologies associated with diabetic cardiomyopathy [55].

Some years after discovering cannabinoids, and because of the large amount of therapeutic properties attributed to them, drug discovery programs were initiated with the aim of modifying their chemical structures in order to enhance their potency, efficacy and pharmacokinetics [56]. The CBD scaffold has been commonly used for the development of new semi-synthetic CBD analogues such as 1',1'–Dimethylheptyl, miscellaneous and quinone derivatives, modifications on the C40-Alkyl chain or in the hydroxyl groups and halogenated substituents on the phenol ring.

In 1968, Mechoulam and co-workers originated HU-331, a quinone derivative of CBD synthetized by an oxidative process [57]. Later on, it was described that HU-331, also known as VCE-004 (Figure 3), presents a potent antineoplastic activity and binding affinity to PPARγ [47, 58]. However, *in vivo* studies carried out with quinones showed some negative effects, including acute cytotoxicity, immunotoxicity, and, unexpectedly, carcinogenesis [59]. Thus, with the aim of avoiding these side effects, a collection of new chemical entities with modifications in position 2 of the benzene ring was generated by the company Emerald Health Biotechnology España (Cordoba, Spain), generating the VCE-004 series exemplified by the compounds VCE-004.8 and VCE-004.3 (Figure 3). These non-electrophilic compounds maintain the agonist activity on PPARγ and have a greater affinity for the CB_2 receptor compared to the natural cannabinoid CBD, making them extremely interesting to be used for the treatment of inflammatory, immunologic, fibrotic or neurodegenerative diseases [60]. In fact, recent studies carried out in *in vitro* and *in vivo* models of skin fibrosis have demonstrated that the compounds VCE-004.3 and VCE-004.8 inhibit inflammatory and profibrotic factors, highlighting their efficacy for the treatment of different forms of scleroderma [60, 61]. Moreover, subsequent studies in multiple sclerosis (MS) models show that VCE-004.8 activates hypoxia-inducible factor (HIF) pathway, resulting in a beneficial effect for MS treatment by ameliorating pro-inflammatory molecule expression and axonal damage [62]. The series 004 were licensed to Emerald Health Pharmaceuticals (San Diego USA). EHP-101, an oral formulation of VCE-004.8, has completed a Phase I clinical study (clinicaltrial.gov: NCT03745001) and initiation of Phase II studies in scleroderma patients are being planned (clinicaltrial.gov: NCT04166552).
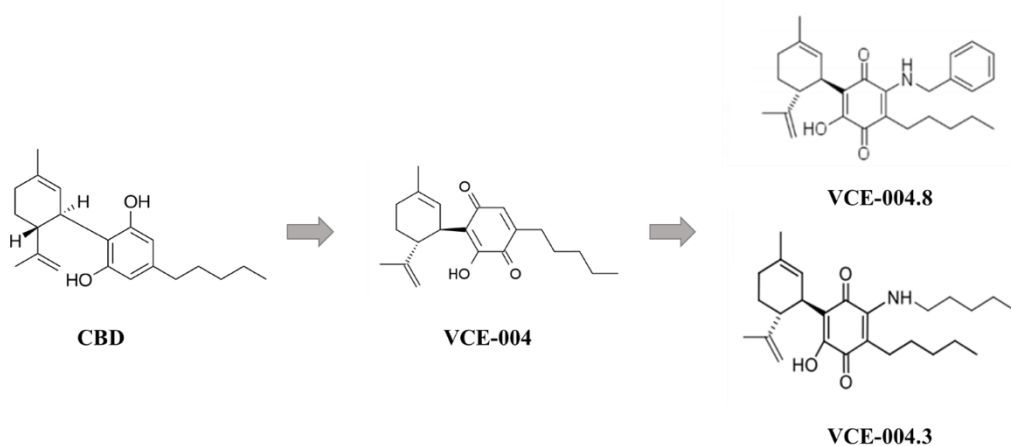
Figure 3. Schematic representation of VCE-004.3 and VCE-004.8 synthesis.

On the other hand, although CBG has been less studied than CBD, some biological effects have been also attributed to it, for example, anti-inflammatory properties [63]. Emerald Health Biotechnology España was also interested in the development of other molecules with a better bioactivity than its precursor CBG. Thus, the company developed a new cannabinoid quinone derivative named VCE-003 (Figure 4). This compound is PPARγ and CB_2 receptors agonist and shows a therapeutic profile for the treatment of neuroinflammatory and neurodegenerative disorders induced or not by abnormal autoimmunity [64, 65]. Later on, they generated a group of non-thiophilic VCE-003 derivatives with different target affinities (PPARγ agonist). After a deep characterization, several studies demonstrated that VCE-003.2 has a high potential to be used for the treatment of neurodegenerative diseases with neuroinflammatory traits, including Huntington's (HD) and Parkinson's (PD) diseases [66-68].
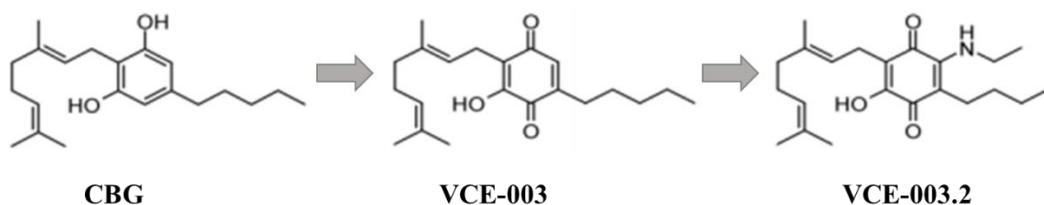
Figure 4. Schematic representation of VCE-003.2 synthesis.

5.   The endocannabinoid system in obesity and peripheral inflammatory diseases

Over the last few decades, the ECS has been involved in multiple physiological and pathological processes, leading to be extremely interesting for drug development.

5.1. Role of the endocannabinoid system in obesity

Obesity is a worldwide disease whose prevalence is around 600 millions of obese and nearly 2 billion people with overweight [69]. Obesity is a multifactorial disease characterized by a chronic inflammation and a high fat accumulation in the organism. Usually, obesity is considered as a significant risk factor for developing many pathologies, mainly including cardiovascular and metabolic disorders, such as type-2 diabetes and metabolic syndrome (MetS) [70, 71], but also musculoskeletal disease (osteoarthritis), Alzheimer's disease and some specific cancers [72-74]. Although the basis of obesity remains uncertain [75], the systematic chronic adipose tissue inflammation seems to be the main factor of the obesity co-morbidities [73]. Despite the first line of management of this disease is lifestyle therapy, its growing incidence is cause of alarm, hence the need to develop more efficient and safe obesity treatments.

Although the adipose tissue was designed to store energy, nowadays this belief is not totally real. Depending on whether we refer to white (WAT) or brown (BAT) adipose tissue, its function will be different. WAT is involved in energy storage and endocrine hormone secretion but, on the contrary, BAT is the responsible of energy expenditure and it is considered an interesting target for obesity treatment [76].

The ECS has a fundamental role in food intake, lipid metabolism and energy expenditure, thus, it is characterized as a potent regulator of energy balance. It has been described that the ECS is a physiological mechanism initially originated to increase food intake and energy storage, leading to survival periods of fasting [77]. It has been reported that the overactivation of the ECS is associated to obesity and metabolic disorders [78]. Confirming this, it was demonstrated that the inhibition of CB_1R activity is involved in the control of food intake and energy expenditure [79]. In fact, rimonabant, an anorectic anti-obesity and systemic CB_1R antagonist drug, was developed and approved in Europe in 2006. However, it had to be withdrawn after two years due to important psychiatric side effects.

Regarding food intake, it is well-known that it depends on different peripheral signals (e.i., leptin, adiponectin, ghrelin, etc.) that come to hypothalamic areas where CB_1Rs and endocannabinoids are highly expressed. The relationship between obesity and activation of ECS can be also observed in genetically-modified murine models of obesity, which have a defective leptin signalling and high hypothalamic endocannabinoid levels [80]. A

number of reports demonstrated that endocannabinoids produced in gut increased the consumption of fat [81, 82] and when animals were pharmacologically blockade with a CB$_1$R antagonist in duodenum, they reduced the fat intake [81]. However, the communication pathway gut-brain is not completely understood, but it is possible that this connection is mediated by a gastric ghrelin secretion when cells are activated through CB$_1$R [83]. The leptin hormone has also been involved in food intake. In fact, a link exists between a leptin-resistance state and hyperphagia [84].

On the other hand, some studies suggest that food intake also depends on the type of neurons where endocannabinoids act and on the subcellular CB$_1$R localization. In 2010, Bellocchio, L. et al showed that endocannabinoids have orexigenic effects when they act at CB$_1$R located at cortical glutamatergic neurons, but in the case of acting at GABAergic neurons, their effects are anorexigenic [85]. In addition, CB$_1$R agonist cannabinoids also promote feeding acting upon hypothalamic proopiomelanocortin (POMC) neurons [86].

Moreover, the ECS also promotes obesity by inhibiting processes modulated by the sympathetic nervous system (SNS), such as energy expenditure, brown adipose tissue (BAT) thermogenesis and white adipose tissue (WAT) lipolysis [87, 88]. In this sense, some *in vitro* studies demonstrated that CB$_1$R agonists induce adipogenic differentiation, whereas CB$_1$R antagonists promote the oxidation of fatty acids, mitochondrial biogenesis and thermogenesis [89]. In obesity, high endocannabinoid levels in the liver have also been found, causing steatosis [90]. Also, the ECS regulates insulin secretion by the pancreas. Whereas the CB$_1$R activation in pancreatic cells increases inflammation and apoptosis, the blockade of CB$_1$R enhances its proliferation [91-93].

On the other hand, CB$_2$R also plays an important role in obesity, particularly improving obesity-associated inflammation in *in vivo* models of diet-induced obesity (DIO) [94]. As earlier mentioned, obesity is usually accompanied of a chronic low-grade inflammation due to an increase of pro-inflammatory cytokines production in adipocytes, which inhibit anti-inflammatory adipokines release, as well as the presence of immune cells into the adipose tissue [95, 96]. Although literature shows contradictions of CB$_2$R as a target for obesity treatment, evidence exists that CB$_2$R activation inhibits the polarization toward the pro-inflammatory M1 macrophage and the release of inflammatory adipokines [94, 97].

5.2. Role of the endocannabinoid system in peripheral inflammatory diseases

The peripheral ECS is also involved in the control of pathological functions, playing an important role in inflammatory processes. Rheumatoid arthritis (RA) is a chronic inflammatory autoimmune disease that is characterized by a persistent synovium inflammation, resulting in an inadequate fibroblast-like synoviocytes (FLSs) proliferation and an increase of pro-inflammatory cytokines and metalloproteinases (MMPs), infiltration of inflammatory cells and production of autoantibodies [98]. This inflammation also affects bone and cartilage, finishing in joint destruction [98]. Current medications for RA are nonsteroidal anti-inflammatory drugs, corticosteroids and disease-modifying antirheumatic drugs. However additional drug candidates with a safe prolife are still needed [99]. Anecdotal and preclinical evidence supported the use of cannabinoids for the treatment of arthritis, being beneficial in decreasing pain and inflammation [100].

2-Arachydonoyl glycerol (2-AG) as well as an enhanced expression of CB_1 and CB_2 receptors have been found in synovial tissues of RA patients but not in control patients [101]. Hence, the ECS could represent a potential therapeutic target for RA treatment by increasing the levels of endogenous cannabinoids or modulating the activity of CB_1 and CB_2 receptors [98]. Notably, the use of allosteric ligands for cannabinoid receptors offers a potential opportunity as therapeutic agents. In this sense, it has been demonstrated that positive allosteric modulators of the CB_1 receptor produce analgesia and attenuate neuropathic pain without cannabimimetic side effects [102, 103]. Indeed, there is evidence that both antagonists and agonists of CB_1 can be useful in the modulation of arthritis [104].

Another important point in this disease is the balance in the number of osteoblasts and osteoclasts, being the later overactivated. Interestingly, CB_1 activation induces osteoblast activity, inhibiting bone resorption, a frequent event in arthritis [105]. On the contrary, Idris et al. demonstrated that the inactivation of CB_1R protected the mice from loss bone by the inhibition of osteoclast formation [106]. In addition, the same protector effect was observed in mice treated with HU-308 and JWH-133 in a collagen-induced arthritis model. *In vitro* experiments also noted that the synthetic cannabinoid agonists HU-210 and Win-55,212-2 inhibited prostaglandin E2 production and MMPs in IL-1β-stimulated chondrocytes [98].

33

Numerous *in vitro* and *in vivo* studies conclude that the activation of CB_2R reduces the immune response in T cells, macrophage migration and the release of pro-inflammatory factors. But also, the agonism of CB_1 has also been shown to have anti-inflammatory effects on immune cells, being involved in the inhibition of T cell signalling [107]. Several studies have revealed that CB_2R agonists, like HU-308 and JWH-133, reduced proliferation and production of interleukin (IL)-6, MMPs and chemokine ligand 2 (CCL2) in FLSs exposed to TNF-α [98]. In addition, the exogenous application of endocannabinoids decreases the production of inflammatory mediator. Another strategy to increase endocannabinoid levels could be by inhibiting their metabolic enzymes [98].

6. PPARs: an attractive target for the treatment of obesity and inflammatory diseases

The peroxisome proliferator-activated receptor belongs to a subfamily of nuclear hormone receptors which function as ligand-inducible transcription factors and regulate numerous physiological processes [108]. There are three groups of PPARs receptors: PPARα, PPARβ/δ, and PPARγ, all of them functioning as transcription factors. PPARs share similar structural features and are constituted by three domains: an amino-terminal domain (NTD) with constitutive activation function 1 (AF-1), a DNA-binding domain (DBD) containing two zinc finger motifs essential for DNA binding, and a carboxi-terminal ligand-binding domain (LBD) with the ligand-dependent AF-2 [108]. Independently of sharing the same structure, their distribution and function is different. To exert biological functions, PPARs have to form a heterodimer with the retinoid X receptor (RXR). When the complex PPAR:RXR is activated by a ligand, it suffers conformational changes that release co-repressors (e.g., SMRT and NCoR) and recruit co-activators (e.g., TRAP220 and PGC-1α), resulting in the activation of a transcriptional machinery of genes containing peroxisome proliferator response element (PPRE) (Figure 5) [109]. PPARs can also repress the activity of other transcription factors, like nuclear factor kappa B (NF-κB), activator protein-1 (AP-1), nuclear factor of activated T cells (NFAT) or signal transducer and activator of transcription 3 (STAT3) by a ligand-dependent mechanism called trans-repression. This effect means a reduction of pro-inflammatory genes expression. Besides, PPARs suppress the transcriptional activity of genes by a ligand-independent process [110].
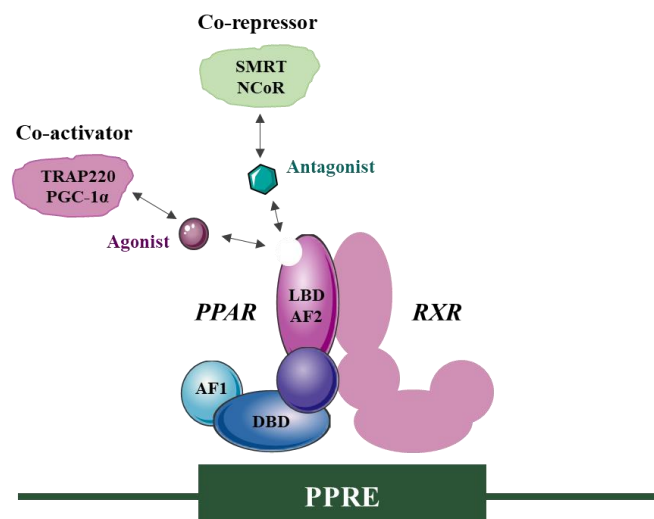
Figure 5. Transcriptional regulation of peroxisome proliferator-activated receptor (PPAR). Binding of agonists or antagonists to PPAR and its dimer partner RXR displays conformational changes of the receptors, inducing co-activator (such as Peroxisome proliferator-activated receptor gamma coactivator 1-alpha (PGC-1α) and Thyroid hormone receptor-associated protein 220 (TRAP220)) or co-repressor (such as Silencing mediator of retinoid and thyroid hormone receptor (SMRT) and Nuclear receptor co-repressor (NCoR)) binding. AF1: activation function 1 domain; DBD: DNA-binding domain; LBD-AF2: ligand binding and activation function 2 domain.

Interestingly, PPARs can also suffer post-translational modifications (PTMs), including SUMOylation, phosphorylation, acetylation, and ubiquitination. For example, it is shown that PPARγ can be phosphorylated at serine 112 (S112ph) through the activation of NF-κB pathway or by CDK7 and CDK9, or at serine 273 (S273-P) by CDK5, having the S273-P a high impact on obesity. Increased levels of PPARγ S273-P in obese humans and mice have been observed, hence it is suggested that PPARγ agonists that are able to block the S273-P could have a potential therapeutic profile by promoting insulin sensitivity in patients suffering from metabolic disorders like type 2 diabetes [111].

There are two isoforms of PPARγ: PPARγ1 and PPARγ2, being the last one differentiated by 30 extra amino acids in the N-terminus region. PPARγ1 is widely distributed in different tissues in the organism, such as immune and inflammatory cells, vascular cells, the gut and brain. However, the expression of PPARγ2 is mainly restricted to adipose tissues, where it plays a key role in adipogenesis [108].

The PPARγ functions are well-known and include the modulation of adipogenesis, glucose homeostasis, lipid metabolism, mitochondrial biogenesis and inflammatory, immunomodulatory and neoplastic processes [112]. According to its functions, many natural and synthetic PPARγ agonists have been used for the treatment of metabolic

disorders such as obesity, type 2 diabetes or MetS. In fact, nowadays, the best known PPARγ agonists are the thiazolidinediones (TZDs), including troglitazone (TGZ), pioglitazone (PGZ) and rosiglitazone (RGZ). For some time, they have been used for the treatment of type 2 diabetes due to their effects in the improvement of insulin sensitivity. However, the clinical use of these full agonist activators (PPARγ-fa) was restricted because of their side effects such as weight gain, oedema, liver injury, cancer, as well as an increased risk of heart failure [113]. Furthermore, reduction of bone mass and an increased risk of peripheral fractures in glitazone-treated patients have also been observed and associated to the inhibition of bone marrow osteoblastogenesis [114]. Thus, PPARγ controls bone mass through differentiation of MSCs towards osteoblasts and adipocytes, and RGZ suppresses osteoblast and promotes adipocyte development [115]. More recently, it has been shown that RGZ stimulates osteoblast differentiation in human MSCs, but this differentiation was followed by oxidative stress and apoptosis, overall resulting in a net loss of osteoblasts in the bone marrow [116]. Therefore, although the physiologic and therapeutic potential of PPARγ modulation remains high, interest has substantially shifted towards partial ligands, and cannabinoid-type molecules have raised considerable interest as safer alternatives to PPARγ-fa for anti-diabetic drug candidates [117].

As previously described, observational and experimental data show a link between obesity and neurodegenerative diseases by inflammatory processes, and the anti-inflammatory effect of PPARγ activators is well-recognized. PPARγ agonists have shown efficacy in both the innate and the adaptive immune system. The high levels of pro-inflammatory cytokines, like resistin, TNF-α, IL-1β and IL-6, are the main cause of developing insulin resistance and neuronal and myelin damage. It has been shown that PPARγ agonists decrease the levels of these pro-inflammatory molecules and suppress NF-κB, AP-1 and STAT3 signalling pathways, which are well-known pathways that control the transcription of pro-inflammatory genes [112, 118].

In both inflammatory and resolution phases, the macrophages and microglia have an important role, being quickly mobilized to the injured area PPARγ takes part in the recruitment and in the induction of phagocytosis. Macrophages are usually classified as classically activated (M1) and alternatively activated (M2), depending on whether they promote a pro-inflammatory or an anti-inflammatory state, respectively. Some studies reported that TZDs enhanced M2 polarization in neurological and diet-induced obesity

models [118, 119]. In physiologic conditions, both M1 and M2 levels are well balanced. However, the prolonged imbalance is the cause of many inflammatory pathologies. Interestingly, it has been reported that PPARγ agonists could re-balance this process [120].

The adaptive immune system also participates in the resolution of inflammation. It has been found that PPARγ agonists suppress the B cells proliferation through the NF-κB inhibition. Moreover, previous studies have demonstrated that PPARγ agonists such as prostaglandin J2 (PGJ2) or TZDs inhibit T cell activation and reduce the T cell differentiation into the Th1 and Th17 phenotype [121]. In addition, it is suggested that PPARγ promotes regulatory T-cell (Treg) survival, which prevents excessive immune responses and autoimmunity.

Studies focusing on the interaction between PPARγ and obesity described that the *in vivo* PPARγ suppression is lethal and its expression is needed for the survival of adipocytes. However, the adipose-specific PPARγ knockout mice subjected to a high-fat diet did not gain weight and did not develop insulin resistance [108].

The activation of PPARγ induces a process of remodelling in the adipocyte, which includes the apoptosis of the existent insulin-resistant adipocytes and the differentiation of preadipocytes, which are smaller and more insulin sensitive [122] (Figure 6). In addition, PPARγ increases the release of the adiponectin hormone, which also enhances insulin sensitivity, in this case, acting in liver and skeletal muscle, and decreasing glucose production in liver. On the other hand, PPARγ activation promotes the glucose uptake by increasing the glucose transporters GLUT1 and GLUT4 in adipose tissue and muscle.
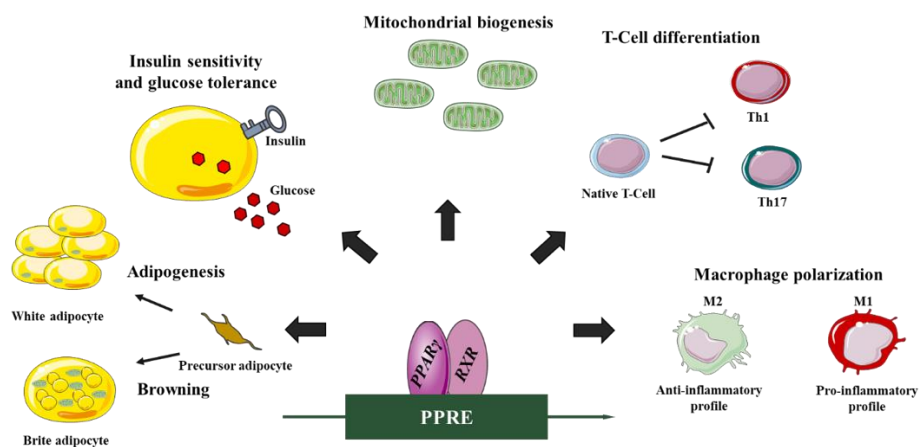

Figure 6. The role of PPARγ in obesity.

Recent research has also identified that PPARγ is involved in the expenditure of energy through browning, a process by which precursor cells of adipocytes acquire brown-like features and are converted into beige or brite adipocytes. This process is derived from the direct stimulation with hormones (adipokines, sex steroids and thyroid hormones) or adrenergic signalling [123]. Both brown and beige adipocytes are characterized by abundant density of mitochondria and high levels of uncoupling protein-1 (UCP-1) expression whose aim is to induce heat dissipation by decreasing synthesis at the respiratory chain [124]. Thus, the induction of browning process by pharmacological manipulation may be a key therapy against obesity.

Although TZDs are the most used PPARγ agonists to assay its effect, other natural products have also been investigated. For example, in a high fat diet (HFD) model, mice treated with amorfrutin B did not gain weight, improved insulin sensitivity and glucose tolerance, and exhibited protecting properties in the liver [125].

Recent evidence suggests that mitochondrial dysfunction is involved in the pathogenesis of many disorders, and especially in neurodegenerative and metabolic diseases. It was shown that the RGZ treatment in mature adipocytes increased mitochondrial biogenesis, which means a major expenditure energy, and *in vitro* experiments carried out in N2a cells treated with Δ^9-THCA increased the mitochondrial mass levels. Thus, targeting mitochondrial biogenesis through PPARγ pathway could be useful to treat obesity or neurological diseases [13, 126].

It is well known that ligands of PPARγ represent a pharmacological approach for the treatment of metabolic and inflammatory disorders, paying a considerable attention to the adverse effects previously observed in TGZs. An emerging trend in the pharmacological industry is the development of ligands with binding affinity for the alternate/allosteric ligand-binding site in the PPARγ LBD. These new compounds could be directed to exert specific effects. For instance, lobeglitazone, a TZD anti-diabetic drug, binds to PPARγ occupying the hydrophobic pocket near the alternate binding site, which results in a higher inhibition of PPARγ S273-P compared to RGZ [127].

Regarding other inflammatory diseases, recent studies have reported that PPARγ is associated with rheumatic diseases [128-130]. In addition, preclinical evidence suggests that PPARγ agonists exert protective effects in experimental models of arthritis, reducing

disease severity, infiltration of inflammatory cells and plasma pro-inflammatory cytokines levels and preventing cartilage and bone loss [130].

7. The hypoxic response pathway. Targeting for therapeutic intervention in obesity and other pathologies

Hypoxia, a state in which oxygen is limited, is a hallmark feature of numerous diseases characterized by inflammatory processes due to hypoxia and inflammation sharing an interdependent relationship [131]. After a deep study of this connection in different pathologies, it has been suggested that the stabilization of Hypoxia-inducible factors (HIFs) by pharmacological intervention could provide tissue protection, triggering potent anti-inflammatory mechanisms [132].

HIFs are heterodimer transcription factors, which can be found in two subunits: α- and β-subunit. Whereas HIF-β, also known as aryl hydrocarbon receptor nuclear translocator (ARNT), is constitutively expressed in the nucleus of all cells, its isoform HIF-α is expressed ubiquitously (HIF-1α) or in specific tissues (HIF-2α and HIF-3α) like in vascular endothelial cells, adipocytes and myeloid-derived cells [133]. Both HIF-1α and HIF-2α are involved in the modulation of several physiological processes including angiogenesis, glucose, fatty acid, cholesterol, mitochondrial metabolism and inflammation. However, HIF-3α has been less studied due to its weak transcriptional activity.

Unlike HIF-1β, which is insensitive to oxygen (O_2), the expression of HIF-1α is regulated by O_2 levels. Under normoxic conditions, α-isoforms are hydroxylated in 402 and 564 proline residues by prolyl-hydroxylases domain proteins (PHDs), which are non-heme Fe (II) dioxygenases that require molecular oxygen and 2-oxoglutarate to hydroxylate. Von Hippel−Lindau protein (pVHL) recognizes the hydroxylation and mediates the HIF-α ubiquitination by an E3-ubiquitin ligase consisting of elongin B/C, cullin 2, and ring-box 1 through 26S proteosome [133] (Figure 7). On the other hand, it has been shown that HIF-α isoforms can also be hydroxylated in 803 asparagine residues by an asparaginyl hydroxylase factor inhibiting HIF-1 (FIH-1).
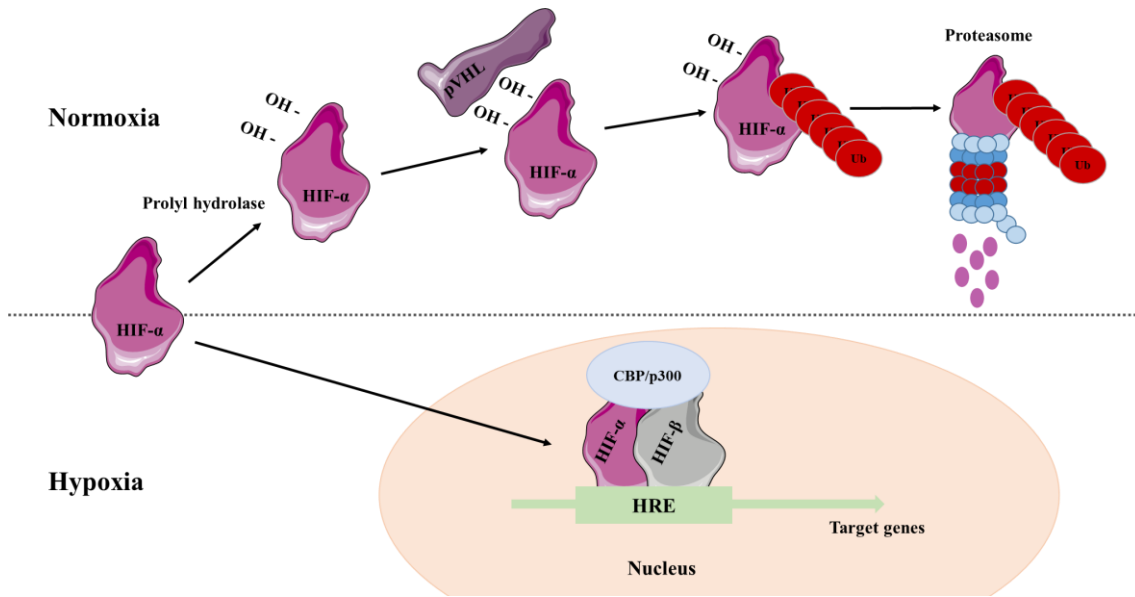
Figure 7. Hypoxia-inducible factor (HIF) regulation during normoxia and hypoxia. In normoxia, HIF-1α is hydroxylated by prolyl hydroxylases (PHDs). Hydroxylated HIF-1α is recognized by pVHL and degraded by the proteasome. In hypoxia, HIF-1α translocates to the nucleus where it dimerises with HIF-1β and recruits co-activators (such as CBP/p300). The HIF heterodimer binds to hypoxia response elements (HRE) within the promoters of target genes to regulate transcription.

There are three well-known PHDs enzyme isoforms: PHD1 is mainly present in testes but it can be also found in brain, kidney, heart and liver. Preferably, it acts over HIF-2α, and hydroxylates in both Pro402 and Pro564 similarly. PHD2 is considered the most important since it is involved in numerous processes and is present in all tissues. It shows preference for HIF-1α, hydroxylating in Pro402 and Pro564 in the same way. PHD3 acts in a similar manner in HIF-1α and HIF-2α, although it only hydroxylates Pro564 [133]. In hypoxic conditions, HIF-1α is translocated to the nucleus where it dimerizes with HIF-1β and recruits coactivators such us Creb Binding Protein (CBP)/p300, binding to hypoxia-response elements (HREs) in the target genes.

Studies on the pathogenic mechanisms of metabolic disease have documented that obesity is a chronic hypoxic state [134] that triggers adaptive responses mediated by hypoxia-inducible factor HIF-1α and HIF-2α and aimed at restoring oxygen homeostasis [134, 135]. Despite a plethora of studies addressing the roles of HIFs in adipose dysfunction [136-139], the involvement of HIF-1α and HIF-2α in obesity remains controversial. On the one hand, the hypertrophic and hyperplasic adipocytes create a hypoxic condition that exacerbates macrophage-mediated inflammation in obesity. Both in obese patients and in mice models of obesity a link between the hypoxic adipose tissue and the migration of M1 polarization of macrophages has been identified, highlighting

that the activation of the HIF pathway might contribute to the obese phenotype [140, 141]. However, other studies have shown that hypoxia actually promotes body weight reduction. In fact, this was observed in a study performed in humans exposed to high altitude (hypobaric hypoxia) whose result was a reduction in food intake and a consequent body weight loss [142]. But also, a body weight reduction was induced in obese patients exposed to the same conditions [143]. Other *in vivo* studies showed that adipocyte-specific HIF-2α-deficient obese mice expressed low levels of UCP-1 and thus a dysregulation in the thermogenic process, indicating that HIF-2α has a protector role against obesity [144]. In addition, HIF also plays an important role at the hypothalamic level targeting genes that prevent overeating and obesity in an obese state [145].

Many other studies have assayed the possible use of PHD inhibitors to induce HIF stabilization as a novel therapy in obesity. In one study, the use of mice with a low expression of PHD2 (hypomorph mouse line (Hif-p4h-2$^{gt/gt}$)) in different tissues enhanced the expression of genes involved in glucose metabolism, cardiac function and blood pressure, promoting cardioprotection. In addition, Hif-p4h-2 mice also reduced significantly the body weight compared to wild-type mice [146]. Subsequent studies also carried out in PHD2-deficient mice showed to have less adipose tissue, lower adipocyte size and inflammation, glucose tolerance and insulin sensitivity increased as well as protection against HFD-induced hepatic steatosis [147]. Similarly, beneficial effects were observed with the administration of a PHD2 inhibitor. Moreover, the HIF target gene erythropoietin has been shown to suppress adipogenesis and improve obesity, reducing insulin resistance and adipose tissue inflammation in HFD mice [148, 149]. These findings indicate that the use of PHD-HIF modulators could provide beneficial effects in the management of MetS.

Nowadays, the development of "hypoxia mimetic agents", which are drugs used to activate the HIF pathway, are having successful results in a wide range of diseases, including anaemia, cancer and ischaemic and neurodegenerative diseases. Sometimes the results have been controversial [150]. However, the beneficial effects overweigh the side effects in most of the studies [150]. Recently, our group has demonstrated that VCE-004.8 inhibits PHD1 and PHD2 activity, resulting in HIF-1α and HIF-2α stabilization. In addition, *in vivo* models of MS showed the potential efficacy of VCE-004.8 against demyelination, axonal damage and immune cell infiltration. A down-regulation of pro-inflammatory genes associated to the disease was also observed [62].

<u>Aims</u>

In the past few years it has become evident that the endocannabinoid system plays a crucial role in regulating food intake and energy metabolism. Moreover, the endocannabinoid system also regulates different elements of the immune system and the inflammatory process, which in addition to be closely linked to obesity and insulin resistance, could be the target of treatment for several inflammatory diseases such as rheumatoid arthritis. Therefore, the pharmacological manipulation of the endocannabinoid system is a major goal for researchers and pharmaceutical companies.

Since research evidence indicates that PPARγ agonists are able to regulate lipid turnover and metabolism and also mediate potent anti-inflammatory activities, the aims of this search project have been the following:

- To investigate the role of VCE-004.8 and Δ^9-THCA on PPARγ modulation and their efficacy in a murine model of metabolic syndrome induced by high fat diet (HFD).

- To identify the ability of Δ^9-THCA to modulate classic cannabinoid receptors (CB$_1$ and CB$_2$) and evaluate its efficacy in a murine model of collagen-induced arthritis (CIA).

Material and Methods

1. Reagents

Rosiglitazone was purchased from Cayman Chemical (Ann Arbor, MI, USA), T0070907 and CP-55,940 from Sigma-Aldrich (St. Louis, MO, USA) and SR141716 from Tocris Bioscience (Bristol, UK). Other reagents were form Sigma.

2. Cannabinoids

VCE-004.8 was obtained from Emerald Health Pharmaceuticals (Córdoba, Spain). Δ^9-THCA-A was purified at >95% from the Cannabis variety Moniek (CPVO/20160114) and was obtained from Phytoplant Research S.L. (Córdoba, Spain).

3. Cell lines

Immortalized murine primary brown adipocytes (pBAT) were kindly provided by Prof Francesc Villarroya (University of Barcelona, Spain). pBAT cells were maintained in Dulbecco's Modified Eagle's Medium (DMEM) with 10% FBS, 2% HEPES, 20 mM L-glutamine, and 1% (v/v) penicillin/streptomycin antibiotics. For pBAT differentiation, cells were cultured in 6-well plates (2,5 x 10^5 cells/well) and T3 (1 nM) and insulin (20 nM) were added to the media (Growth media) for 24 hours. Then, IBMX (500 μM), dexamethasone (500 nM) and indomethacin (125 μM) were added to the growth media for 48 h (Differentiation media), before changing back to the growth media with just T3 and insulin for an additional 48 h to allow acquisition of a differentiated morphology. Treatment with RGZ (1 μM) and VCE-004.8 (1 μM) in the presence and the absence of T0070907 (5 μM) started at the same time as the differentiation process. Pancreatic acinar-derived AR42J, HEK293 and HEK293-CB_1-CRE-Luc cells were maintained in DMEM, containing 20 mM L-glutamine and supplemented with 10% FBS and antibiotics. HEK293-CB_1-β-arrestin Nomad were cultured in DMEM supplemented with MEM Non-essential Amino Acid Solution (100×) (Sigma-Aldrich), 10% FBS, 20 mM L-glutamine, puromycin (5 μg/ml), hygromycin (80 μg/ml) and G418 (250 μg/ml). AR42J and HEK293 cells were obtained from ATCC (Manassas, VA, USA), HEK293-CB_1-CRE-Luc cells were obtained from Innohealth Group S.L. (Madrid, Spain) and HEK293-CB_1-β-arrestin Nomad cells were purchased to Innoprot S.L. (Derio, Bizkaia, Spain). Human chondrocytes (Sigma-Aldrich) were cultured in Chondrocyte Growth Medium (Sigma-Aldrich). All the cells were maintained at 37 °C in a humidified atmosphere containing 5% CO2.

4. Cytotoxicity assays

Cytotoxicity assays were performed using standard YOYO-1 and MTT methods depending of the cell line. For YOYO-1, HEK-293T (1 x 10^4) cells were seeded in 96-wells plates. Next day, the cells were treated with the compounds and YOYO-1 reagent (250nM). After 6 hours, the cytotoxicity was measured using the Live Content Cell Imaging System IncuCyte HD (Sartorius, Göttingen, DE). For MTT, after 21 days of adipogenic differentiation in 96-wells plates, 50 µl of 3-MTT (5 mg/ml) from a mixture solution of MTT: DMEM (1:2) was added to each well for 4 h at 37º C in darkness. Supernatants were removed, and 100 µL DMSO was added to each well for 10 min, in gentle shaking. Absorbance was measured at 550 nm using a TriStar^2 Berthold/LB942 multimode reader (Berthold Technologies, Oak Ride, TN, USA). In both assays each set of experiments was done by triplicate. The value of untreated control was taken as 100% survival.

5. Transient transfections and luciferase assays

To analyse PPARs transcriptional activities, HEK-293 (1 x 10^5) cells were cultured in 24-well plates and transiently co-transfected with the indicated constructs containing human LBDs (GAL4-PPARγ-LBD, GAL4-PPARδ-LBD, GAL4-PPARα-LBD) together with the luciferase reporter vector GAL4-luc (firefly luciferase) using Roti©-Fect (Carl Roth, Karlsruhe, Germany). To study CB$_1$-mediated functional activities, HEK293-CB$_1$-CRE-Luc (5 x 10^4) cells were seeded in 96-well plates. After stimulation for 6 hours, the cells were lysed in 50 µl lysis buffer containing 25 mM Tris–phosphate pH 7.8, 8 mM MgCl2, 1 mM DTT, 1% Triton X-100, and 7% glycerol during 15 min at RT in a horizontal shaker. Luciferase activity was measured using a TriStar^2 Berthold/LB942 multimode reader (Berthold Technologies) following the instructions of the luciferase assay kit (Promega). Luciferase activity was normalized with protein concentration.

6. Docking analysis

6.1. PPARγ-binding affinity

Ligand docking, and binding properties were calculated by using the *AutoDock4* [151] and the *Vina* software [152] with the virtual screening tool PyMOL [153]. The receptor models used were the PDB references 5Y2O57 [154], 4EMA56 [155] and

5LGS58 [156]. Search space for the docking was set around the binding sites described previously [157, 158].

6.2. CB₁-binding affinity

Three available structures of CB_1 receptor in an active-agonist bound state were used to prepare a grid for receptor docking; an X-ray structure (PDB code 5XR8) of CB_1 in complex with tricyclic compound AM841 [159], a cryo-EM structure (PDB code 6N4B) of CB_1 in complex with an indazole derivative [160] and an X-ray structure (PDB code 6KQI) of CB_1 in complex with CP-55,940 in the orthosteric site and the negative allosteric modulator (NAM) OR275569 bound to an extrahelical pocket overlapping with the cholesterol interaction site [161]. All docking calculations on the CB_1 structures were carried out with Schrodinger's GLIDE 2019-2 using its Standard Precision (SP) [162] scoring and rescoring function with the extra precision (XP) [163] scoring function. The ligand molecules were first processed with Schrodinger's Ligprep (protonation state at pH 7.4 ± 0,5), to generate 3D energy-minimized molecular structures with correct tautomeric and ionization states. The receptor grid was centered on the agonist bound orthosteric site in docking attempts to predict ligand-binding modes. Results were assessed by examining the best 10 energy poses in terms of the docking glidescore.

Protein Energy Landscape Exploration (PELE) is a highly efficient Monte Carlo (MC) algorithm that has been shown to perform extremely well at reproducing experimental binding modes in cross-docking scenarios [164, 165]. The basic algorithm works as follows: each MC move consists of three main steps: i) ligand and protein perturbation; ii) side chain rotamer sampling; and iii) system minimization. The ligand is perturbed in a series of rotations and translations with a set of user-defined variables, whereas the protein is perturbed based on a minimization with constrained displacements along the Cα-atoms following a set of given modes which can derived from an anisotropic network model (ANM) [166] or on a principal component analysis (PCA) [165]. The resulting structure obtained in the final minimization step is accepted or rejected by applying a Metropolis criterion. Backbone movements were performed by displacing backbone atoms along the first six ANM modes. This was accomplished by performing an all-atom geometry optimization, where a constraint was added to each alpha carbon along a randomly chosen mode (with displacements of 1.0 Å). Finally, a relaxation was accomplished with a 10° resolution side chain sampling for those residues within a

distance of 4Å to any ligand atom. In all calculations, PELE used the all atom OPLS2005 force field [167] with an OBC implicit solvent model [168] for protein and ligands. Interaction energies referred to in the results section are defined by E(AB) - E(A) - E(B), where AB stands for the complex, A for the receptor and B the ligand. Two different PELE protocols were applied depending on the specific purpose: <u>PELE induced fit docking:</u> This protocol was applied to improve the binding modes predicted from GLIDE rigid (receptor) docking for the THC series to the cryo-EM structure (PDB 6N4B). Ligand perturbation was switched between the low and medium range rotations and translations (0-15° and 0.5-1.5Å, respectively) and only allowed to explore the area around the orthosteric binding site. A total of 1000 PELE step simulations were run on 240 processors for 18-24 hours. <u>PELE global search:</u> This protocol performed a dynamic exploration over the whole surface of <u>CB$_1$</u> receptor in order to locate any possible binding site for Δ^9-THCA-A once its orthosteric site was occupied by an agonist. This protocol was performed with 40 initial positions of the ligand randomly placed around the entire protein surface (extracellular, intracellular and membrane exposed). Since the binding site was assumed to be unknown, large rotations and translations were applied to the ligand at high SASA values and were gradually decreased at lower values of SASA (as the molecule gains more and more contacts with the receptor, translations and rotations are smaller). The simulation was run for a total of 1000 MC steps on 240 processors for 20 hours; results were analyzed by inspecting the lowest interaction energy poses.

7. Mesenchymal stem cells (MSCs) differentiation

The Reina Sofia University Hospital approved this study and the procedures followed were in accordance with the ethical standards of the ethic committee from Hospital Reina Sofía (Cordoba, Spain) and with the Declaration of Helsinki. The Haematology Service recruited bone marrow donors. All subjects gave their informed consent so that the bone marrow aliquots extracted for clinical purposes could also be used for mesenchymal bone marrow research. MSCs were seeded in α-MEM containing, 10% FBS, 2 mM Glutamine, 1 ng/ml bFGF and antibiotics. For adipogenic and osteoblast differentiation, the cells were plated at 500 cells/cm^2 in 6 or 24 wells plates until came closer to confluence. At that time, the same media without bFGF were supplemented with 1×10^{-8} M dexamethasone, 10 mM β-glycerophosphate, and 0.2 mM ascorbic acid (Osteoblast media; OM) or 5×10^{-7} M dexamethasone, 0.5 mM isobutylmethylxanthine, and 50 µM indomethacin (Adipocyte media, AM). Treatments with RGZ (1 µM), VCE-004.8 (1 µM)

and Δ^9-THCA-A (1, 5 and 10 µM) in the presence and the absence of T0070907 (5 µM) started at the same time as the differentiation process. After 7 or 14 days of differentiation, the mRNA was analyzed by qPCR and, after 21 days, adipogenesis and osteoblastogenesis were analyzed by Oil red O and Alizarin red staining, respectively. Lipid accumulation was detected by Oil Red O staining. Cells were fixed in 3,7 % paraformaldehyde for 10 min, washed with 60 % isopropanol for 5 min, incubated with an Oil Red O solution for 20 min at room temperature, followed by washing twice with dH$_2$O and counterstaining with DAPI (0,5 µg/ml in PBS) for 5 min. For quantification, the staining lipid droplets were dissolved in isopropanol and measured at 540 nm using a microplate reader. The mineralization was evaluated by Alizarin red staining. The cells were fixed in 3.7% paraformaldehyde for 10 min, rinsed in dH$_2$O and stained with Alizarin red (40mM) for 5-10 min at room temperature. Finally, the cells were washed with dH$_2$O. For quantification, the mineral content was dissolved in 10 % acetic acid for 30 min with rotation at room temperature. The solution was extracted and heated to 85ºC for 10 min. Then, the pH (4.1-4.5) was neutralized with ammonium hydroxide and the optical density was measured at 405 nm using a microplate reader. Images captured with the light microscope were analyzed with the ImageJ Software (NIH; Bethesda, MD, USA).

8. CB$_1$ and CB$_2$ receptor binding assay

Δ^9-THCA-A (10^{-11}-10^{-4} M) was investigated by competition studies against [^{3}H]CP-55,940 (164.5 Ci/mmol, Perkin Elmer, Boston, MA, USA) to determine its binding affinity (Ki value) at both cannabinoid receptors using commercially available membranes prepared from CB$_1$ or CB$_2$ receptor-stably transfected HEK-293 cells (RBHCB1M400UA and RBXCB2M400UA, respectively; Perkin-Elmer) [169]. Briefly, membranes were added in assay buffer (for CB$_1$: 50 mM Tris-Cl, 5 mM MgCl$_2$.H$_2$O, 2.5 mM EDTA, 0.5 mg/ml bovine serum albumin, pH 7.4, or for CB$_2$: 50 mM Tris-Cl, 5 mM MgCl$_2$.H$_2$O, 2.5 mM EGTA, 1 mg/ml bovine serum albumin, pH 7.5) at a final concentration of 8 µg/well and 4 µg/well for CB$_1$ and for CB$_2$ receptors, respectively. The radioligand was used at 0.4 nM for CB$_1$ receptors or 0.53 nM for CB$_2$ receptors and in a final volume of 200 µl for both receptors. The reaction was stirred for 90 min at 30°C. Non-specific binding was determined with non-radiolabelled WIN55,212-2 (Sigma Aldrich, 10 µM) in the presence of radioligand. 100% binding of the [^{3}H]CP-55,940 was determined by incubation of the membranes with radioligand in the absence of Δ^9-THCA-

A. All of the plastic material employed were siliconized with Sigmacote (Sigma-Aldrich) to prevent possible adhesion of compounds. After incubation, free radioligand was separated from bound radioligand, by filtration in GF/C filters, previously treated with a 0.05% (v/v) polyethylethylenimine solution. Then, filters were washed nine times with cold assay buffer, using the Harvester® filtermate equipment (Perkin Elmer). Radioactivity was measured using a liquid scintillation spectrometer (Microbeta Trilux 1450 LSC & Luminiscence Counter (Perkin Elmer)). Data were expressed as percentage of [^{3}H]CP-55,940 binding.

9. [^{35}S]GTPγS binding analysis

The intrinsic activity of Δ^9-THCA-A at the cannabinoid receptors was analyzed using a [^{35}S]-GTPγS binding assay with increasing concentrations (10^{-11}-10^{-4} M) of this compound [169]. The assay buffer was prepared by adding 10 µM GDP (Sigma-Aldrich) to 20 mM HEPES (Sigma-Aldrich) buffer containing 100 mM NaCl and 10 mM MgCl$_2$ at pH 7.4. Later, the radiolabelled, non-hydrolysable G-protein-activating analogue of guanosine triphosphate, [^{35}S]-GTPγS (PerkinElmer) was added at a final concentration of 0.3 nM in assay buffer. The assay started once membranes (previously permeabilized with 5 µg of saponin; Sigma-Aldrich) containing CB$_1$ (HTSO19M) or CB$_2$ receptors (HTS020M) (5 µg/well; Eurofins Discovery Services, Saint Charles, MO, USA) were added. The reaction had a final volume of 100 µl and was stirred for 30 minutes at 30ºC. To determine the non-specific signal, 10 µM GTPγS (Sigma-Aldrich) was employed. Again, 96-well plates and the tubes needed for the experiment were siliconized with Sigmacote (Sigma-Aldrich). The reaction was terminated by rapid vacuum filtration with a Harvester® filtermate equipment (Perkin Elmer) through Filtermat A GF/C filters. The filters were washed nine times with ice-cold filtration buffer (10 mM sodium phosphate, pH 7.4), and bound radioactivity was measured with a 1450 LSC & Luminiscence counter Wallac MicroBeta TriLux (Perkin-Elmer).

10. Analysis of allosteric properties of Δ^9-THCA-A at the CB$_1$ receptor

For the study of allosteric properties of Δ^9-THCA-A at the CB$_1$ receptor, the activation of this receptor elicited by increasing concentrations (10^{-11}-10^{-4} M) of CP-55,940, was quantified alone or in presence of Δ^9-THCA-A at three concentrations (10^{-6}, 10^{-10} and 10^{-13} M) following a modification of the procedure for [^{35}S]-GTPγS binding.

11. CB₁ functional assays (Arrestin and proliferation)

HEK293-CB$_1$-β-arrestin Nomad (1 x 10^4) cells were cultured in 96-well plates. Next day, the culture was stimulated as indicated and fluorescence was measured at different times for 24h using Live Content Cell Imaging System IncuCyte HD (Sartorius, Göttingen, DE). Cells confluence as a tool to measure proliferation was determined by IncuCyte HD Confluence Processing analysis tool.

12. Animals and experimental designs
12.1. High fat diet (HFD) model

Six-week old male C57BL/6 mice, obtained from Charles Rivers Laboratories (l'Arbresle, France), were pair-housed at 20–22 °C, under constant conditions of light (14 hours of light; lights on at 7:00 am), and free access to food and water. All experiments were performed in accordance with European Union guideline and approved by the Animal Research Ethic Committee of Cordoba University (2014PI/025). Procedures were designed to minimize the number of animals used and their suffering. At 8 weeks of age, the animals were randomly assigned in two groups (N = 20) to receive either a high-fat diet (HFD), D12451 (Research Diets, New Brunswick, NJ, USA; 45%, 20%, and 35% calories from fat, protein and carbohydrate, respectively) or standard diet (CD), A04 SAFE Diets (Augy, France; 8,4%, 19,3% and 72,4% calories from fat, protein, and carbohydrate, respectively) for 15 weeks. A04 SAFE was used as control diet in our experiments since this is used routinely in our animal facilities and has a percentage of calorie content from fat sources grossly similar to that of other control diets (e.g., D12450B diet from Research Diets, with 10% calories from fat), with an stable nutritional composition in terms of percentage of main nutrients and calorie sources. Body weight (BW) gain and daily energy intake were monitored once weekly during the first 12 weeks, and twice a week during treatment period. The latter was calculated from mean food ingestion per week using the energy density index provided by the manufacturer (3.34 kcal/g for CD or 4.73 kcal/g for HFD). In order to assess the potential metabolic effects of VCE-004.8 and Δ^9-THCA-A, mice were treated by daily intraperitoneal injection (i.p) of these compounds (20 mg/Kg dissolved in ethanol/cremophor/saline 1:1:18) during three weeks, from week 12 onwards, in CD and HFD groups (n = 10/group). Body composition analyses were performed by quantitative magnetic resonance (QMR), using

the EchoMRI™ 700 analyzer (Houston, TX, software v.2.0). MRI scans were taken before starting diet exposure, at the start of treatment (week 12), and at the end of experimental procedures (week 15). At the end of the experiment, mice were euthanized and blood and tissues were collected. Tissues were immediately frozen using dry ice and then stored at -80ºC and/or fixed by immersion in a 4 % formalin solution for further analysis of molecular expression and histology, respectively. Blood was collected into heparin tubes and centrifuged at 2000 rpm for 20 minutes at 4ºC.

In another experiment, eight-week old male C57BL6 mice fed with CD were treated with Δ^9-THCA-A (20 mg/Kg i.p.), with or without the selective PPARγ inhibitor, T0070907 (5 mg/Kg i.p.), for 3 weeks (n = 10/group). Pair-aged mice (n=10) treated with vehicle served as controls.

12.2. Collagen-induced arthritis (CIA) model

Seven-week old male DBA/1 mice were purchased from Janvier Labs (Le Genest Saint Isle, France). The mice were housed in cages at controlled temperature (20 ± 2°C) and relative humidity (40–50%), with alternating 12 h light–dark cycles. All experiments were performed in accordance with European Union guideline and approved by the Animal Research Ethic Committee of Cordoba University (2018PI/18).

On day 0, mice received the first immunization injecting 100 μL of type II bovine collagen (2 mg/mL) (Sigma-Aldrich) emulsified in equal volumes of Freund's complete adjuvant (Sigma-Aldrich) by intradermal administration at the base of the tail. On day 21, the mice were given a booster immunisation with 100 μL of type II bovine collagen (2 mg/mL) emulsified in equal volumes of Freund's incomplete adjuvant. Following the second immunization, mice without evident symptoms, were randomly assigned in different groups (n=9/group) and treated daily by intra-peritoneal injection with Δ^9-THCA-A (20 mg/Kg), with or without the selective PPARγ inhibitor, T0070907 (5 mg/Kg), the CB_1 inhibitor, SR141716 (3 mg/Kg) or the vehicle (ethanol/cremophor/saline in the proportion of 1:1:18) until day 36. BW change was monitored every 2-3 days during treatment period. Besides, also the paw edema was controlled using a Vernier caliper and a plethysmometer (LE7500, Panlab, Barcelona, Spain). The clinical evaluation of arthritis severity was scored on a scale from 0 to 4 as follows: 0 = normal; 1 = detectable swelling in one joint or toe; 2 = swelling in two types of toes or joints but not entire paw inflamed; 3 = entire paw inflamed and swollen; 4 = severe swelling in the entire paw or ankylosed.

At the end of the treatment period, mice were euthanized, and blood and hind limb tissue were collected for analysis.

In a separate set of experiments, we tested the hypolocomotion and catalepsy effects of both Δ^9-THC and Δ^9-THCA-A at 10 mg/Kg during 30 min in control mice

13. Intraperitoneal glucose and insulin tolerance tests, and triglyceride determinations

The animals were intraperitoneal injected with a bolus of 2 g of glucose per kg BW, after a 5 h period of food deprivation, and blood glucose levels were determined at 0, 20, 60 and 120 min after injection. For ITT, the animals were subjected to intraperitoneal injection of 1 U of insulin (Sigma-Aldrich) per kg body weight, after a 5 h fasting. Blood glucose levels were measured at 0, 20, 60 and 120 minutes. All glucose concentrations were measured using a handheld glucometer (Accu-Check Advantage®; Roche Diagnostics, Rotkreuz, Switzerland).

14. Determination of hormonal, metabolic and inflammatory markers, and autoantibodies

Circulating adipokine levels of leptin, insulin, ghrelin, resistin, glucagon, gastric inhibitory peptide (GIP), glucagon-like peptide 1 (GLP-1), plasminogen-activator inhibitor-1 (PAI-1) and adiponectin were measured using quantitative Bio-Plex Pro™ Mouse Diabetes 8-Plex immunoassay (#171F7001M; Bio-Rad Laboratories, Hercules, CA, USA) and Bio-Plex Pro Mouse Diabetes Adiponectin assay #171F7002M (Bio-Rad). Additionally, serum FGF21 levels were measured using a commercial ELISA kit (Quantikine MF2100; R&D Systems, Minneapolis, MN, USA) and serum triglyceride levels were assayed, using a GPO-POD assay kit (Triglyceride Liquid kit 992320, Quimica Analitica Aplicada SA, Tarragona, Spain). Cytokine levels (IFNγ, IL-6, IL-10, IL-17A and TNF-α) and IgG antibody levels against type II collagen were measured using a quantitative Bio-Plex Pro™ Mouse Cytokine Th17 Panel A 6-Plex immunoassay (#m6000007ny; Bio-Rad) and Mouse Anti-Type II Collagen IgG Assay Kit (Chondrex, Redmond, WA, USA), respectively. For other biomarkers, serum samples from mice were pooled (n = 6 mice per group) and assayed for cytokine and adipokine expression using the Proteome Profiler Mouse XL Cytokine Array and the Proteome Profiler Mouse Adipokine Array (R&D Systems). Spot density was determined using Quick Spots image

analysis software (R&D Systems). All assays were carried out according to the manufacturer's instructions.

To determine insulin secretion *in vitro* AR42J cells were stimulated with VCE-004.8 for 24 h and after that the cell were washed and incubated with 1.5 mL of Krebs-Ringer bicarbonate buffer (KRBB) containing 143.5 mM NaCl, 5.8 mM KCl, 2.5 mM CaCl2, 25 mM HCO3, 0.3% BSA (Sigma-Aldrich) and 3.3 mM glucose at 37 °C for 1 h. Then, cells were washed and incubated with 1.5 mL KRBB buffer with 27.7 mM glucose at 37 °C for 1 h. Total insulin was measured in the supernatants using a rat (10-1250-01) ELISA (Mercodia AB, Uppsala, Sweden).

15. Histological analysis

From HFD model, brown adipose tissue (BAT), white adipose tissue (WAT,) and liver were collected and fixed in 4% formalin for 24 hours. From CIA model, the knee joint of each mouse was isolated and fixed in 4% formalin for 2 days and decalcified in 7% nitric acid for 5 days. Once tissues were fixed and decalcified, they were processed through several steps of dehydration with a series of alcohols (70% to 100%). The next step was xylene clearing and finally, paraffin embedding. After paraffin blocks inclusion, the samples were cut into section and deparaffinized by running them through xylene to alcohols (100% to 70%). All pictures of histologic analysis were taken using a Leica DM2000 microscope and Leica MC190 camera.

15.1. Hematoxylin & eosin

H&E staining discloses abundant structural information, displaying a wide range of cytoplasmic, nuclear, and extracellular matrix differences. Liver tissue and knee sagittal sections (5 µm) were stained with haematoxylin for 1 min and eosin for 30sec. Following, the section were dehydrated (from 80%-96%-100% alcohols to xylene) and mounted using Eukitt (Sigma-Aldrich). The liver sections were evaluated for steatosis according to the Kleiner system [170]. A semi-quantitative score was assigned to describe the extent of steatosis (0, <5%; 1, 5–33%; 2, 33–66%; and 3, >66%). The degree of inflammation in knee sections was examined according to the following scheme: 0, normal knee joint; 1, normal synovium with occasional mononuclear cells; 2, definite arthritis, a few layers of flat to rounded synovial lining cells and scattered mononuclear cells; 3, clear hyperplasia of the synovium with three or more layers of loosely arranged lining cells and

dense infiltration with mononuclear cells; 4, severe synovitis with pannus and erosions of articular cartilage and subchondral bone.

15.2. Safranin O and Toluidine blue

These staining are cationic dyes that stain both proteoglycans and glycosaminoglycans, having the toluidine blue a higher affinity for the sulfur in cartilage compared to Safranin O. For safranin O staining, rehydrated sections (5 µm) were stained with Weigert's hematoxylin working solution for 10 min and rinsed in tap water until clear. Sections were stained sequentially with 0.02% Fast Green solution for 5 min, 1% acetic acid solution for 15 sec, and 0.1% Safranin O solution for 5 min. Subsequently, the sections were dehydrated (from 80%-96%-100% alcohols to xylene) and mounted using Eukitt (Sigma-Aldrich). For toluidine blue staining, rehydrated sections (5 µm) were stained with toluidine blue working solution for 3 min, dehydrated (from 80%-96%-100% alcohols to xylene) and mounted using Eukitt (Sigma-Aldrich).

Based on safranin O and toluidine blue staining, a score was assigned to describe the cartilage damage: 0, no destruction; 1, minimal erosion, limited to single spots; 2, slight to moderate erosion in a limited area; 3, more extensive erosion; and 4, general destruction.

15.3. Immunohistochemistry

For IHC analysis, 7 µM-thick paraffin-embedded tissue sections of inguinal white (iWAT) adipose tissue were used. Antigen retrieval was performed in 37 °C trypsin (pH 7.8) for 1 h or 10 mM sodium citrate buffer (pH 6) at 95 °C for 10 min. Sections were incubated with F4/80 antibody (1:50; MCA497, Bio-Rad) or UCP-1 antibody (1:500; ab10983, Abcam, Cambridge, UK) overnight at 4 °C, respectively. Then, the slides were incubated for 1 h at room temperature with the appropriate biotin-conjugated secondary antibody (Merck Millipore, Billerica, MA, USA). Reaction was stained with DAB substrate kit (Merck Millipore), and subsequent counterstaining with hematoxylin and mounting.

16. Western Blots
16.1. Protein expression from *in vivo* studies

Proteins were isolated from brown (BAT) and inguinal white (iWAT) adipose tissues in 50 µl of NP-40 lysis buffer (50 mM Tris‑HCl pH 7.5, 150 mM NaCl, 10% glycerol y

1% NP-40) supplemented with 10 mM NaF, 1 mM Na3VO4, 10 µg/ml leupeptin, 1µg/ml pepstatin and aprotinin, and 1 µl/ml PMSF; 30 µg samples were boiled at 95 °C in Laemmli buffer and electrophoresed in 10% SDS/PAGE gels. Separated proteins were transferred (20 V for 30 min) to PVDF membranes and blocked in 0.1% Tween 20 in TBS solution containing 5% non-fat dry milk for 1 h at room temperature. Membranes were incubated with the UCP-1 antibody overnight at 4 °C (1:2000; ab10983, Abcam). For loading control, α-tubulin levels were assayed in the same samples (1:10.000; DM-1A, Sigma-Aldrich). Membranes were washed and incubated with the appropriate horseradish peroxidase-conjugated secondary antibody for 1 h at room temperature and detected by chemiluminescence system (GE Healthcare Europe GmbH, Freiburg, Germany).

16.2. Protein expression from *in vitro* studies

AR42J cells (4 x 10^5) were seeded in 6-wells plates and treated with VCE-004.8, DFX and CBD for 6 hours. To measure the state levels of HIF-1α protein we used the anti-HIF-1α mAb (1:1.000, 610959, BD Biosciences, Madrid, Spain) and normalized to anti-β-Actin (1:10.000, A2228, Sigma-Aldrich). HEK293-CB$_1$-β-arrestin Nomad and HEK293 cells (3,5 x 10^5) were seeded in 6-wells plates. Next day, the cells were deprived of serum (1% FBS) for 18 hours, after which they were pre-incubated with SR141716 for 5 min and then treated with Δ^9-THCA-A and CP-55,940 for 25 min. The expression of phospho-ERK1/2 and total ERK were analyzed with the antibody anti-phospho-ERK1/2 (1:2000, 9101, Cell Signaling Technology, Danvers, MA, USA) and anti-MAP Kinase (ERK1/2) (1:10.000, M5670, Sigma-Aldrich). Anti-β-Actin was used for loading control (1:50.000, 40900, Abcam). The proteins were isolated and separated by the same process than in *in vivo* studies.

17. mRNA extraction and qPCR

17.1. mRNA extraction from *in vivo* studies

mRNA was extracted from liver and BAT tissues using the FavorPrep™ Tissue Total RNA Purification Mini Kit (Favorgen Biotech Corp., Ping-Tung, Taiwan) and from eWAT, iWAT and knee tissues using QIAzol Lysis Reagent (Qiagen, Hilden, Germany) and purified with Qiagen RNeasy Lipid Kit (Qiagen, Hilden, Germany) or RNeasy Mini Kit (Qiagen).

17.2. mRNA extraction from *in vitro* studies

MSCs cells were collected at day 7 or 14 of differentiation. Primary human chondrocytes were seeded in Chondrocyte Growth Medium until confluence. Then, the medium was replaced by DMEM/Nutrient Mixture F-12 supplemented with 1% FBS and antibiotics. At that moment, chondrocytes were pre-treated with 5 μM T0070907 and 1 μM SR141716 for 30 min, then with 5 μM Δ^9-THCA-A for 30 min more and, finally, with IL-1β (10 ng/mL) for 48 h. For gene expression, total RNA was extracted using the High Pure RNA Isolation kit (Roche Diagnostics). RNA integrity was checked on an agarose gel.

17.3. qPCR

Complementary DNA was synthesized using the the iScript™ cDNA Synthesis Kit (Bio-Rad). A CFX96 Real-Time PCR Detection System (Bio-Rad) was used for PCR amplification. All reactions were performed using the iQTM SYBR Green Supermix (Bio-Rad). Gene expression was standardized to HPRT-1 or GADPH mRNA levels in each sample

17.4. Primers used in this study

The primer sequences for the quantitative real-time PCR were:

Gene	Forward (5´ → 3´)	Reverse (5´ → 3´)
h-PPARγ2	GCGATTCCTTCACTGATACACTG	GAGTGGGAGTGGTCTTCCATTAC
h-LPL	GGCGCTACCTTGAGATAGAGTTCTG	TGTTTTCTACAGGGTGCTTTAGATGAC
h-aP2a	CCAGGAATTTGACGAAGT	TCTCTTTATGGTGGTTGATT
h-CEBPA	CCTTGTGCCTTGGAAATGCAAAC	CTGCTCCCCTCCTTCTCTCA
h-ADIPOQ	CATGACCAGGAAACCACGACTC	CCGATGTCTCCCTTAGGACCA
h-RUNX2	TGGTTAATCTCCGCAGGTCAC	ACTGTGCTGAAGAGGCTGTTG
h-ALP	CCAACGTGGCTAAGAATGTCATC	TGGGCATTGGTGTTGTACGTC
h-SP7	AGCCAGAAGCTGTGAAACCTC	AGCTGCAAGCTCTCCATAACC
h-IBSP	AGGGCAGTAGTGACTCATCCG	CGTCCTCTCCATAGCCCAGTGTTG
h-COX-2	CATTCTTTGCCCAGCACTTCAC	CGTGGTAAGAGGAACTTTCC
h-IL-6	GGTACATCCTCGACGGCATCT	GTGCCTCTTTGCTGCTTTCAC
h-iNOS	GTTCTCAAGGCACAGGTCTC	GCAGGTCACTTATGTCACTTATC
h-HPRT	ATGGGAGGCCATCACATTGT	ATGTAATCCAGCAGGTCAGCAA
m-TNFα	CTACTCCCAGGTTCTCTTCAA	GCAGAGAGGAGGTTGACTTTC
m-ICAM1	GTGGCGGGAAAGTTCCTG	CGTCTTGCAGGTCATCTTAGGAG
m-CD4	TCCTTCCCACTCAACTTTGC	AAGCGAGACCTGGGGTATCT

m-CXCL16	CGTTGTCCATTCTTTATCAGGTTCC	TTGCGCTCAAAGCAGTCCA
m-CCL22	AAGACAGTATCTGCTGCCAGG	GATCGGCACAGATATCTCGG
m-CXCR5	ACTCCTTACCACAGTGCACCTT	GGAAACGGGAGGTGAACCA
m-CXCR2	CACCGATGTCTACCTGCTGA	CACAGGGTTGAGCCAAAA
m-FGF21	TGTTTGACCGGATCTACACAC	CCCACAAGAGCACTCCAA
m-ADAMTS5	GGCATCATTCATGTGACACC	CGAGTACTCAGGCCCAAATG
m-IL-17	TTCATGTGGTGGTCCAGCTTTC	CCTCAGACTACCTCAACCGTTC
m-MMP-13	CTTGATGCCATTACCAGTC	GGTTGGGAAGTTCTGGCCA
m-iNOS	AACGGAGAACGTTGGATTTG	CAGCACAAGGGGTTTTCTTC
m-COX-2	TGAGCAACTATTCCAAACCAGC	GCACGTAGTCTTCGATCACTATC
m-RANKL	ATGATGGAAGGCTCATGGTTGG	CAGCATTGATGGTGAGGTGTG
m-IL-1β	CTCCACCTCAATGGACAGAA	GCCGTCTTTCATTACACAGG
m-IL-6	GTATGAACAACGATGATGCACTTG	ATGGTACTCCAGAAGACCAGAGGA
m-MCP-1	AAGTCCCTGTCATGCTTCTG	TCTGGACCCATTCCTTCTTG
m-GAPDH	TGGCAAAGTGGAGATTGTTGCC	AAGATGGTGATGGGCTTCCCG

18. RNA-Seq analysis

For each group, total RNA was extracted from iWAT, prepared, pooled, and run on an Agilent Bioanalyzer system to confirm quality (RNA integrity number >8). Transcriptome libraries were then constructed using poly-A selection with the TruSeq Stranded mRNA Library Prep Kit (Cat. No. RS-122-2101, Illumina, San Diego, CA, USA). In brief, 300 ng of total RNA from each sample was used to construct a cDNA library, followed by sequencing on the Illumina HiSeq 2500 with single end 50 bp reads and ~30 millions of reads per sample. The FASTQ files were pre-processed with Trimmomatic (v0.36) to remove adapter sequences and aligned to the mm10 assembly of the mouse genome using HISAT2 (v2.1.0). The counts per gene matrix were obtained from the alignments with featureCounts (v1.6.1) using the in-built RefSeq annotation for the mm10 genome assembly. After filtering genes with less than 15 reads across samples, the raw counts were analyzed with DESeq2 (v1.20.0) to obtain the regularized log transformed expression matrix and the differential expression analysis results. We used a threshold of an absolute fold change ≥ 2 and an adjusted P value ≤ 0.01 to consider a gene as differentially expressed in any comparison. Heatmaps were generated using the scaled mean of the regularized log expression for each group with the R package ComplexHeatmap (v1.20.0). The gene set enrichment analysis (GSEA) [171] and the over-representation analysis were performed using the R package ClusterProfiler (v3.10.1) [172]. For GSEA, genes were pre-ranked using the log2 transformed fold

change. The KEGG pathway database and Gene Ontology (Biological Process) annotation were used to group genes by biological function. All the P values were adjusted using the Benjamini and Hochberg correction to control the false discovery rate (FDR). RNA-seq data have been deposited in the Gene Expression Omnibus databank (accession no. GSE129573).

19. Proteomic analysis

The depletion of the three most abundant protein in the plasma was performed using the Hu-7 Multiple Affinity Removal System kit (Agilent Technologies, Wilmington, DE, USA) following the manufacturer's instructions. The remaining proteins were concentrated using 5000 molecular weight cut-off (MWCO) spin concentrators (Agilent Technologies); then the cells were lysed and cleaned to remove any contaminants by protein precipitation with TCA/acetone and solubilised in 50 μL of 0.2% RapiGest SF (Waters, Milford, MA, USA) in 50 mM $(NH_4)HCO_3$. The total protein was measured using the Qubit Protein Assay Kit (Thermo Fisher Scientific, Waltham, MA, USA) and 50 μg of protein from each sample was subjected to trypsin digestion. In order to build the spectral library and quantified the samples by SWATH acquisition, the solution of peptides was analysed by a shotgun data-dependent acquisition (DDA) approach using nanoLC-MS/MS. Then, the samples were pooled in five group of 6 samples each and 1 μg was separated into a nano-LC system Ekspert nLC400 (Eksigent, Dublin, CA, USA). Peptide and protein identifications were performed using Protein Pilot software v5.0 (Sciex) with a human UniProtKB concatenated target-reverse decoy database, specifying iodoacetamide as alkylation. The false discovery rate (FDR) was set to 0.01 for both peptides and proteins. The MS/MS spectra of the identified peptides were used to generate the spectral library for SWATH peak extraction using the add-in for PeakView Software v2.1 (Sciex) MS/MS^{ALL} with SWATH Acquisition MicroApp v2.0 (Sciex). The normalized SWATH areas matrix was then imported into the R statistical programming environment for further analyses and visualization. Pairwise data comparisons were performed for every condition against the control by applying a Welch Two Sample T-Test, and resultant p values were adjusted to control the False Discovery Rate (FDR) using the Benjamini and Hochberg approach. The MS proteomic data have been deposited in the ProteomeXchange Consortium via the PRIDE partner repository (accession no. PXD015274).

20. Statistical analysis

In vitro data are expressed as mean ± S.D. and, *in vivo* and binding assays results are represented as mean ± SEM. Data that showed a normal distribution from two groups were tested using a Students T-test. The significance between three or more independent groups was analyzed using one-way ANOVA followed by Tukey's post hoc test. The data that involved two independent variables were tested using a two-way ANOVA followed a Bonferroni multiple comparison test. Data not normally distributed were analyzed by the Kruskall–Wallis followed by Dunn's post hoc test. Post hoc analysis in ANOVA tests were carried out when F achieved was $P < 0.05$, and there was no significant variance in homogeneity. The value of $P < 0.05$ was considered significant. N values were derived from independent animals or experiments, not replicates. Some results were normalized to minimize variations between independent experiments. Statistical analysis was performed using GraphPad Prism® version 6.01-7.

Results

1. VCE-004.8, A Multitarget Cannabinoquinone, Attenuates Adipogenesis and Prevents Diet-Induced Obesity

VCE-004.8, A Multitarget Cannabinoquinone, Attenuates Adipogenesis and Prevents Diet-Induced Obesity

Belen Palomares[1,2,3], Francisco Ruiz-Pino[1,2,3], Carmen Navarrete[4], Inmaculada Velasco[1,2,3], Miguel A. Sánchez-Garrido[1,2,3], Carla Jimenez-Jimenez[1,2,3], Carolina Pavicic[5], Maria J. Vazquez[1,2,3], Giovanni Appendino[6], M. Luz Bellido[4,7], Marco A. Calzado[1,2,3], Manuel Tena-Sempere[1,2,3] & Eduardo Muñoz[1,2,3]

1.1. VCE-004.8 is a selective PPARγ modulator

We have previously found that VCE-004.8 binds and activates PPARγ [60], and were interested to analyse whether or not this compound was able to activate other PPAR family members. We found that VCE-004.8, at non-toxic concentrations, selectively induced PPARγ-dependent transcriptional activity, although with lower potency than RGZ ((PPARγ: $p < 0.001$ RGZ vs untreated; $p = 0.0407$ VCE-004.8 vs untreated; Fig. 1a-b), suggesting that VCE-004.8 is a selective agonist of the PPARγ isoform.
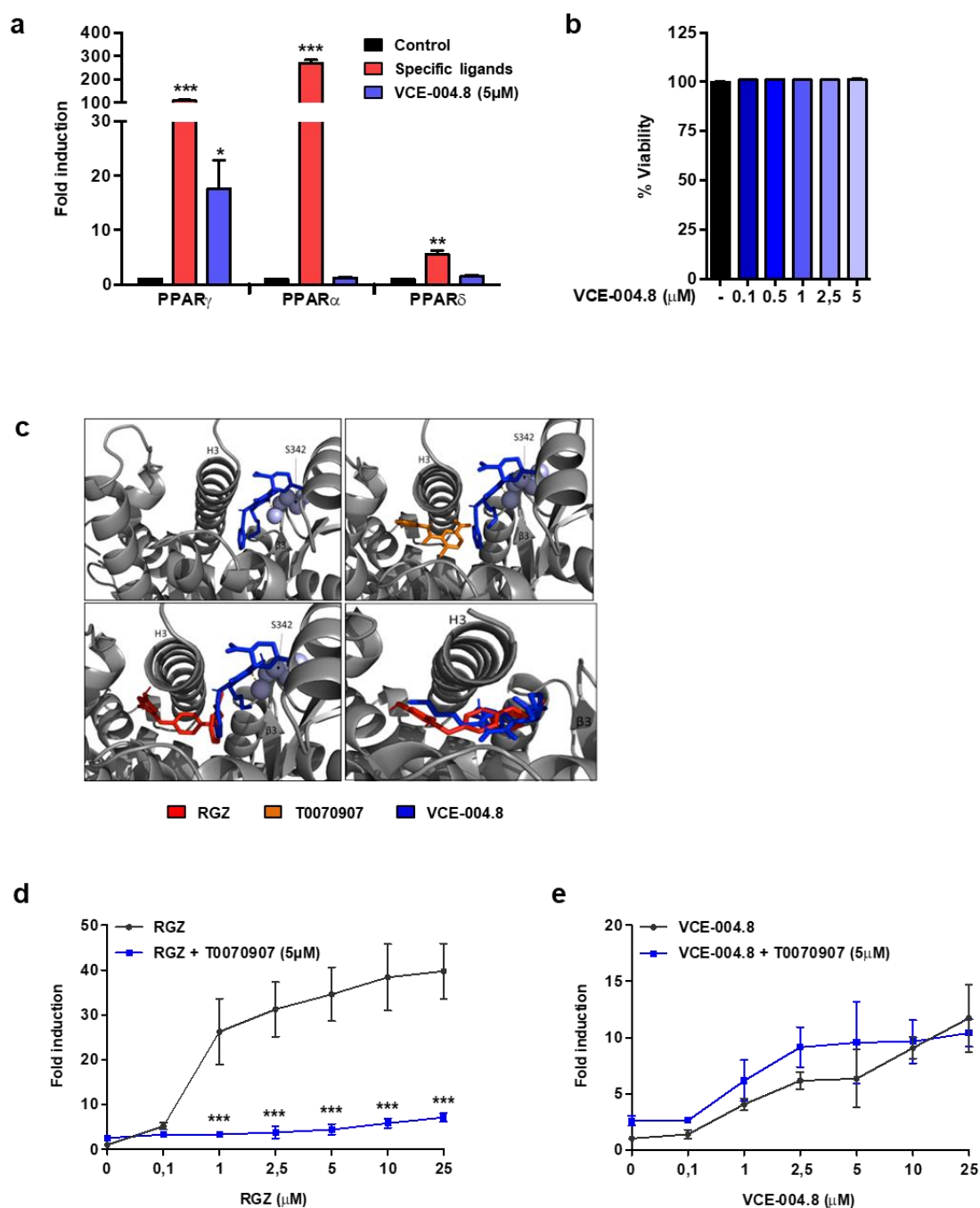
Results

Figure 1. Characterization of VCE-004.8 as a selective PPARγ agonist. (a) Receptor-specific transactivation by VCE-004.8. HEK-293T cells were co-transfected with a GAL4-luc reporter and GAL4-PPARγ, GAL4-PPARα and GAL4-PPARδ and treated with VCE-004.8 (5 μM) for 6 hours and luciferase activity measured in the cell lysates. Results are expressed as the fold induction ± SD (n=3) relative to untreated control. Control (black bars), VCE-004.8 (blue bars) and specific ligands for each receptor (red bars): RGZ (5 μM) for PPARγ, WY14643 (5 μM) for PPARα, and GW0742 (5 μM) for PPARδ. Results are shown as mean ± S.D. **(b)** Cytotoxic activity of VCE-004.8. HEK-293T cells were treated with the compounds at the indicated concentrations for 6 hours and cell viability was analyzed by the YOYO-1 method. Results are shown as mean ± SD and expressed as percentage of cell viability (n=3). **(c)** PPARγ LBD structure 3B0R bound to VCE-004.8 (blue) with and without of T0070907 (orange) or RGZ (red). PPARγ LBD structure 4EMA bound to VCE-004.8 and RGZ (lower right panel). **(d, e)** PPARγ transcriptional activity of VCE-004.8 and RGZ in the presence and the absence of T0070907 is shown. HEK-293T cells were co-transfected with GAL4-PPARγ and GAL4-luc, pre-treated with T0070907 for 15 min and then stimulated with increasing concentrations of either RGZ or VCE-004.8 for 6 hours and luciferase activity measured. Results are expressed as the fold induction ± SD relative to RGZ (d) or VCE-004.8 (e) (n=4). *P<0.05, **P<0.01 and ***P<0.001 agonist ligands or VCE-004.8 treatment vs. control or RGZ+T0090709 vs. RGZ. (ANOVA followed by Tukey's test or unpaired two-tailed Student's t-test).

PPARγ has a large ligand-binding pocket (LBP), and the diversity of modes in which ligands can be accommodated is associated to distinct biological profiles. The LBP extends from the C-terminal helix H12 to the β-sheet S1/S2 and is divided into AF-2 and β-sheet sub-pockets[173]. Based on different PPARγ complex structures, it has been proposed that full agonists, such as RGZ, bind to both sub-pockets, establishing hydrogen bonds with residues Tyr473 (H12) on AF-2 (also called canonical binding site) and Ser342 (S1/S2) on β-sheet sub-pocket (also called alternative binding site), whereas partial agonists only significantly bind to the alternate site [157, 158]. Docking experiments based on the crystal structures 3B0R, 4EMA, 5Y20 and 5LGS deposited in the Protein Data Bank (PDB) were carried out on VCE-004.8. As depicted in Fig. 1c, molecular docking with 3B0R indicated that in the absence of T0070907, an irreversible PPARγ antagonist covalently binding to Cys285 into the PPARγ LBP canonical binding site, VCE-004.8 binds to Ser342 in Ω-loop β3 (alternative site) with a predicted *Ki* of 448.03 nM. Docking analysis using 4EMA and 5Y20 predicts a similar binding pattern, with calculated *Ki* of 95.59 nM and 67.68 nM, respectively. In addition, VCE-004.8 also showed a predicted binding to I218 in Helix 3, rationalizing its higher affinity to crystal 5Y20. Docking analysis (3B0R) in the presence of T0070907 and RGZ, which bind to the canonical site, did not displace the hydrogen bonding interaction of VCE-004.8 with Ser342 (Fig. 1c), rather enhancing the binding its affinity to the alternative site (*Ki* 236.22 nM in the presence of T0070907 and *Ki* 121.55 nM in the presence of RGZ). Interestingly, in the presence of RGZ, VCE-004.8 could also interact with the canonical binding site, suggesting that VCE-004.8 could, in principle, mediate biological activities through both the canonical and the alternative LBP PPARγ sites. To assess this, the potential

functionality of the canonical and alternative PPARγ sites involved in the response to VCE-004.8 were investigated. Luciferase reporter assays were used to study the participation of the canonical and alternative binding sites in the response to VCE-004.8 in comparison with RGZ. As expected, pre-incubation with the selective inhibitor of the canonical PPARγ site, T0070907, effectively blocked RGZ-induced PPARγ transactivation ($p < 0.001$ RGZ+T0070907 vs RGZ; Fig. 1d). Conversely, T0070907 did not block VCE-004.8-induced PPARγ transcriptional activity (Fig. 1e). These findings are consistent with the fact that RGZ activates PPARγ by acting mainly, but not exclusively, through the canonical binding site [158].

1.2. Effect of VCE-004.8 on adipogenic and osteoblastogenic differentiation

Our initial results strongly suggested that, in contrast to RGZ, VCE-004.8 is a PPARγ partial ligand agonist. Since PPARγ is a master regulator of adipogenesis[174], we studied the ability of VCE-004.8 to influence MSCs differentiation into adipocytes. To this purpose, MSCs were cultured in adipogenic medium (AM) for either 7 days or 21 days to study, respectively, the mRNA expression of adipogenic markers or detect lipid droplets. In the event, hMSC treated with VCE-004.8 showed fewer and smaller lipid droplets (Fig. 2a and 2b). In addition, VCE-004.8 prevented mitotic expansion of hMSCs (Fig. 2c) and the reduction in the number of cells was not caused by cytotoxicity (Fig. 2d). VCE-004.8 induced lower expression of the adipogenic differentiation markers PPARγ, aP2a, ADIPOQ, LPL and CEBPA (PPARγ2: $p = 0.0415$; aP2a: $p < 0.0001$; Fig.2e) as compared to cells treated with the PPARγ-fa, RGZ (PPARγ2: $p < 0.0001$; aP2a: $p < 0.0001$; ADIPOQ: $p < 0.0001$; LPL: $p < 0.0001$; CEBPA: $p < 0.0001$; Fig.2e). Interestingly, the effect of VCE-004.8 on adipocyte differentiation was prevented by T0070907 (PPARγ2: $p = 0.0012$; aP2a: $p < 0.0001$; ADIPOQ: $p < 0.0003$; Fig.2e), suggesting that this PPARγ ligand can signal through both the canonical and alternative LBP binding site (Fig. 2e compared to Fig. 1e).
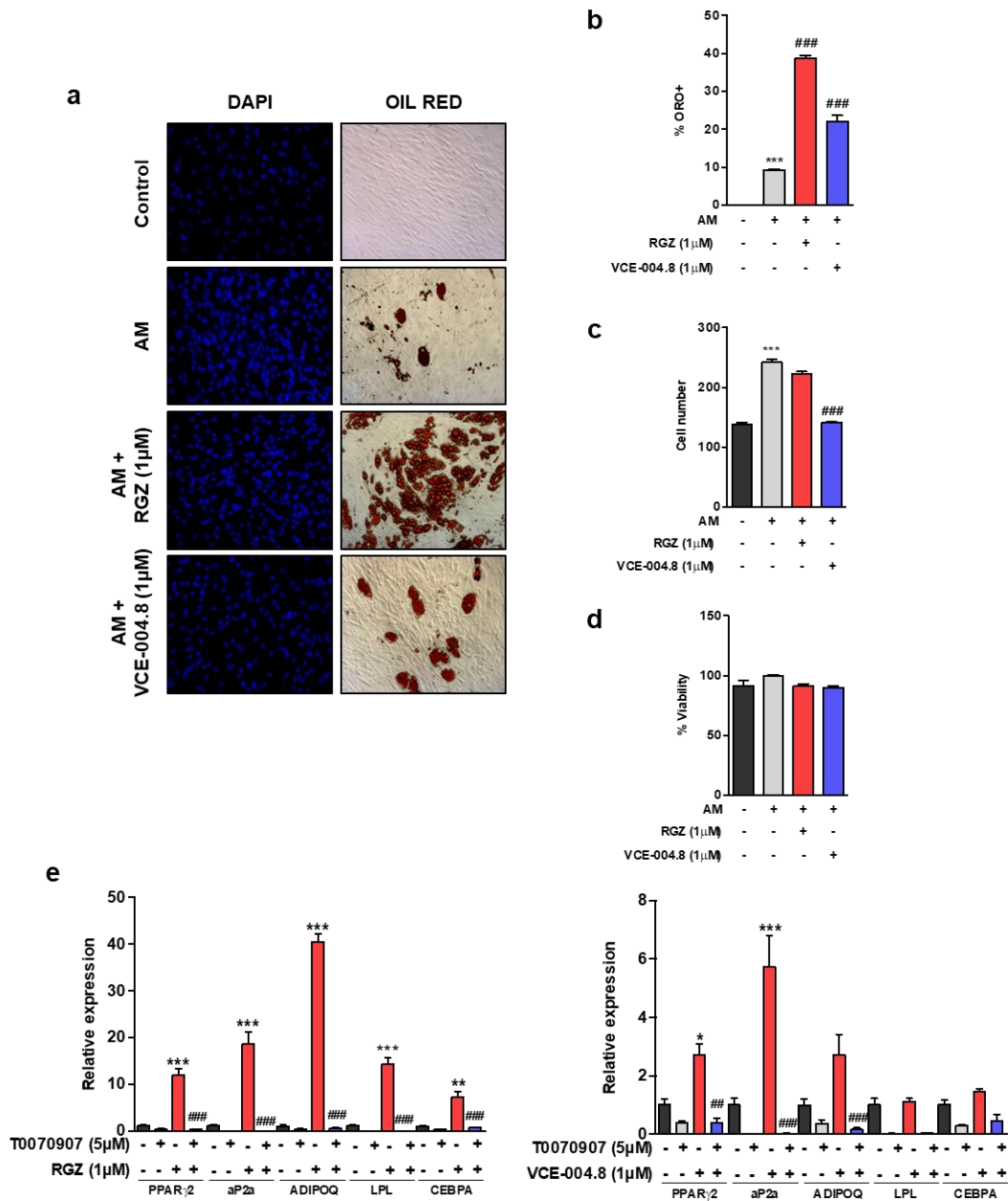
Figure 2. Effect of VCE-004.8 on MSCs differentiation. MSCs were differentiated in adipogenic medium (AM) in the presence of RGZ or VCE-004.8. **(a)** Representative images of Oil Red O (ORO) staining and DAPI nuclear counterstain of MSCs undergoing adipogenic differentiation. Quantification of Oil Red O positive cells **(b)** and DAPI nuclear cells **(c)** after 21 days of differentiation is presented. **(d)** Cytotoxicity of RGZ and VCE-004.8 was evaluated by the MTT method. **(e)** MSCs were differentiated in AM with RGZ or VCE-004.8 in the presence and the absence of T0070907 for 7 days and gene expression of adipogenic markers measured by qPCR. Results represent the mean $\pm$ S.D (n=3). For (B, C) ***$P<0.001$ AM vs. control; ### $P<0.001$ RGZ or VCE-004.8 + AM vs. AM; for (E) *$P<0.05$, **$p<0.01$ and ***$P<0.001$ RGZ or VCE-004.8 vs. the control cells; #$P<0.05$, ##$P<0.01$ and ###$P<0.001$ RGZ or VCE-004.8 + T0070907 vs. RGZ or VCE-004.8. (ANOVA followed by Tukey's test).

There is evidence that glitazones, like RGZ, suppress MSC osteoblast development through the PPARγ pathway, mechanistically rationalizing the observation of bone loss after prolonged use of this class of drugs [175]. However, other authors have shown that

72

RGZ does not interfere directly with osteoblastogenesis in hMSCs [116]. Nevertheless, we found that VCE-004.8 neither inhibited osteoblast mineralization, nor suppressed the expression of osteogenic differentiation markers, such as Runx2 and ALP, in hMSC differentiated in an osteoblastogenic medium (OM) for 21 days (Supplementary Fig. 1). Altogether, these data indicate that VCE-004.8 qualifies as a partial PPARγ ligand, being significantly less adipogenic than RZG and not interfering with osteoblasts differentiation.

1.3. VCE-004.8 treatment ameliorates HFD-induced metabolic perturbations

To evaluate the potential beneficial effects of VCE-004.8 on metabolic disease, we studied the impact of chronic administration of this compound in a mouse model of HFD-induced obesity, which displays features of MetS. HFD exposure for up to 15 weeks caused a significant increase in body weight ($p = 0.015$ in 2nd wk; $p = 0.0015$ in 3rd wk and $p < 0.0001$ during the rest of diet exposure), caloric intake ($p = 0.0013$), fat mass ($p < 0.0001$) and adiposity index (calculated as fat / fat + lean mass) ($p < 0.0001$), with a decrease in % lean mass ($p < 0.0001$) (Fig. 3a-f). Treatment with VCE-004.8 significantly reduced BW gain ($p = 0.0005$ in 1st wk of treatment; $p = 0.0011$ in the 2nd wk; $p = 0.0088$ in the 3rd wk; $p = 0.0068$ in the 4th wk and $p = 0.031$ in the last wk of treatment), fat mass ($p = 0.029$) and adiposity ($p = 0.042$), while it increased % lean mass ($p = 0.046$), without affecting total calorie intake. Modest albeit significant effects of VCE-004.8 on BW gain ($p = 0.048$), % fat ($p = 0.0056$) and lean mass ($p = 0.031$), and adiposity index were detected also in CD mice ($p = 0.032$) (Fig. 3).

Macrophage infiltration of white adipose tissue is implicated in the metabolic complications of obesity. A notable feature of adipose tissue in obese mice is the presence of unique clusters of macrophages that surround dead adipocytes, called crown-like structures (CLS). Therefore, to determine the effect of VCE-004.8 on adipose tissue morphology and inflammation, we analyzed adipocyte size by H&E staining and measured the number of CLS by staining iWAT sections with the macrophage marker F4/80. We observed a significant increase in adipocyte volume that paralleled a reduction in the number of adipocytes per field in HFD animals compared to the CD group. VCE-004.8 treatment prevented HFD-induced adipocyte hypertrophy, normalized adipocyte number and caused a reduction in the presence of CLS (Adipocyte area: $p < 0.0001$ HFD

vs CD; p < 0.0001 HFD+VCE-004.8 vs HFD; Adipocyte number: p = 0.0034 HFD vs CD; p = 0.0498 HFD+VCE-004.8 vs HFD; Fig. 4a-c).
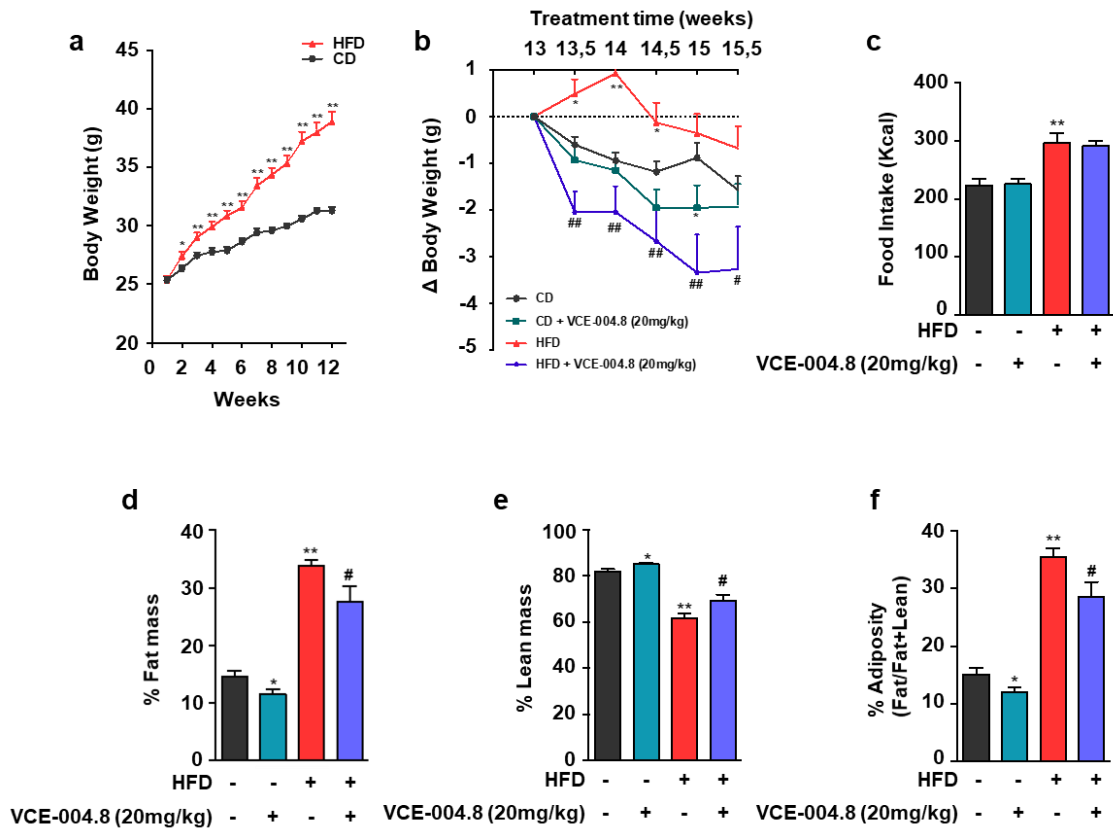

Figure 3. Effect of VCE-004.8 on body weight gain, food intake and body composition. (**a**) Body weight (BW) curves of adult male mice fed for 15-weeks with high fat diet (HFD) or the corresponding control diet (CD). (**b**) BW gain (g) in HFD and CD mice treated for the last three weeks with VCE-004.8 or vehicle; values are referenced to BW at the beginning of treatment (taken as 0). (**c**) Total calorie intake (Kcal) during the treatment period in HFD and CD mice injected with VCE-004.8 or vehicle. In addition, the percentage fat and lean mass, as well as percentage of adiposity, at the end of treatments are presented in (**d-f**) for the four experimental groups. Values correspond to means ± SEM of at least 8 mice per group. **P<0.01 and ***P<0.001 VCE-004.8-treated mice or HFD mice vs. control (CD) mice; #P<0.05 and ##P<0.01 VCE-004.8-treated HFD mice vs. HFD mice treated with vehicle (ANOVA followed by Tukey's test or unpaired two-tailed Student's t-test).
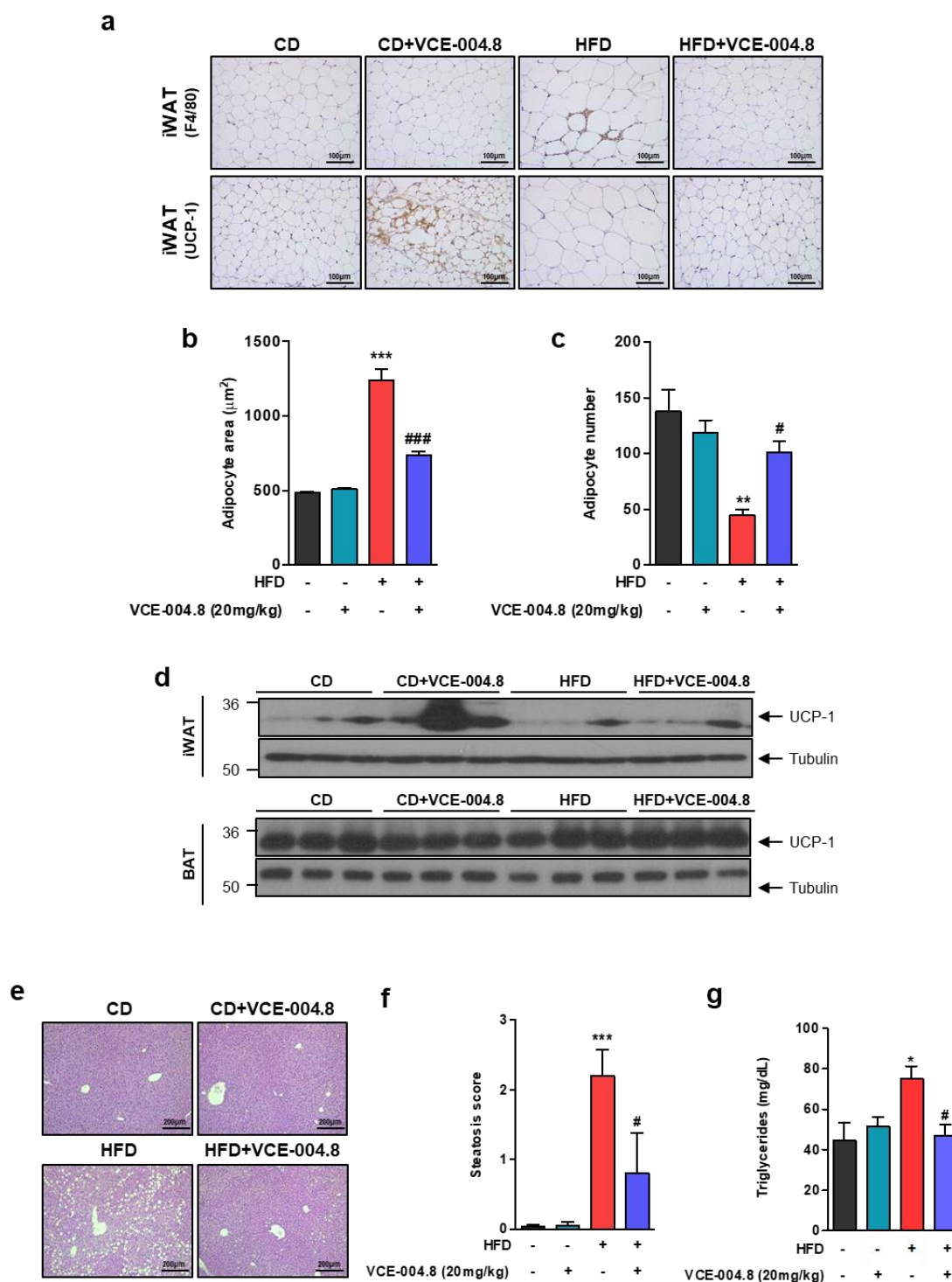
Figure 4. Effect of VCE-004.8 on adiposity and liver steatosis in HFD animal. (**a**) Crown Like Structures (CLS) and browning in iWAT. Representative immuno-histochemistry with anti-F4/80 and anti-UCP-1 antibodies (original magnification ×20, scale bar: 100 μm), (**b**) Adipocyte area (n = 6 animals per group), (**c**) Adipocyte number (n = 6 animals per group). (**d**) Representative Western blot images of UCP-1 protein expression in iWAT and BAT tissues (n=3). (**e**) H&E-stained liver sections (original magnification ×10, scale bar: 200 μm). (**f**) Steatosis scores (n = 6 animals per group). (**g**) Triglycerides plasma levels (Values correspond to means ± SEM; n = 6 animals per group). *P<0.05, **P<0.01 and ***P<0.001 HFD mice vs. control (CD) mice; #P<0.05 and ###P<0.001 VCE-004.8-treated HFD mice vs. HFD mice (ANOVA followed by Tukey's test).

Next, to investigate the potential effect of VCE-004.8 on the thermogenic pathway we investigated the adipose expression of UCP-1 by immunochemistry and Western blot. Interestingly, VCE-004.8 induced a clear iWAT browning in control mice, but responses were less clear in HFD mice. Moreover, the expression of UCP-1 in the BAT was not modified after VCE-004.8 treatment, in either control or HFD animals (Fig. 4d).

To assess the effect of VCE-004-8 on lipid metabolism, we next analyzed the degree of fat infiltration in the liver and the circulating levels of triglycerides. As expected, liver histochemistry demonstrated the presence of hepatic steatosis in mice fed HFD ($p = 0.0006$ HFD vs CD; Fig. 4e-f), which displayed also a significant increase in serum triglyceride levels ($p = 0.030$ in HFD vs CD) (Fig. 4g). Treatment with VCE-004.8, did not affect the architecture of the hepatic parenchyma nor altered triglyceride concentrations in CD mice, but significantly reduced hepatic steatosis, and fully normalized circulating triglyceride levels in HFD mice (Hepatic steatosis: $p = 0.0343$ HFD+VCE-004.8 vs HFD; triglyceride levels: $p = 0.022$ HFD+VCE-004.8 vs HFD Fig. 4e-g).

Continuous exposure of male mice to HFD caused also perturbations in glycemic homeostasis, characteristic of MetS, which were documented by a significant worsening of glucose tolerance, as revealed by GTT ($p = 0.026$) (Fig. 5a-b), and a (moderate) decrease in insulin sensitivity in ITT (Fig. 5c), compared to CD mice. In addition, HFD mice displayed elevated basal glucose (200.74 ± 8.9 mg/dl vs. 153.3 ± 4.73, N=20/group – measured before initiation of the pharmacological intervention; $p = 0.012$) and insulin levels ($p = 0.028$; Fig. 5d), as evidence for a state of insulin resistance. Treatment of HFD mice with VCE-004.8 significantly improved glucose tolerance, as demonstrated by individual time-course profiles ($p = 0.0063$ in HFD+VCE-004.8 vs HFD at 60 minutes) (Fig. 5a) and integral area-under-the-curve (AUC) responses ($p = 0.012$) (Fig. 5b), and enhanced insulin sensitivity, as documented by ITT profiles and the normalization of basal insulin levels ($p = 0.028$) (Fig. 5c-d). Notably, VCE-004.8 administration to CD mice also tended to improve also glucose tolerance ($p = 0.0008$ at 60 minutes) and insulin sensitivity ($p = 0.042$ at 60 minutes) and significantly increased basal insulin levels in lean animals ($p = 0.021$).
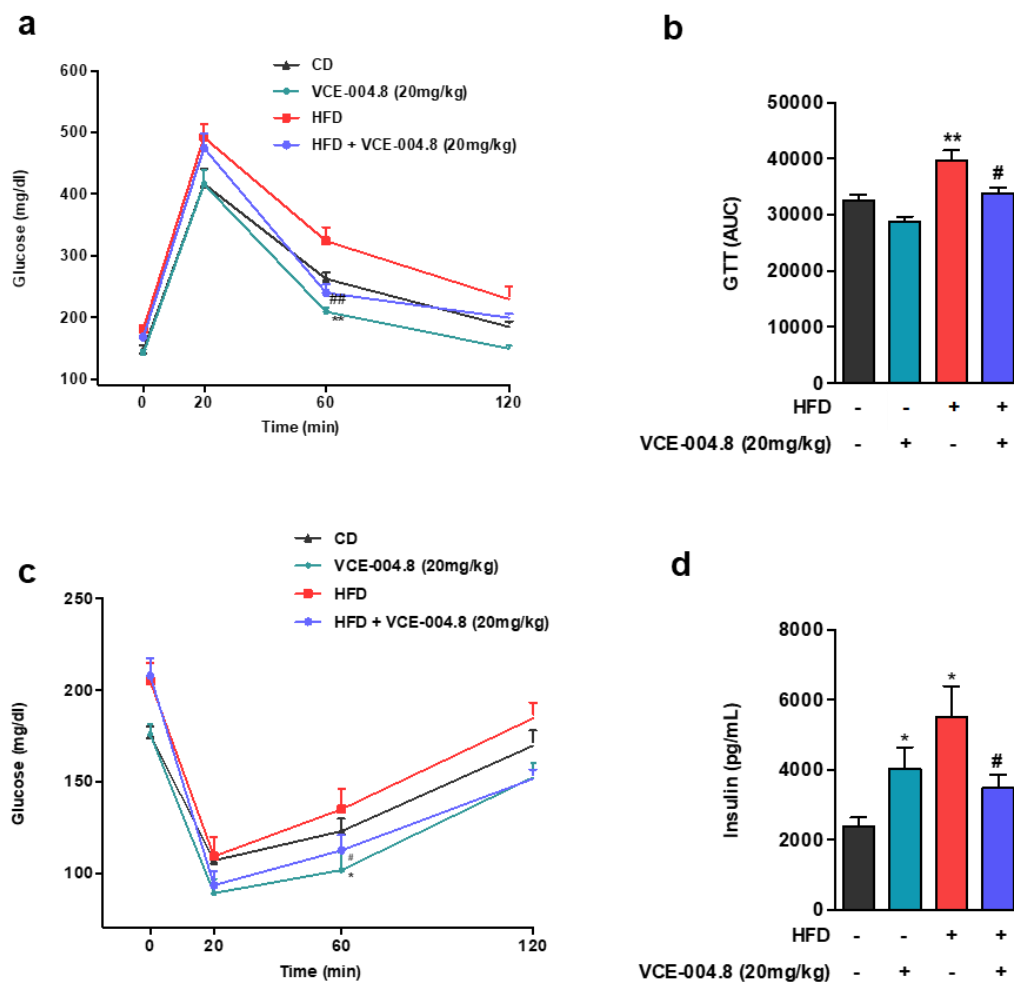
76

Figure 5. Effect of VCE-004.8 on glucose tolerance and insulin sensitivity. (**a**) Glucose tolerance tests in control (CD) and HFD mice treated with VCE-004.8 or vehicle for three weeks. In addition to time-course profiles, integral glucose responses in GTT are presented in (**b**), calculated as area-under-the-curve (AUC). (**c**) Insulin tolerance tests in CD and HFD treated with VCE-004.8 or vehicle for three weeks. In addition, in (**d**) basal insulin levels at the end of the three-week treatment period are shown for the four experimental groups. Values correspond to means ± SEM of at least 8 mice per group. $*P<0.05$ and $**P<0.01$ VCE-004.8-treated mice or HFD mice vs. control (CD) mice; $\#P<0.05$ and $\#\#P<0.01$ VCE-004.8-treated HFD mice vs. HFD mice treated with vehicle (ANOVA followed by Tukey's test).

1.4. Effect of VCE-004.8 on metabolic and hormonal markers

To gain deeper insight into the effects of VCE-004.8 in the context of metabolic disease, a panel of hormonal markers, with pivotal roles in energy and metabolic homeostasis, was assayed in our HFD model. Chronic exposure to HFD resulted in dramatically increased leptin levels ($p < 0.0001$) (Fig. 6b), together with significant reductions in adiponectin ($p = 0.0058$) (Fig. 6c), ghrelin ($p = 0.0478$) (Fig. 6a) and glucagon levels ($p = 0.035$) (Fig. 6d); changes that altogether might contribute to deterioration of the metabolic profile of HFD animals. In addition, HFD mice showed

elevated PAI-1 levels (p = 0.027) (Fig. 6f), and unaltered concentrations of resistin, GIP and GLP-1 (Fig. 6e, g-h). Treatment with VCE-004.8 partially normalized leptin concentrations (p = 0.016), in keeping with the associated reduction of adiposity, and lowered resistin levels (p = 0.037), while it increased adiponectin (p = 0.028); these joint changes might partially explain the improved metabolic profile of VCE-004.8 treated obese animals. In contrast, no effect on ghrelin or glucagon levels was found after VCE-004.8 treatment in HFD mice. Notably, administration of VCE-004.8 to lean CD animals significantly increased GIP (p = 0.027) and GLP-1 levels (p = 0.0029), as well as PAI-1 concentrations (p < 0.0001). Yet, in HFD mice, the stimulatory effect for incretins (GIP, GLP-1) disappeared, while it persisted for PAI-1 (p = 0.0003).

Several lines of evidence indicate that the metabolic hormone, FGF21, plays a key role in obesity-associated metabolic syndrome [176]. Indeed, increased plasmatic levels of FGF21 have been found in HFD mice [177] and metabolically unhealthy obese patients [176]. Since FGF21 can be induced in BAT by PPARγ agonists [178], we were interested to explore whether or not VCE-004.8 had some role on FGF21 in different tissues and cell types. Our results showed that in control mice, VCE-004.8 enhanced the expression of FGF21 in BAT and iWAT (BAT: p = 0.0295 VCE-004.8 vs CD; iWAT: p = 0.0301 Fig. 7a), which may reflect the activation of PPARγ by VCE-004.8 in these tissues. Accordingly, VCE-004.8, as well as RGZ, also induced the expression of FGF21 mRNA in the pBAT cell line, although to different extent, which confirms that VCE-004.8 is a PPARγ partial agonist. Interestingly, T0070907 greatly inhibited RGZ-induced FGF21 expression but did not show a significant effect on the expression of this gene mediated by VCE-004.8, highlighting the importance of the alternative binding in the PPARγ LBP for the biological activity of VCE-004.8 (p < 0.0001 RGZ vs untreated; p = 0.0040 VCE-004.8 vs untreated; p < 0.0001 RGZ+T0070907 vs RGZ; Fig. 7b). HFD mice showed an enhanced expression of FGF21 mRNA in liver, eWAT and iWAT tissues that was reduced by VCE-004.8, especially in iWAT. In addition, the circulating levels of FGF21 were significantly increased in HFD, while treatment with VCE-004.8 normalized them (p = 0.0095 HFD vs CD; p = 0.0382 HFD+VCE-004.8 vs HFD; Fig. 7c).
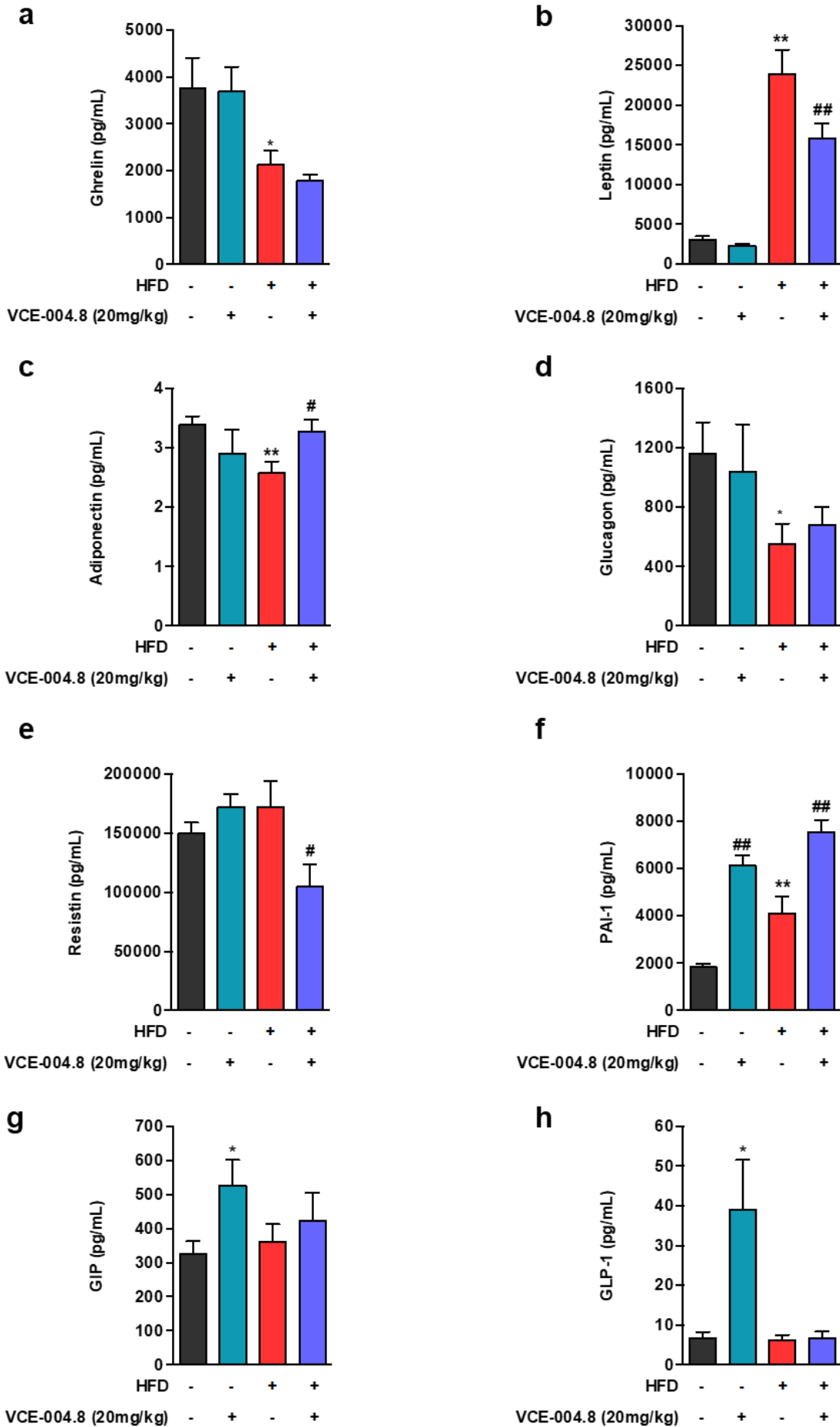
Figure 6. Effect of VCE-004.8 on different metabolic hormones. A panel of hormones and circulating factors, with key roles in metabolic homeostasis, were assayed in control (CD) and HFD male mice, at the end of the three-week period of treatment with VCE-004.8 or vehicle. The factors assayed were: (**a**) ghrelin; (**b**) leptin; (**c**) adiponectin; (**d**) glucagon; (**e**) resistin; (**f**) PAI-1; (**g**) GIP; and (**h**) GLP-1. Values correspond to means ± SEM of at least 8 mice per group. *P<0.05 and **P<0.01 VCE-004.8-treated mice or HFD mice vs. control (CD) mice; #p<0.05 and ##p<0.01 VCE-004.8-treated HFD mice vs. HFD mice treated with vehicle (ANOVA followed by Tukey's test).
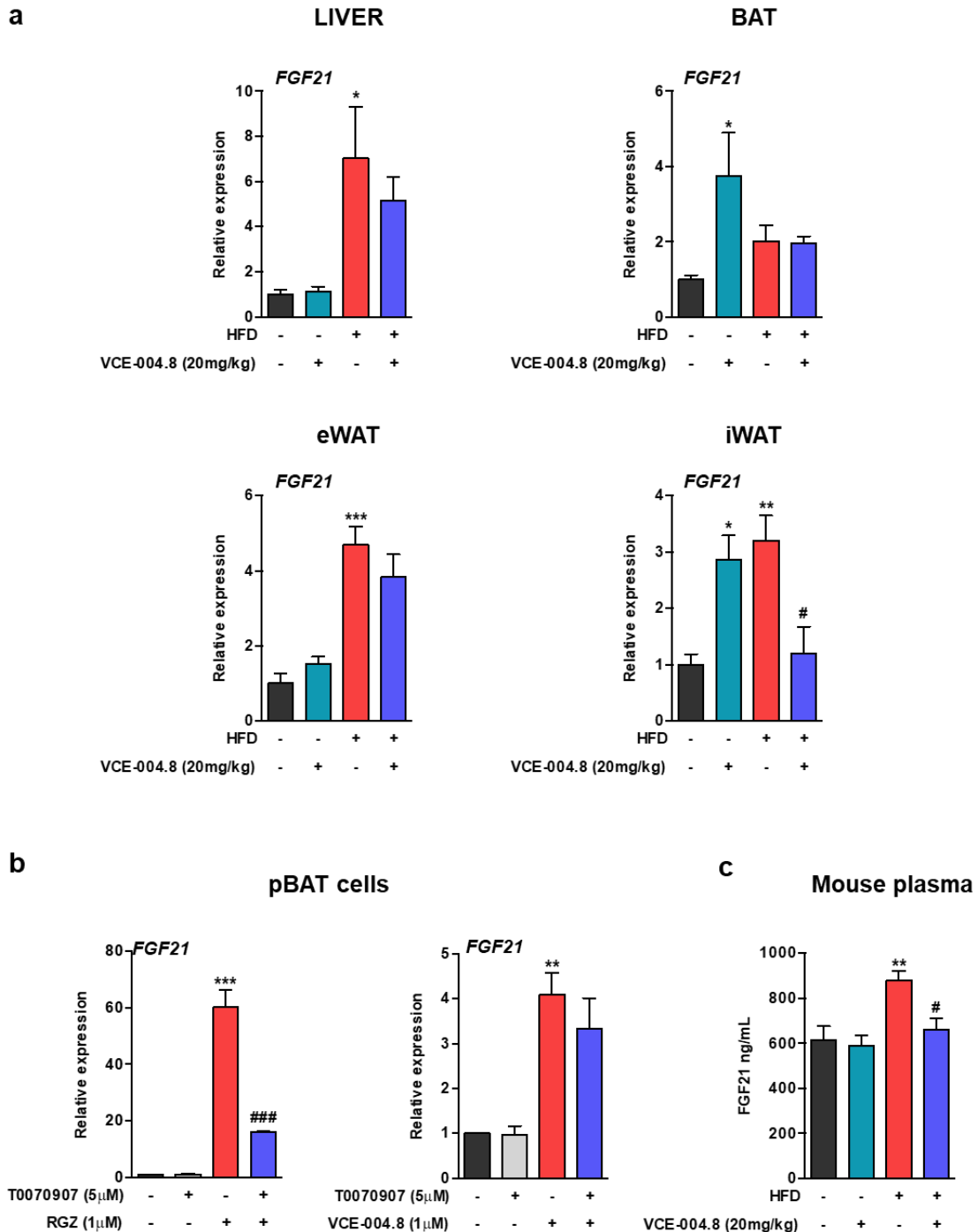
Figure 7. VCE-004.8 modulates the expression of FGF21. (**a**) FGF21 mRNA levels in the liver, BAT, eWAT and iWAT extracted from control and HFD mice treated or untreated with VCE-004.8. Values correspond to means ± SEM of 5–8 mice per group. (**b**) FGF21 gene expression in RGZ- or VCE-004.8-treated pBAT cells in the presence and the absence of T0070907. Results represent the mean ± SD (n=3). (**c**) FGF21 plasmatic levels were examined using the Mouse FGF21 Quantikine ELISA Kit. Values

correspond to means ± SEM of 5–8 mice per group. For (a, c) *P<0.05, **P<0.01 and ***P<0.001 VCE-004.8-treated mice or HFD mice compared to the control mice; #p<0.05 VCE-004.8-treated HFD mice compared to HFD mice; for (b) **P<0.01 and ***P<0.001 RGZ or VCE-004.8 vs. control; ##P<0.01 RGZ + T0070907 vs. RGZ. Data were assessed by ANOVA followed by Tukey's test.

1.5. Supplementary information

ALIZARIN RED STAINING
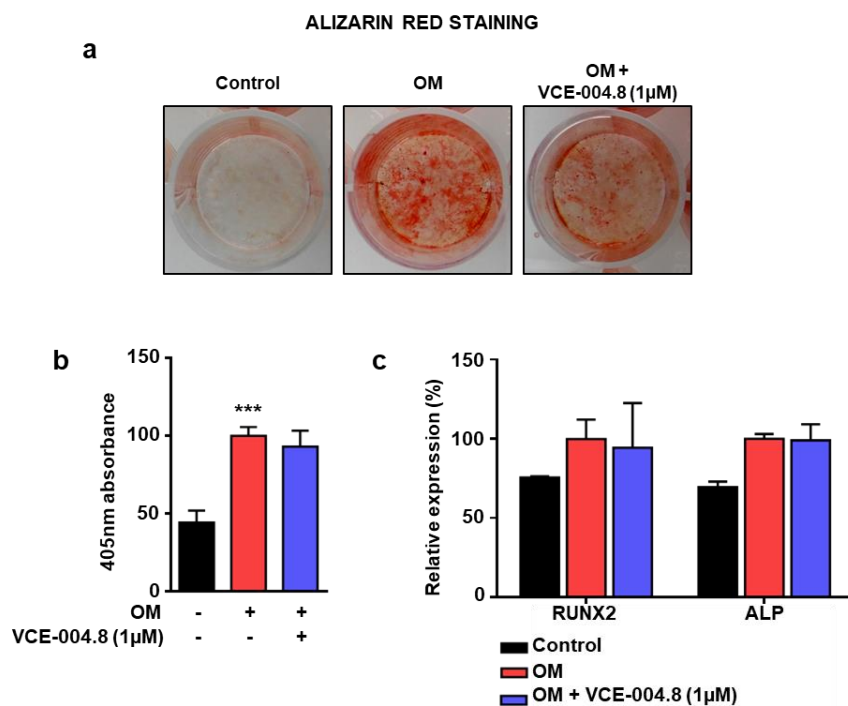
Figure S1. VCE-004.8 does not affect osteoblastogenic differentiation in MSCs. (a) Alizarin red staining after 21 days of subculture. **(b)** Quantification of calcium mineral deposits by absorbance at 405 nm. **(c)** Gene expression of RUNX2 and ALP in MSCs differentiated for 14 days. Data represent the percentage of increase over OM considered as the 100% of osteoblastogenic induction. Results represent the mean ± S.D (n=3). *P<0.05 OM vs. control. (ANOVA followed by Tukey's test).

BEFORE DIET INTERVENTION (WEEK-0)

AFTER DIET INTERVENTION (WEEK-12)

■ CD + Veh   ■ CD + VCE-004.8   ■ HFD + Veh   ■ HFD + VCE-004.8

Figure S2. Body composition analysis of experimental animals before initiation of the pharmacological intervention wit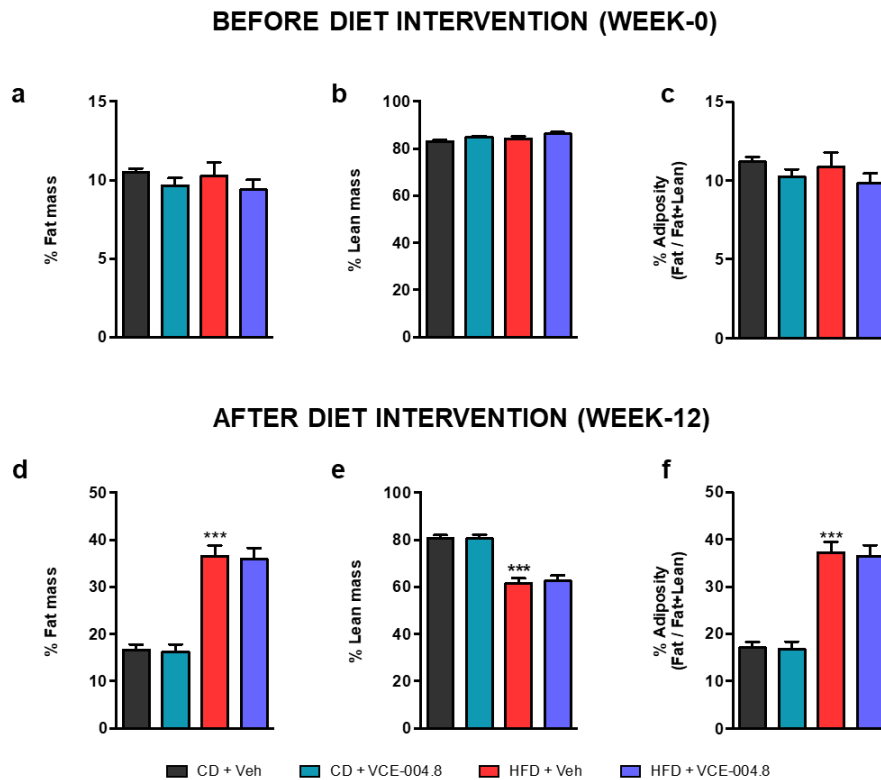h VCE-004.8. In the *upper panels*, body composition indices are shown from the different experimental groups before initiation of the diet intervention (week-0): % of body fat (**a**), % of lean mass (**b**), and % of percentage of adiposity (calculated as Fat/Fat + Lean mass) are shown. In the *lower panels* (**d-f**), similar indices were recorded after 12 weeks of nutritional intervention with either control diet (CD) or High Fat Diet (HFD), immediately before initiation of pharmacological treatment with VCE-004.8. Note that the 50 animals were divided at the beginning of the study into the four experimental groups: CD + Veh; CD + VCE-004.8; HFD + Veh; and HFD + VCE-004.8, which are presented here to ease comparison with data shown in Figure 3. ***P<0.001 HFD mice vs. control (CD) mice (ANOVA followed by Tukey's test).

a

DFX (µM)	-	10	-	-	-	-
CBD (µM)	-	-	5	-	-	-
VCE-004.8 (µM)	-	-	-	1	2,5	5

120—   ← HIF-1α

50—   ← Actin

b
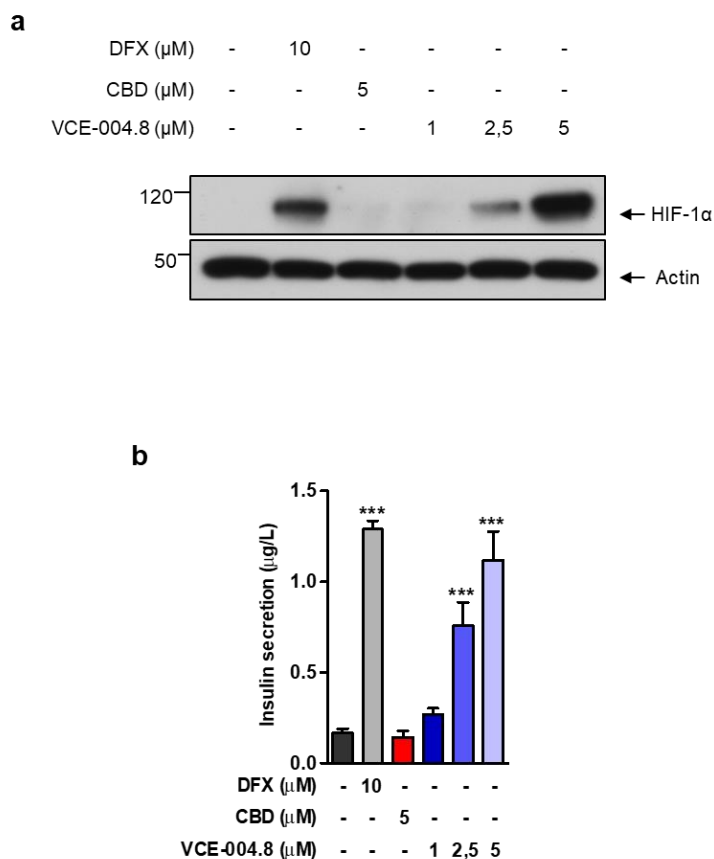
Figure S3. VCE-004.8 stabilises HIF-1α and induces insulin secretion in AR42J cells. AR42J cells were stimulated with DFX (10 µM), CBD (5 µM) or VCE-004.8 at the indicated concentrations for 6 hours, respectively. Cell lysates were analysed for protein expression by immunoblots (**a**). We show a representative western blot of three independent experiments. (**b**) AR42J cells were seeded in 24 well plates, stimulated with the same treatments and incubated with KRBB supplemented with 27.7 mM glucose for 1 h. Insulin secretion was analysed by ELISA. Data are mean ± SD of n = 3 experiments. ***$P < 0.001$ vs. control group (one-way ANOVA followed Dunnett's test).

2. Tetrahydrocannabinolic acid A (THCA-A) reduces adiposity and prevents metabolic disease caused by diet-induced obesity

Tetrahydrocannabinolic acid A (THCA-A) reduces adiposity and prevents metabolic disease caused by diet-induced obesity

Belén Palomares[a,b,c], Francisco Ruiz-Pino[a,b,c], Martin Garrido-Rodriguez[a,d], M. Eugenia Prados[e], Miguel A. Sánchez-Garrido[a,b,c], Inmaculada Velasco[a,b,c], María J. Vazquez[a,b,c], Xavier Nadal[f], Carlos Ferreiro-Vera[f], Rosario Morrugares[a,b,c], Giovanni Appendino[g], Marco A Calzado[a,b,c], Manuel Tena-Sempere[a,b,c,1], Eduardo Muñoz[a,b,c,*,1]

2.1. Δ⁹-THCA-A is a selective and non-adipogenic PPARγ ligand agonist that induces iWAT browning through a PPARγ-dependent pathway

We have previously shown that Δ^9-THCA-A is a PPARγ agonist at nanomolar concentrations [13]. Herein, we have studied the selectivity of Δ^9-THCA-A on different PPARs, showing that, when compared to the full ligand agonist rosiglitazone (RGZ), Δ^9-THCA-A is a partial ligand activator for PPARγ, devoid of PPARα and PPARδ transcriptional activities (Figure 1A).
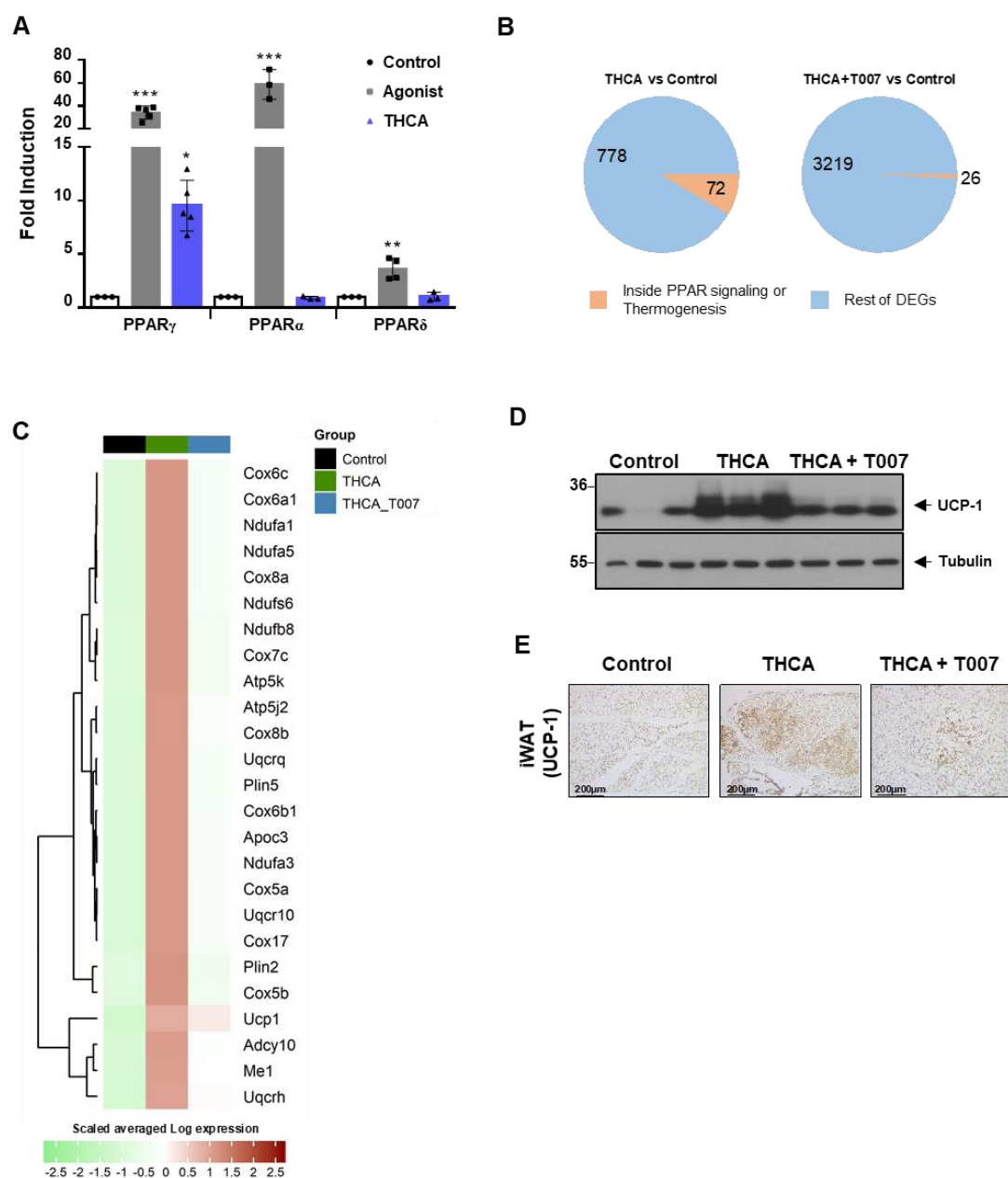
Results

Figure 1. Characterization of Δ⁹-THCA-A as a selective PPARγ agonist. (A) Receptor-specific transactivation by Δ⁹-THCA-A. HEK-293T cells were co-transfected with the plasmids encoding nuclear receptors (GAL4-PPARγ, GAL4-PPARα and GAL4-PPARδ) and their cognate luciferase reporter (GAL4-luc). After transfection, cells were treated with Δ⁹-THCA-A (10 μM) and receptor-specific agonists for 6 hours. Control (white bars), Δ⁹-THCA-A (blue bars) and specific ligands for each receptor (grey bars): RGZ (1 μM) for PPARγ, WY14643 (5 μM) for PPARα, and GW0742 (5 μM) for PPARδ. Results are expressed as the fold induction ± SD (n = 3-5) relative to untreated control. *$P < 0.05$, **$P < 0.01$ and ***$P < 0.001$ agonist ligands or Δ⁹-THCA-A treatment vs. control (ANOVA followed by Tukey's test). **(B)** Representative Western blot images of PPARγ phosphorylation at Ser273 in 3T3L1 adipocytes pre-treated with Δ⁹-THCA-A and RGZ for 30 min, followed by treatment with TNF-α for 30min (n = 3). (B) Pie charts indicating the number and proportion of differentially expressed genes included in the KEGG pathways of interest for each comparison. **(C)** Heatmap of the top 25 genes induced by Δ⁹-THCA-A inside the PPAR signaling or thermogenesis pathways that are not differentially expressed in the Δ⁹-THCA-A+T0070907 vs control comparison. **(D, E)** Representative Western blot images of UCP-1 protein expression and immunohistochemistry with anti-UCP-1 antibodies in iWAT tissue (original magnification × 10, scale bar: 200 μm) (n = 3).

To further investigate the effect of Δ⁹-THCA-A on PPARγ *in vivo*, mice were treated with Δ⁹-THCA-A in the presence or not of T0070907, and transcriptomic analyses in inguinal white adipose tissue (iWAT) were performed. Differential expression analysis of both conditions versus control mice identified a total of 3719 genes with an adjusted P ≤ 0.01 and an absolute fold change ≥ 2 (Figures 1B and 2A). From the 850 genes changing in response to THCA, 72 belonged to the PPAR signaling or thermogenesis pathways. On the other hand, in presence of the antagonist T0070907, from the 3245 with significant changes, only 26 were found in those pathways (Figure 1C and 2A). UCP-1 gene, a key marker of the iWAT browning process, was found among the top 25 genes upregulated by Δ⁹-THCA-A in a T0070907-sensitive manner (Figures 1C). Moreover, western blotting and immunohistochemistry showed that Δ⁹-THCA-A induced the expression of UCP-1 protein in iWAT (Figure 1D, 1E).

As we shown in Figures 2A and 2B, PPAR and thermogenesis pathways share a group of commons genes indicating that both present similar regulatory mechanisms. In line with such putative thermogenic activation, Δ⁹-THCA-A treatment caused a trend for suppression of body weight gain that was independent of food intake changes but blocked by co-administration of T0070907 (Figure 3).
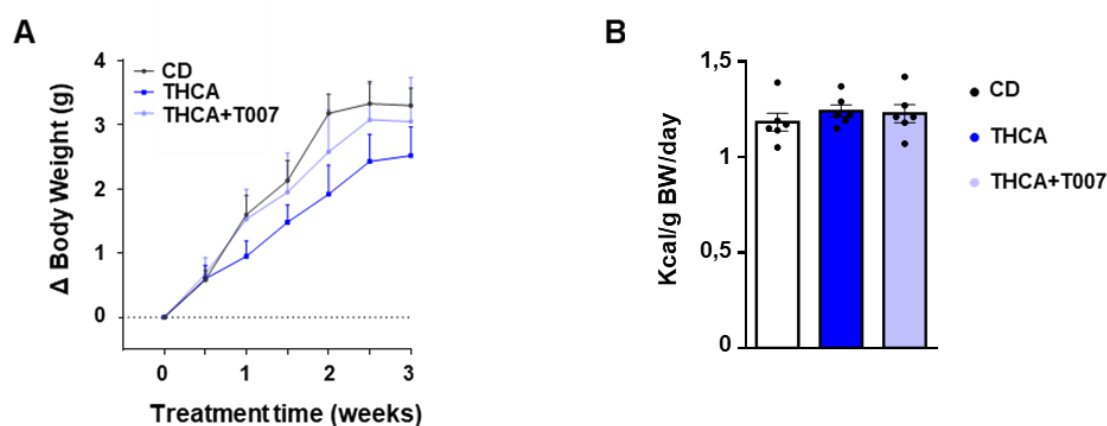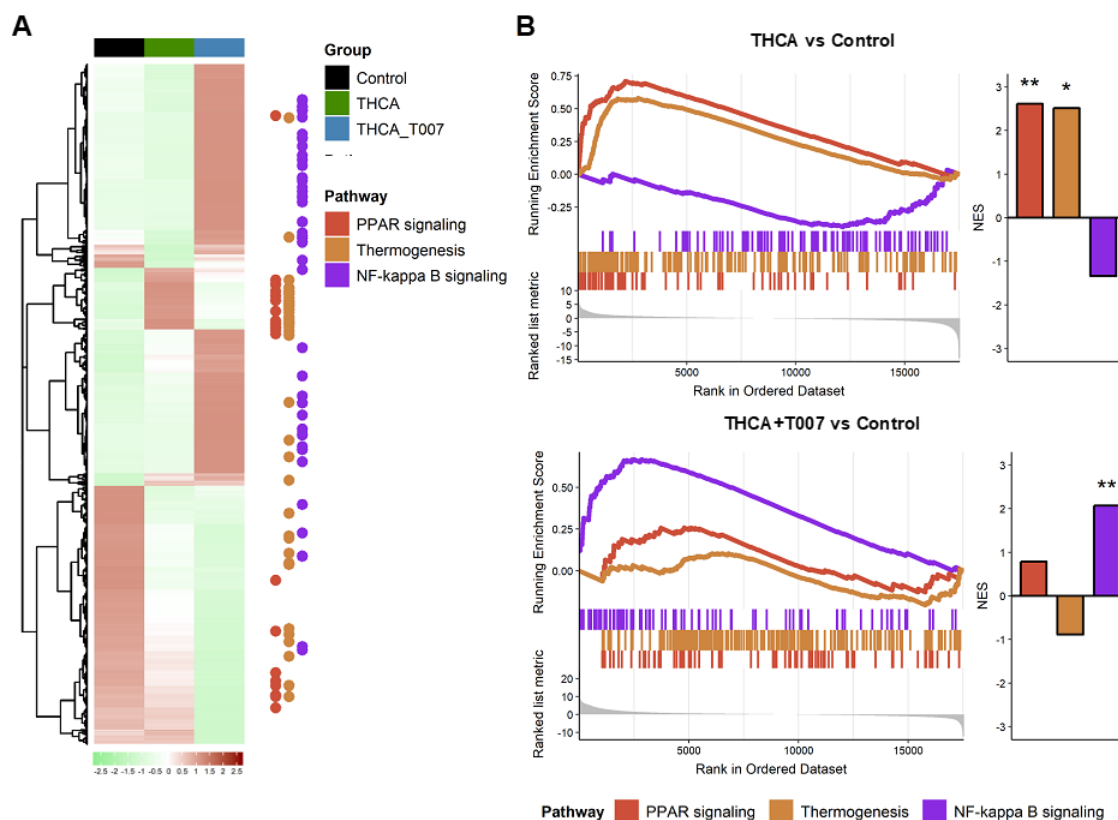
Figure 2. Transcriptomic analysis of the PPARγ dependent activity of Δ⁹-THCA-A in iWAT. (A) Heatmap of all the differentially expressed genes (absolute fold change ≥ 2 and an adjusted P value ≤ 0.01) in Δ⁹-THCA-A versus control or Δ⁹-THCA-A+T0070907 versus control comparisons. The color represents the scaled mean of log transformed expression. The column annotations indicate the sample group and the points at the right side highlight the position of genes belonging to the KEGG pathways of interest. **(B)** Gene set enrichment analysis results for the KEGG pathways of interest. The left side enrich plots indicate the position of the genes belonging to each pathway in the pre-ranked list per comparison. The right-side bar plots represent the normalized enrichment score (NES) and significance of the GSEA result *P ≤ 0.05; **P ≤ 0.01; ***P ≤ 0.001.

Figure 3. Effect of 3 weeks treatment of Δ⁹-THCA-A combined or not with of T0070907 on body weight gain and food intake. (A) BW gain, and **(B)** Daily food intake (Kcal/g BW/day) during the treatment, for the three experimental groups. Data are presented as mean ± SEM (n= 6 mice per group).

In addition, we identified 70 upregulated genes linked to NF-κB and cytokine-cytokine-receptor signaling, whose expression was largely prevented by treatment with Δ⁹-THCA-A (Fig 2A, B).
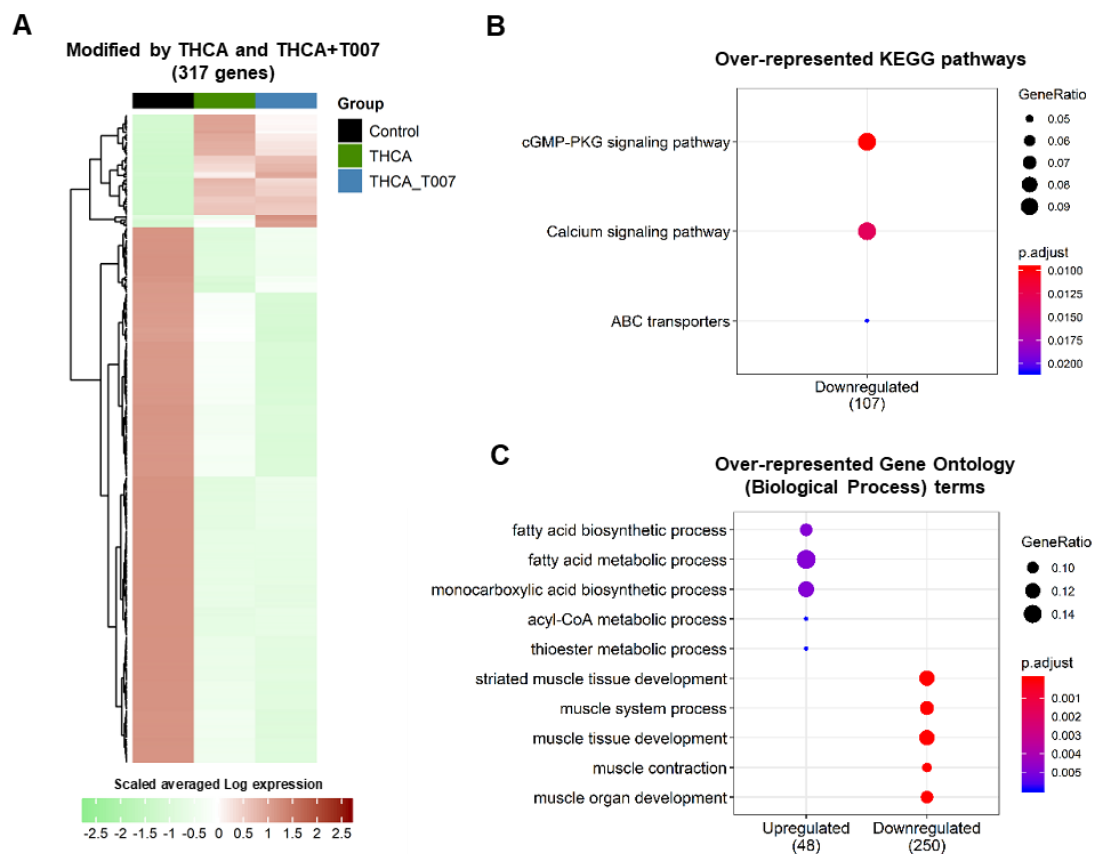
Figure 4. Transcriptomic analysis of the PPARγ independent activity of Δ⁹-THCA-A in iWAT. (A) Heatmap of the 317 genes that are modified in the same direction by both Δ⁹-THCA-A and Δ⁹-THCA-A+T0070907 treatments. The color represents the scaled mean of log transformed expression. The column annotations indicate the sample group. **(B, C)** Over-represented KEGG pathways and Gene Ontology (Biological Process) terms in the clusters of up or down regulated genes by both treatments. The presence of a point indicates the over representation (Fisher Exact Test Adjusted $P \leq 0.05$) of a pathway or term (Y axis) in a group of genes (X axis).

We also found 317 genes that were modified by Δ⁹-THCA-A in a way insensitive to T0070907 (Figure 4A). To functionally evaluate this gene cluster, we performed an over-representation analysis using the KEGG pathways and Gene Ontology annotations (Figure 4B-C). Among them, upregulation of genes related with the fatty acid metabolism and downregulation of genes belonging to cGMP-PKG, calcium signaling pathways and muscle tissue development, was found. Docking analysis revealed that Δ⁹-THCA-A may exert its PPARγ activity by acting at both canonical and alternative binding sites of the PPARγ LBD. Δ⁹-THCA-A binds to the alternative site by interacting with Ser342 at the β-sheet (Ω-loop) through its carboxylate group (Figure 5).
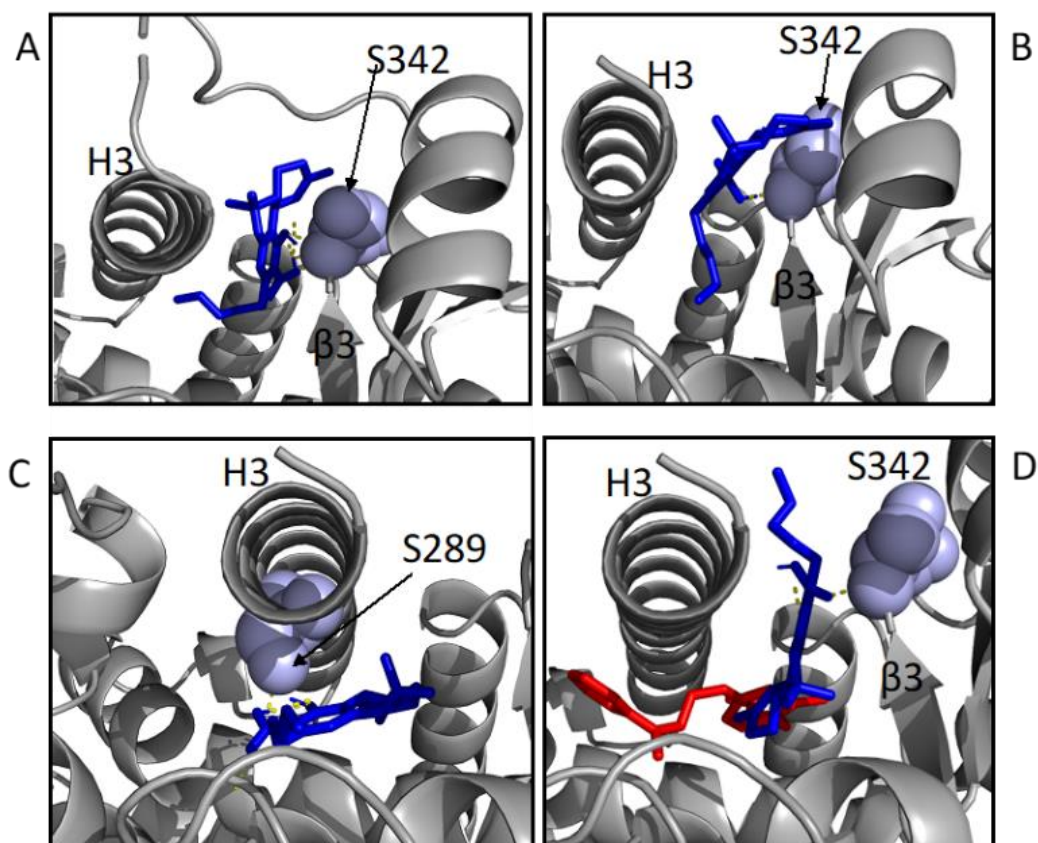
Figure 5. Ligand docking, and binding properties of Δ⁹-THCA-A to PPARγ. (**A**) PPARγ LBD structure 5Y2O ser342 bound to Δ^9-THCA-A (blue), B.E. VINA Kcal/mol= -8.8; B.E. AutoDock Kcal/mol= -10.58; Predicted Ki 17.45 nM. (**B**) PPARγ LBD structure 4EMA ser342 bound to Δ^9-THCA-A (blue), B.E. VINA Kcal/mol= -7.8; B.E. AutoDock Kcal/mol= -8.2; Predicted Ki 982.28 nM. (**C**) PPARγ LBD structure 5LSG ser289 in Helix 3 bound to Δ^9-THCA-A in the orthosteric site (blue), B.E. VINA Kcal/mol= -7.5; B.E. AutoDock Kcal/mol= -8.8; Predicted Ki 302.1 nM. (**D**) PPARγ LBD structure 5LSG bound to RGZ in the orthosteric site (red), and Δ^9-THCA-A in the alternative site (blue).

However, in fluorescence resonance energy transfer (FRET) assays we found that Δ⁹-THCA-A does not affect PPARγ co-regulators interaction (Figure 6). Taken together, our results showed that the bioactivity of Δ⁹-THCA-A was mediated by the PPARγ canonical pathway as well as by other pathways.
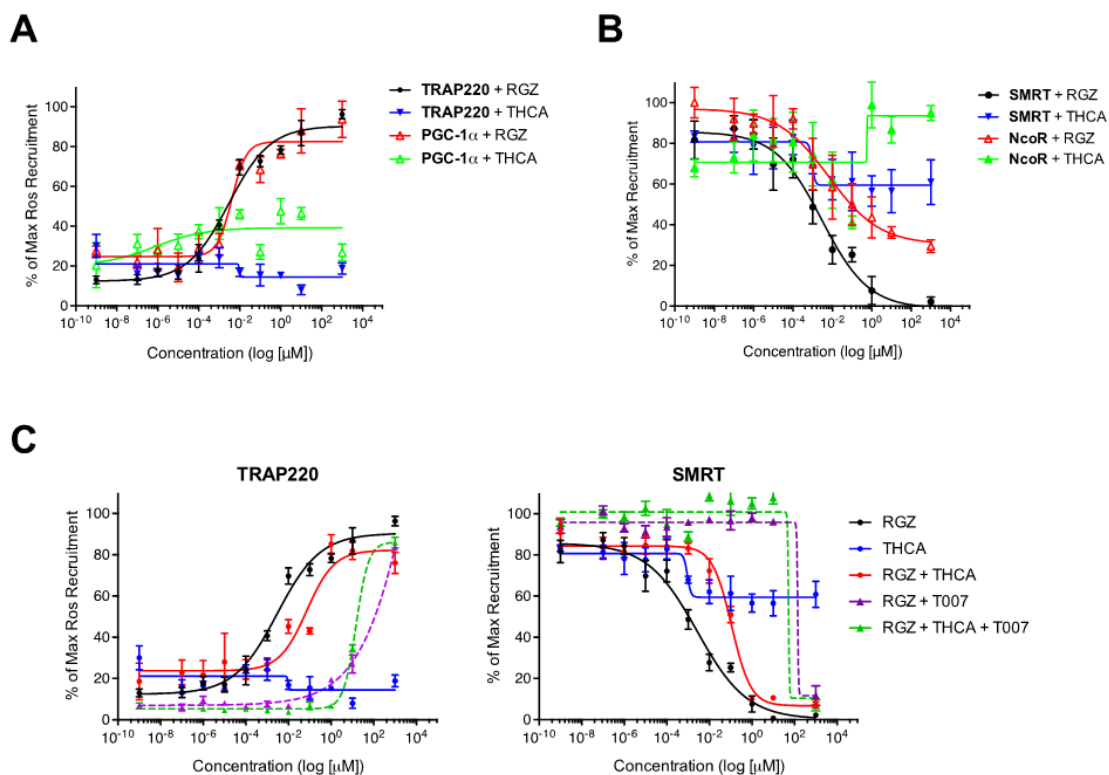
Figure 6. Effects on PPARγ-ligand interactions in presence of Δ⁹-THCA-A in LanthaScreen assays. (**A**) TR-FRET assay was employed to study coactivator peptide recruitment to the human PPARγ LBD in response to RGZ or Δ⁹-THCA-A. Data are expressed as a percentage of the maximum RGZ response. Three experiments were performed, and representative graphs are shown. (**B**) Corepressor peptide displacement to human PPARγ LBD in response to RGZ or Δ⁹-THCA-A was examined by TR-FRET assay. Data are expressed as a percentage of the maximum recruitment in the absence of ligand. Representative data from three experiments are shown. (**C**) Alternative site binding for Δ⁹-THCA-A in PPARγ was tested by using increasing concentrations of RGZ or Δ⁹-THCA-A both in the absence or the presence of 5 µM T0070907 PPARγ antagonist. TRAP220 data are expressed as a percentage of the maximum RGZ response, while SMRT data are expressed as a percentage of the maximum recruitment in the absence of ligand. Representative graphs from three experiments are shown.

The ability of Δ⁹-THCA-A to influence MSCs differentiation into adipocytes or osteoblasts was studied *in vitro*, after culture of MSCs in adipogenic medium. Figure 7A-B show that MSC treated with Δ⁹-THCA-A contained fewer and smaller lipid droplets compared to RGZ treatment. Moreover, Δ⁹-THCA-A induced lower expression of the adipogenic differentiation markers, PPARγ, aP2a, ADIPOQ, LPL and CEBPA, as compared to cells treated with RGZ (Figure 7C). In contrast, we found that Δ⁹-THCA-A enhanced osteoblast mineralization as well as the expression of the osteogenic differentiation markers, Runx2, SP7, IBS and ALP, (Figure 7D-F). These data indicate that Δ⁹-THCA-A qualifies as a partial PPARγ ligand significantly less adipogenic than RZG and with an enhanced osteoblasts differentiation capacity.
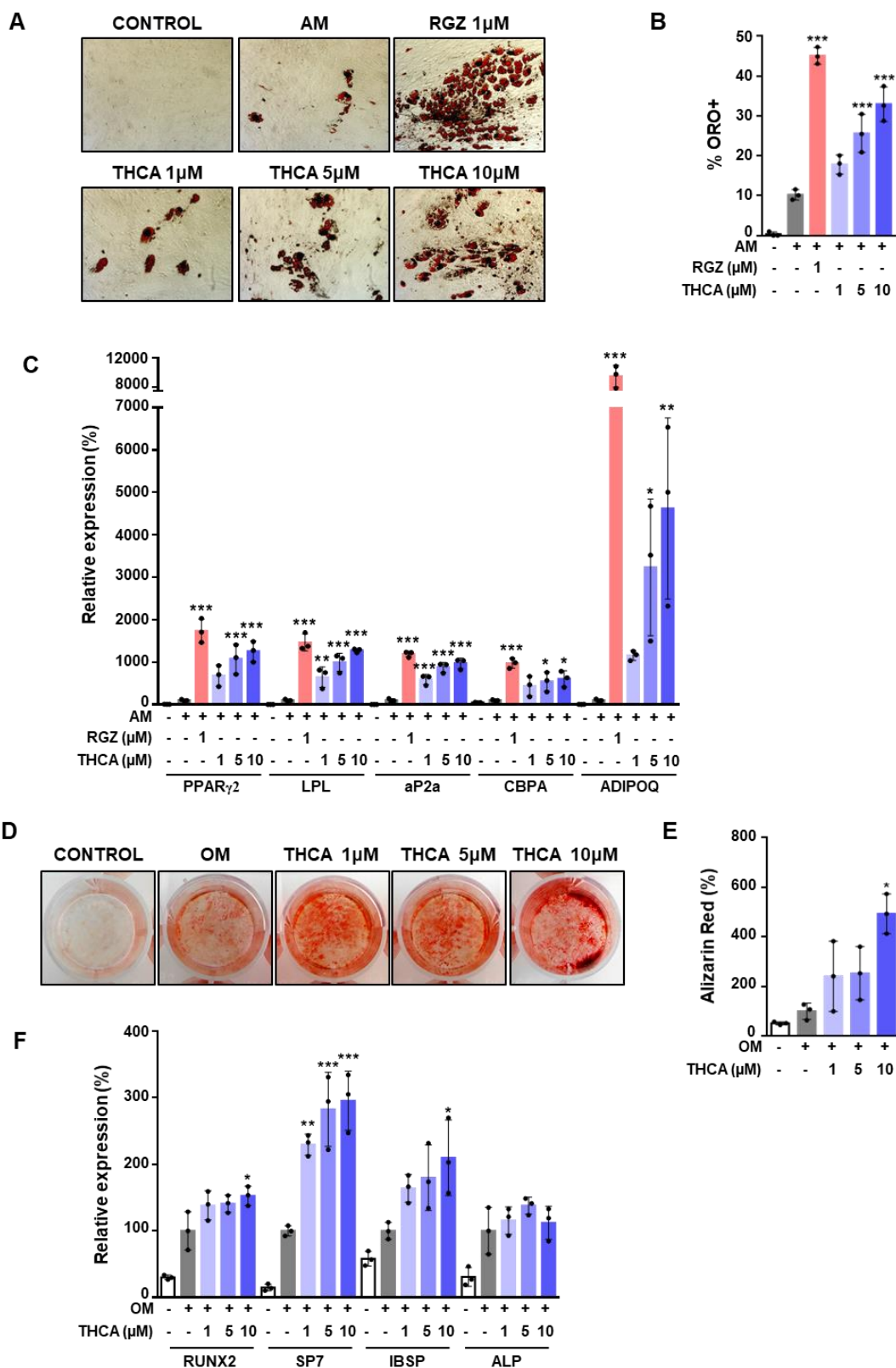
Figure 7. Effect of Δ⁹-THCA-A on MSCs adipogenic and osteoblastogenic differentiation. MSCs were cultured under adipogenic medium (AM) in the presence of RGZ or Δ⁹-THCA-A. **(A)** Representative images of the cells stained with Oil Red O assayed by light microscopy (×10) after 21 days of differentiation. **(B)** Quantification of the stained lipid droplets in Oil Red O (ORO⁺ cells) was performed measuring absorbance at 540nm. **(C)** mRNA levels of adipogenic markers were analyzed by qPCR after 14

days of differentiation. **(D)** MSCs were cultured under osteoblastogenic medium (OM) in the presence of Δ^9-THCA-A and mineralization detected by Alizarin red staining was assessed by gross appearance after 21 days of differentiation. **(E)** Quantification of the eluted Alizarin Red stain measuring absorbance at 405nm. **(F)** Gene expression of osteoblastogenic markers analyzed by qPCR. Results represent the mean ± S.D (n = 3). *P < 0.05, **p < 0.01 and ***P < 0.001 RGZ or Δ^9-THCA-A vs. AM; Δ^9-THCA-A vs. OM. (ANOVA followed by Tukey's test).

2.2. Δ^9-THCA-A ameliorates HFD-induced metabolic perturbations and iWAT inflammation

Next, we analyzed the effects of Δ^9-THCA-A (20 mg/kg BW/day) in a mouse model of HFD-induced obesity. Feeding a HFD for 12-wks resulted in a significant increase in body weight over CD controls (BW; Figure 8A), together with enhanced fat mass (35.89 ± 2.63 g vs. 16.19 ± 1.45 g in CD; P>0.001) and adiposity index, calculated as ratio between fat mass and fat + lean mass (36.43 ± 2.62 vs. 16.56 ± 1.49 % in CD; P=0.001). Δ^9-THCA-A treatment caused a marked suppression of BW gain in HFD mice (Figure 8B), observed also, albeit with lesser amplitude, in CD mice. The increased adiposity caused by HFD was reversed by Δ^9-THCA-A treatment, which caused also a significant suppression of the adiposity index in control lean mice, as determined by Student t-test between the CD and CD+Δ^9-THCA-A groups (Figure 8C). In contrast, treatment with Δ^9-THCA-A failed to significantly modify daily food intake neither in the HFD (0.89 ± 0.08 in Δ^9-THCA-A-treated vs. 1.01 ± 0.06 kcal/g BW/d in vehicle-treated mice; P=0.2626) or the CD (1.08 ± 0.06 in Δ^9-THCA-A-treated vs. 1.04 ± 0.05 kcal/g BW/d in vehicle-treated mice; P=0.0617) groups.

Δ^9-THCA-A improved also glucose homeostasis in HFD-induced obese mice. While HFD exposure for 15-wks evoked an elevation of basal glucose levels, worsened glucose tolerance after glucose bolus injection (Figure 8D) and reduced insulin sensitivity (Figure 8E), treatment of HFD mice with Δ^9-THCA-A for 3-wks resulted in lowering of basal glycemia, and markedly improved glucose profiles, both in glucose and insulin tolerance tests, which displayed better profiles than those of CD mice without pharmacological intervention. Moreover, positive effects of Δ^9-THCA-A in terms of glucose tolerance and insulin sensitivity were also detected in lean control mice (Figure 8D-E). This was associated to a significant lowering of basal insulin levels after Δ^9-THCA-A administration to CD and HFD mice (Figure 8F), possibly reflecting a state of enhanced insulin sensitivity. Δ^9-THCA-A treatment of obese mice largely prevented liver fat infiltration caused by HFD and markedly reduced the steatosis score (Figure 8G-H). In

94

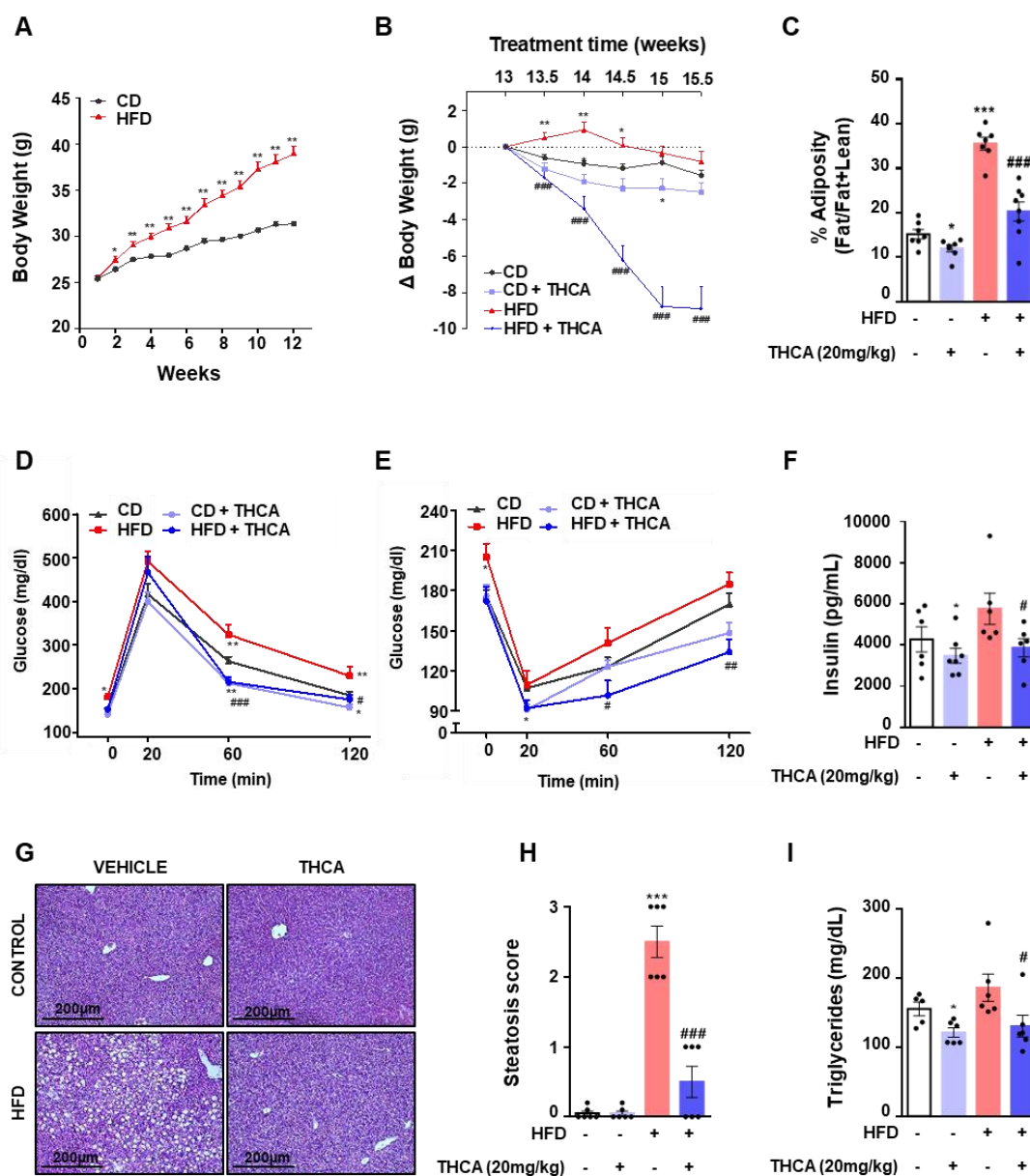addition, Δ^9-THCA-A significantly decreased serum triglyceride levels both in obese and lean mice (Figure 8I).

Figure 8. Effect of administration of Δ^9-THCA-A on metabolic and hormonal parameters in a mouse model of HFD-induced obesity. **(A)** Body weight evolution of adult male mice fed for 12-weeks with high fat diet (HFD) or the corresponding control diet (CD). **(B)** BW change in HFD and CD mice treated for three weeks with Δ^9-THCA-A or vehicle; values are referenced to BW at the beginning of treatment (taken as 0). **(C)** Percentage of adiposity, at the end of treatments in the four experimental groups. **(D-E)** Glucose and Insulin tolerance tests in CD and HFD mice treated with Δ^9-THCA-A or vehicle for three weeks. **(F)** Basal insulin levels at the end of the three-week treatment period are shown for the four experimental groups. **(G)** Liver sections with hematoxylin and eosin (H&E) staining (original magnification x10, scale bar: 200 μm). **(H)** Steatosis scores (n = 6 mice per group) and **(I)** plasma levels of triglycerides. Values correspond to means ± SEM (n= 5-8 mice per group). *$P<0.05$, **$P<0.01$, ***$P<0.001$ Δ^9-THCA-A-treated mice or HFD mice vs. control (CD) mice; #$P<0.05$, ##$P<0.01$, ###$P<0.001$ Δ^9-THCA-A-treated HFD mice vs. HFD mice treated with vehicle (ANOVA followed by Tukey's test).

95

The iWAT transcriptomic profile in control and HFD mice, untreated or treated with Δ^9-THCA-A, was next investigated. Differential expression analysis revealed a total of 1387 genes overcoming the cutoff of an adjusted $P \leq 0.01$ and an absolute fold change ≥ 2 in any of the two comparisons (Figure 9A). Among them, KEGG pathway analyses revealed that genes involved in NF-κB signaling and cytokine-cytokine receptor were upregulated in HFD mice, which matches their inflammatory phenotype in iWAT [179]. As described above in figures 2A and 2B, the group of common genes between cytokine-cytokine receptor and NF-κB signaling pathways indicate the shared regulatory mechanisms between both processes. Additionally, genes belonging to the insulin receptor signaling pathway showed lower expression in HFD mice, in line with a state of insulin resistance. Interestingly, Δ^9-THCA-A treatment of HFD mice reduced the expression of genes belonging to the inflammatory pathways, partially recovering the expression of those linked to the insulin signaling process (Figure 9A-B). In total, DEGs analysis revealed that 1014 genes including those related to NF-κB signaling and cytokine-cytokine receptor (70 genes) were modified in HFD mice and normalized in Δ^9-THCA-A-treated HFD mice (Figure 9C). Finally, to confirm the anti-inflammatory profile of Δ^9-THCA-A, we analyzed by qPCR the top 25 upregulated inflammatory genes in the iWAT of HFD mice (Figure 9D), confirming the increased expression of key components of this gene-set, including TNFα, ICAM-1, CD4, CXCL-16, CCL22, CXCR5 and CXCR2 (Figure 9E).
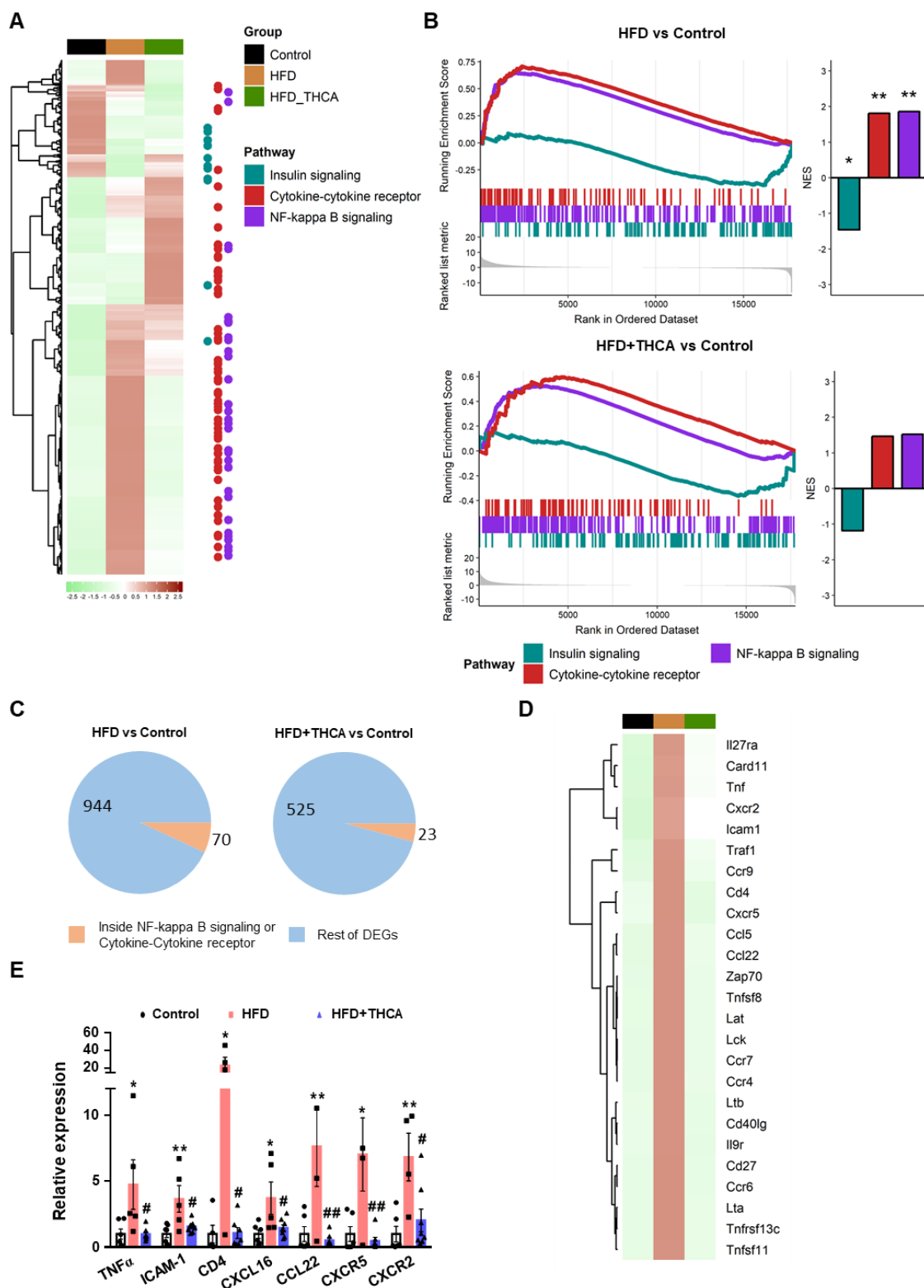
Figure 9. Transcriptomic analysis of Δ⁹-THCA-A effects in the iWAT of HFD mice. (A) Heatmap of all the differentially expressed genes (absolute fold change $\geq$ 2 and an adjusted P value $\leq$ 0.01) in HFD (brown box) versus control (black box) or HFD+Δ⁹-THCA-A (green box) versus control comparisons. The color represents the scaled mean of log transformed expression. The column annotations indicate the sample group and the points at the right side highlight the position of genes belonging to the KEGG pathways of interest. **(B)** Gene set enrichment analysis results for the KEGG pathways of interest. The left side enrich

plots indicate the position of the genes belonging to each pathway in the pre-ranked list per comparison. The right-side bar plots represent the normalized enrichment score (NES) and significance of the GSEA result *P ≤ 0.05; **P ≤ 0.01; ***P ≤ 0.001. **(C)** Pie charts indicating the number and proportion of differentially expressed genes included in the KEGG pathways of interest for each comparison. **(D)** Heatmap of the top 25 genes induced by HFD (brown box) inside the NF-κB or cytokine-cytokine receptor pathways that are not differentially expressed in the HFD+Δ^9-THCA-A (green box) vs control (black box) comparison. **(E)** Gene expression of pro-inflammatory genes were measured by qPCR. Results are presented as mean ± SEM (n= 4-8 mice per group). *P<0.05, **P<0.01 HFD mice vs. control mice; #P<0.05, ##P<0.01 Δ^9-THCA-A-treated HFD mice vs. HFD mice treated with vehicle (ANOVA followed by Tukey's test)

In keeping with their obese phenotype, HFD mice also displayed features of adipose tissue enlargement and inflammation. Thus, a significant increase in adipocyte volume was observed, accompanied by signs of macrophage infiltration of WAT, assessed by F4/80 staining of clusters of macrophages surrounding dead adipocytes, in the so-called crown-like structures (CLS) (Figure 10A-B). Δ^9-THCA-A administration fully prevented adipocyte enlargement and the appearance of CLS in the iWAT of HFD-induced obese mice, while substantially increasing UCP-1 content in iWAT (Figure 10A-C).

Finally, changes in the circulating levels of key metabolic hormones were assessed in HFD-induced obese mice, treated or not with Δ^9-THCA-A. In line with their obese phenotype, HFD mice showed increased leptin and glucagon levels, and decreased GLP-1 concentrations vs. lean CD animals. Treatment with Δ^9-THCA-A fully normalized leptin, GLP-1 and glucagon levels, and evoked a modest, albeit significant increase in adiponectin concentrations in HFD mice (Figure 10D-G). Alike, proteome profiler arrays targeting a comprehensive set of circulating adipokines and cytokines confirmed the increase of the levels of leptin, together with other adipose born-factors, such as Oncostatin M and Serpin E1, in HFD mice, which were decreased by Δ^9-THCA-A, while adiponectin concentrations were increased. Likewise, a set of cytokines including Endostatin, IGFBp-5, PCSK9, Adipsin and IGFBP-3 were suppressed by HFD but increased by Δ^9-THCA-A in HFD mice, while an opposite pattern was observed for CCL11 and CCL6 (Figure 10H).
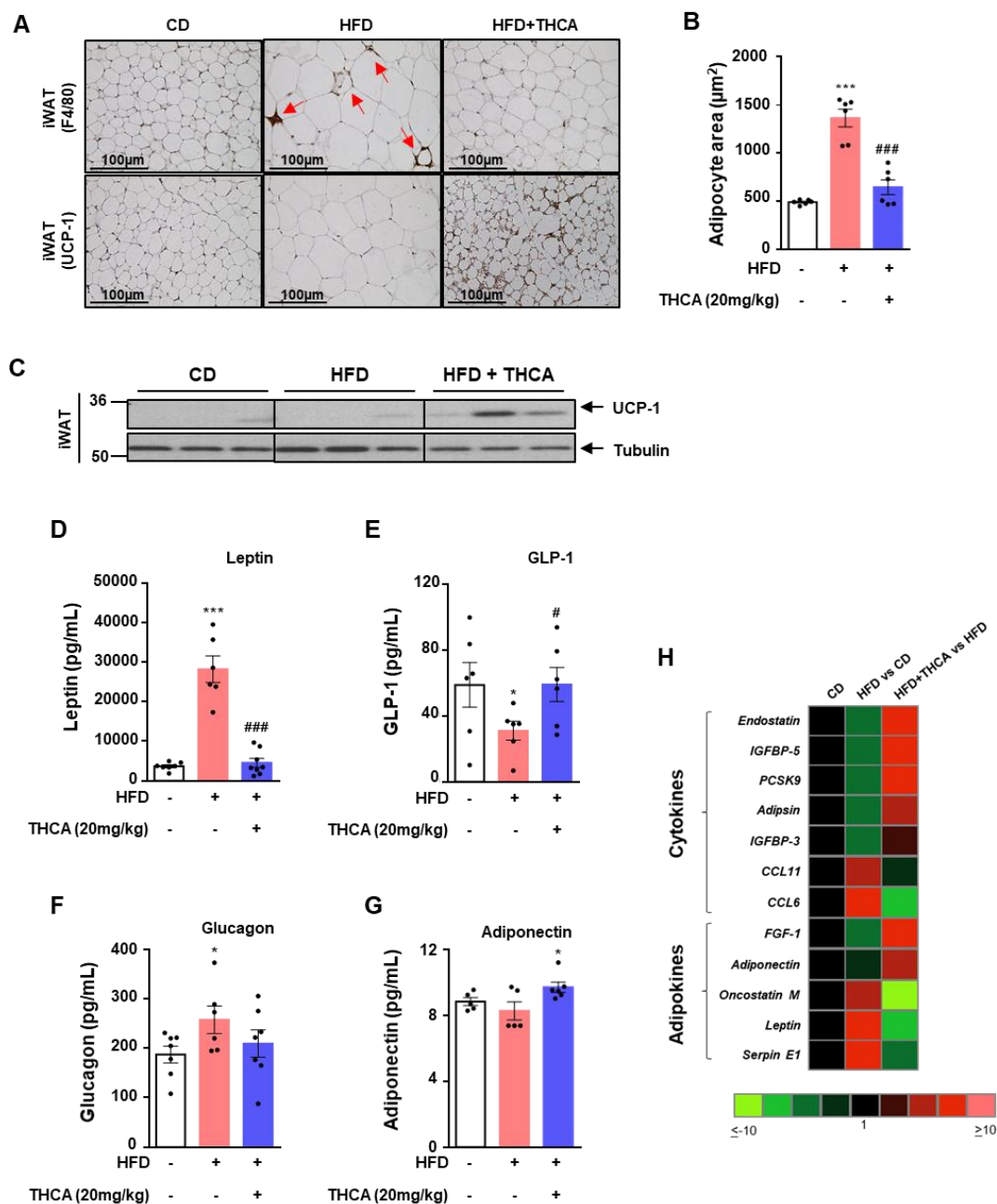
Figure 10. Effects of Δ^9-THCA-A on iWAT browning, adiposity and circulating factors, with key roles in metabolic homeostasis in CD and HFD animals. (**A**) Crown Like Structures (CLS) and browning in iWAT. Representative immunohistochemical detection of anti-F4/80 and anti-UCP-1 antibodies (original magnification x20, scale bar: 100 μm), (**B**) Quantification of adipocyte area (n = 6 animals per group), (**C**) UCP-1 protein levels determined by western blotting in iWAT tissue (n=3). Hormonal markers linked to energy and metabolic homeostasis assayed: (**D**) Leptin, (**E**) GLP-1, (**F**) Glucagon and (**G**) Adiponectin. (**H**) Heatmap showing the plasma profile of cytokines and adipokines. Values correspond to means ± SEM (n= 5-8 mice per group). *P<0.05, ***P<0.001 HFD mice vs. control (CD) mice; #P<0.05, ###P<0.001 Δ^9-THCA-A-treated HFD mice vs. HFD mice treated with vehicle (ANOVA followed by Tukey's test).

3. Δ⁹-Tetrahydrocannabinolic acid alleviates collagen-induced arthritis through PPARγ- and CB₁-dependent pathways

Δ9-TETRAHYDROCANNABINOLIC ACID ALLEVIATES COLLAGEN-INDUCED ARTHRITIS THROUGH PPARγ- AND CB1-DEPENDENT PATHWAYS

(Manuscript submitted to journal)

3.1. Affinity, intrinsic activity and potential allosteric properties of Δ^9-THCA-A at cannabinoid receptors

We first analyzed Δ^9-THCA-A in competition studies to determine its affinity at the CB_1 and CB_2 receptors. Δ^9-THCA-A has a modest affinity (Ki values in the submicromolar range) at both receptors, with a 2-fold higher affinity for CB_1 (Ki = 252 ± 140 nM) than for CB_2 (Ki = 506 ± 198 nM) (Figure 1A). Compared to a classic ligand for both receptors such as CP-55,940, the binding of Δ^9-THCA-A to CB_1 and CB_2 receptors was more than 50 and 100-fold lower respectively [180]. The study of its intrinsic activity at the CB_1 receptor in an [^{35}S]-GTPγS binding assay supported Δ^9-THCA-A to be a partial agonist with an EC50 = 3.8 ± 0.5 µM (more than 100-fold higher (reflecting lower activity) compared to CP-55,940 [180], whereas it apparently behaved as an antagonist/inverse agonist, with an IC50 = 1.3 ± 0.4 µM at the CB_2 receptor (Figure 1B). Lastly, we also wanted to explore whether Δ^9-THCA-A may have any allosteric activity at the CB_1 receptor. To this end, we compared the activation of the CB_1 receptor in the [^{35}S]-GTPγS binding assay elicited by increasing concentrations of CP-55,940 in the absence or the presence of Δ^9-THCA-A at 0.1 nM, a concentration at which the compound was not able to bind and activate the orthosteric site at the CB_1 receptor according to our competition studies (see Figure 1A). Our data indicated that, at this concentration, however, Δ^9-THCA-A enhanced the CP-55,940-dependent activation of the CB_1 receptor, as was confirmed by the statistical significance for the Δ^9-THCA-A effect ($F_{(1,16)}$=12.40, $p<0.005$; see Figure 1C) seen when the two curves were analyzed with a two-way (CP55,940 x Δ^9-THCA-A) ANOVA. This effect of Δ^9-THCA-A was seen at both high (E*max* (% over basal) = 125.1 in the absence of Δ^9-THCA-A *versus* E*max* (%) = 151.5 in the presence of Δ^9-THCA-A) and low (*E*min (%) = -13.1 in the absence of Δ^9-THCA-A *versus E*min (%) = 43.9 in the presence of Δ^9-THCA-A) concentrations of CP-55,940 (Figure 1C). These differences were not found at lower (0.1 pM; $F_{(1,16)}$=2.867, ns) or higher (1 µM, $F_{(1,16)}$=0.950, ns; this is a concentration at which Δ^9-THCA-A is already able to bind the orthosteric site; see Figure 1A) concentrations (data presented in supplementary Figure 1).

The binding affinity of Δ^9-THCA-A for CB_1 receptor inspired us to study its effect on downstream signalling. We stimulated HEK293-CB_1-CRE-Luc cells with either Δ^9-THCA-A or CP-55,940 separately or in combination and the luciferase activity was

measured as indicative of cAMP induction. Δ^9-THCA-A did not induce CRE-Luc activity but enhanced significatively the effect of the orthosteric ligand CP-55,940 (Figure 1D).
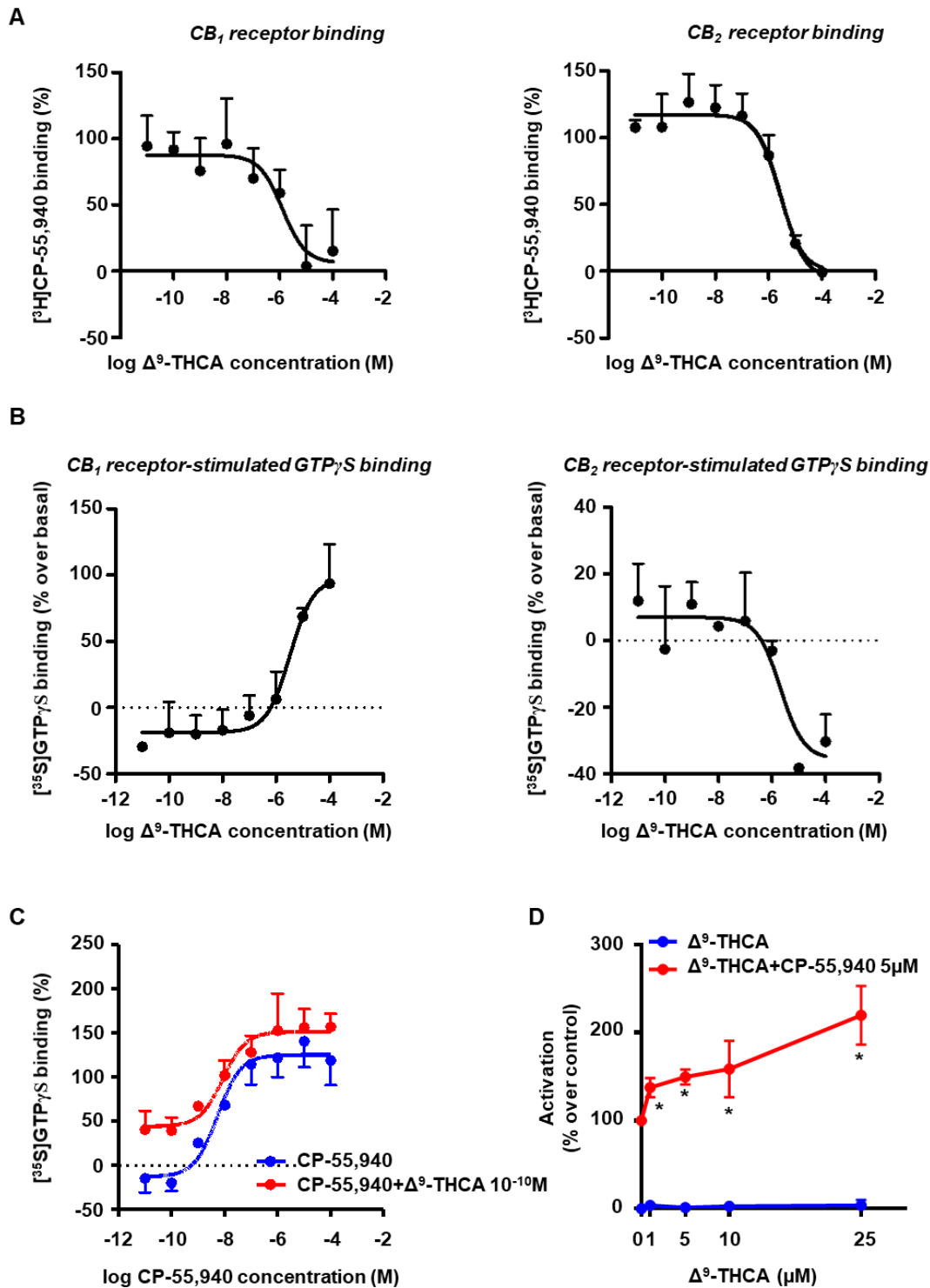
Figure 1. Identification of Δ^9-THCA-A as a positive allosteric CB_1 modulator. (A) Binding affinity of Δ^9-THCA-A to CB_1 and CB_2 receptor. Ki values obtained from competition studies using [^{3}H]CP-55,940 as radioligand for hCB_1 and hCB_2 receptor. **(B)** Average concentration-response curves for the stimulation of [^{35}S]GTPγS binding by Δ^9-THCA-A. **(C)** [^{35}S]-GTPγS binding stimulated by CP-55,940 (10^{-4}-10^{-11} M) in the absence or presence of Δ^9-THCA-A (10^{-10} M). Data were expressed as mean ± SEM of five experiments performed in triplicate for each point. Ki values for each receptor and, the Emax and EC50 (or

104

IC50) values were determined by using GraphPad Prism® version 7. Statistical significance was determined by a two-way ANOVA, followed by Bonferroni's posthoc test to compare CP-55,940+Δ^9-THCA-A vs. CP-55,940. **(D)** Receptor-specific transactivation by Δ^9-THCA-A. HEK293-CB$_1$-CRE-Luc cells were pre-incubated with increased concentration of Δ^9-THCA-A for 20 min and then stimulated with CP-55,940 (5µM) for 6 hours. The values of untreated controls were taken as 100% activation ± SD (n = 5). Statistics: *p<0.05, **p<0.01 and ***p<0.001 CP-55,940+Δ^9-THCA-A vs. CP-55,940.

Next, we analyzed whether Δ^9-THCA-A was also able to activate CB$_1$ through β-arrestin and we found that Δ^9-THCA-A alone slightly induced β-arrestin recruitment compared to CP-55,940, which exhibited a pronounced increment of β-arrestin recruitment (Fig. 2A and 2B). Interestingly, Δ^9-THCA-A was able to enhance β-arrestin recruitment induced by CP-55,940 but it did not affect cell proliferation (Fig. 2C). As expected, the CB$_1$ antagonist SR141716 decreased the β-arrestin recruitment induced by CP-55,940 (Fig. 2A and 2B). Next, we evaluated the signalling pathway involving the phosphorylation of ERK1/2 induced by CB$_1$ activation. Δ^9-THCA-A and CP-55,940 treatments at different concentrations induced the phosphorylation of ERK 1/2 (pERK1/2) at 30 min. Δ^9-THCA-A and CP-55,940 were able to induce pERK1/2 in HEK293-CB$_1$ cells but not in HEK293 cells (Figure 2D). The induction of pERK1/2 by both Δ^9-THCA-A and CP-55,940 was inhibited by SR141716 and no additive effect was observed when both compounds were used in combination (Fig. 2E). Altogether our results suggest that Δ^9-THCA-A may exert biological activities by acting as an orthosteric ligand and also as a positive allosteric modulator (PAM) of CB$_1$.

3.2. Docking

To identify the binding mode of CP-55,940, Δ^9-THC and Δ^9-THCA-A (Fig. 3A) to CB$_1$ a set of *in silico* experiments were performed. Rigid (receptor) cross-docking calculations could reproduce the correct binding mode for CP-55,940 and Δ^9-THC when using the CB$_1$ structure of PDB code 5XR8 (Figure 3B). The top docking pose for Δ^9-THC binds with the core tricyclic rings sandwiched between TM2, TM3 and TM7 in a hydrophobic pocket surrounded by residues (Figure 3B). The most critical H-bond interaction to the hydroxyl sidechain of Ser383 (TM7), with the hydroxyl moiety highlighted in Figure 3A, is preserved. Previous mutagenesis experiments identified Ser383, Phe174, Leu193, Phe379 and Tyr275 as important residues for the binding of Δ^9-THC and CP-55,940 (labelled in Figure 3B and C with asterisk) [159, 181, 182]. The alkyl chain is placed perpendicular to the tricyclic core contacting Leu193, Trp279 and Tyr275, giving the molecule an "L-shaped" bioactive conformation.
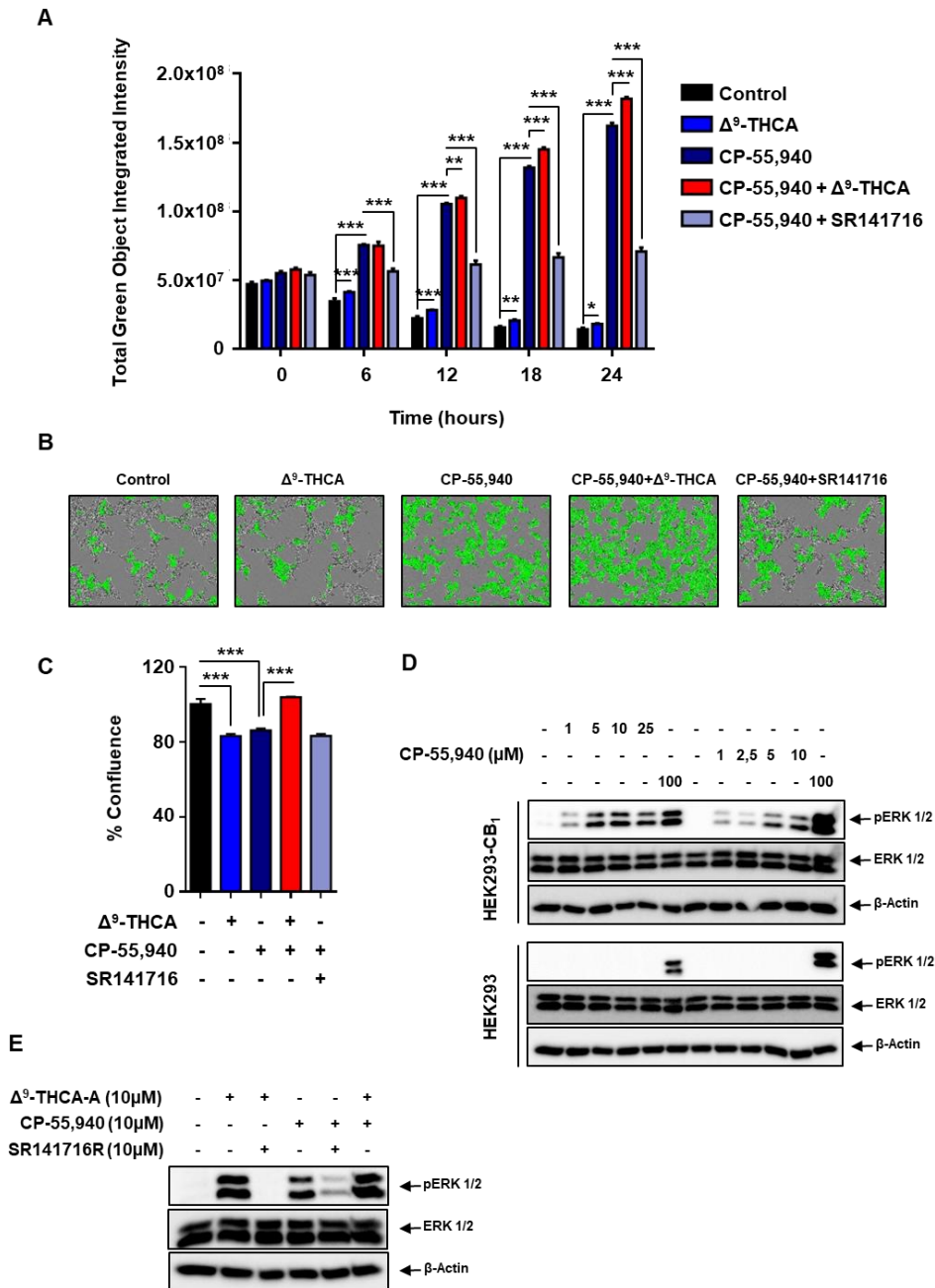
Figure 2. Impact of Δ⁹-THCA-A on β-arrestin recruitment and ERK1/2 Phosphorylation. HEK293-CB₁-β-arrestin Nomad cells were pre-incubated with Δ⁹-THCA-A (1μM) and SR141716 (1μM) for 20min and then treated with CP-55,940 (2,5 μM) for 24 hours. **(A)** Quantification of β-arrestin recruitment on living cells at the times indicated are shown by fluorescence intensity changes. **(B)** Representative images of cytoplasmatic granularity changes (20x magnification) and **(C)** cell confluence of endpoint were determined using the IncuCyte system. Control group was taken as 100 % of confluence. Western blot analysis showing p-ERK1/2, total ERK1/2 and actin levels in **(D)** HEK293-CB₁-β-arrestin Nomad cells and HEK293 cells exposed to increased concentrations of Δ⁹-THCA-A and CP-55,940 for 30 min, and in **(E)** HEK293-CB₁-β-arrestin Nomad cells pre-stimulated with Δ⁹-THCA-A (10μM) and SR141716 (10μM) for 5min and treated with CP-55,940 (10μM). PMA (100nM) was used as a positive control of ERK1/2 phosphorylation. Data are means ± SD (n=5). Statistics: *p<0.05, **p<0.01 and ***p<0.001.
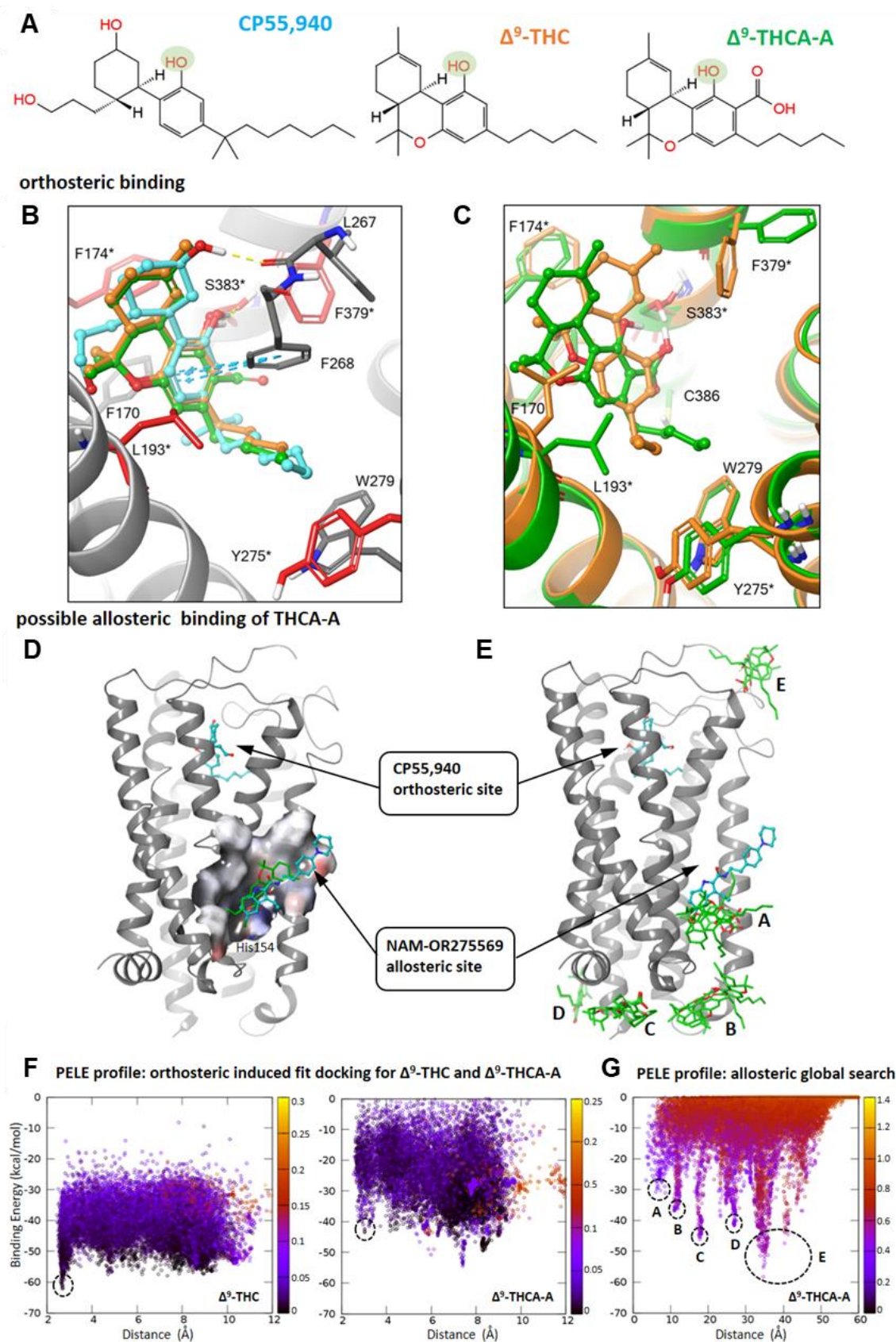
Figure 3. Binding mode prediction from docking and PELE simulations for three CB1 modulators.
(**A**) 2D chemical structure of compounds CP-55,940, Δ⁹-THC and Δ⁹-THCA-A. A key hydroxyl functional
group present in all compounds is highlighted in green. Color coding for (A), (B) and (C) is: CP-55,940,
Δ⁹-THC and Δ⁹-THCA-A in blue, orange and green, respectively. *Binding mode prediction at orthosteric*

site: **(B)** Rigid (receptor) top docking results of CP-55,940 and Δ^9-THC to the orthosteric site of CB1 X-RAY structure PDB 5XR8. Residues interacting with ligands are shown and important residues identified by mutagenesis experiments are depicted in red sticks and labelled with an asterisk. **(C)** PELE induced-fit binding simulation results for Δ^9-THC and Δ^9-THCA-A to the CB1 cryo-EM structure PDB 6N4B. *Binding mode prediction at possible allosteric site.* **(D)** Rigid (receptor) top docking pose of Δ^9-THCA-A to the allosteric site of NAM-OR275569 (represented in blue) for CB1 X-RAY structure PDB 6KQI where the orthosteric site is occupied by CP-55,940. The allosteric pocket is represented with molecular surface showing His154 making H-bonded interaction with carboxylate functional group of Δ^9-THCA-A (in green). **(E)** PELE global search simulation depicted position on the CB1 surface corresponding to the lowest energy poses, black dash circles in PELE profile (G). **(F)** PELE energy profiles for induced-fit docking representing interaction energy (in kcal mol^{-1}) vs. distance between the key hydroxyl group on all modulators and the sidechain OG atom of Ser383 (in Å). The black dash circles in all three plots represent the binding conformation for each molecule that best overlaps with the docking results of CP-55,940 and Δ^9-THC and the recently disclosed binding mode of CP-55,940 in the orthosteric site. **(G)** PELE energy profile for global search, interaction energy (in kcal mol^{-1}) plots vs. distance between the carboxylate group of Δ^9-THCA-A and the sidechain of His154 lying at the base of the NAM- OR275569 allosteric site (in Å). The black dash circles represent the low energy minima corresponding to the representative structures depicted in (C) and (E).

Although CP-55,940 shares a similar binding mode with Δ^9-THC, it has an additional interaction other than the hydroxyl-Ser383 H-bond, namely an extra H-bond to the backbone carbonyl of Leu267 (Figure 3B) through its second hydroxyl group. The stronger electrostatic interaction probably explains its higher potency. Remarkably, the predicted binding mode of CP-55,940 on PDB 5XR8 coincides perfectly with the recently published X-ray structure of CB$_1$ in complex with this molecule occupying the orthosteric site (PDB entry 6KQI). [161]. Docking to the same X-ray CB$_1$ receptor structure of Δ^9-THCA-A suggests that it shares the same binding mode with CP-55,940 and Δ^9-THC. The most important H-bond interaction to Ser383 is preserved (Figure 3B). However, the Glide XP predicted affinity is much weaker for Δ^9-THCA-A, (-8.9) than that of CP-55,940 and Δ^9-THC, probably due to its carboxylic acid does not engage the protein in any electrostatic interaction.

Our PELE-induced fit simulation for Δ^9-THC generated a lowest energy minimum binding mode that perfectly matches the docking pose and X-ray structures, placing it on the orthosteric site (Figure 3F) and recovering all key interactions (H-bond to Ser383, overall L-shape; Figure 3C, orange compound). Thus, the same PELE simulations were repeated for Δ^9-THCA-A to estimate whether it also engages the orthosteric site. However, as seen in their interaction energy plots (Figure 3F), Δ^9-THCA-A seems to engage CB$_1$ in the orthosteric site as well as many other sites involving the extracellular loops with similar interaction energies. In other words, the energy profile leading to the orthosteric site is pronounced for Δ^9-THC, but not for Δ^9-THCA-A, which could have additional interaction sites involving the entrance to the orthosteric site.

The recently solved X-ray structure of CB_1 in complex with agonist CP-55,940 and the NAM ORG27569 (PDB code 6KQI) [161] revealed the allosteric modulator bound to an extrahelical site within the inner leaflet of the membrane, overlapping with a conserved cholesterol binding site seen for many GPCRs (Figure 3D). As a first attempt, tests with rigid (receptor) docking of Δ^9-THCA-A to this site predicted a binding mode that overlaps with the OR27569. However, the interaction is very week, Glide XP giving a score of -5.78 kcal/mol (Figure 3D). As a more thorough test of possible interaction sites for Δ^9-THCA-A on any pocket of CB_1, an exhaustive global exploration with this molecule was performed on the same X-ray structure (PDB code 6KQI) with CP-55,940 occupying the orthosteric site. The energy profile for the global search is presented in Figure 3G as a plot of interaction energy versus the distance between the carboxylate group of Δ^9-THCA-A and the side chain of His154 located at the base of the allosteric pocket. The global exploration generates 5 energy minima (A-E), highlighting potential interaction hotspots for Δ^9-THCA-A when the orthosteric site is occupied with an agonist CP-55,940. The structural location for each of the A-E minima on the plot is shown in Figure 3E. Inspection of these hotspots suggests Δ^9-THCA-A could be binding on the extracellular loops, the intracellular side of CB_1 contacting G proteins or the NAM-OR27569 /cholesterol site mentioned above.

3.3. Δ^9-THCA-A ameliorates IL-1β-induced inflammatory response in human chondrocytes

IL-1β is considered a key proinflammatory mediator in the pathogenesis of arthritis [183]. Thus, we evaluated the effect of Δ^9-THCA-A on the expression of inflammatory factors in human chondrocytes treated with IL-1β. Pre-treatment with Δ^9-THCA-A resulted in a significant inhibition of IL-6, COX-2 and iNOS gene expression induced by IL-1β stimulation. Since Δ^9-THCA-A is a PPARγ agonist [13] and a ligand activator of CB_1 we investigated if the effect of Δ^9-THCA-A was mediated via PPARγ and/or CB_1. Preincubation of chondrocytes with T0070907 (PPARγ antagonist) and SR141716 (CB_1 antagonist) significantly reversed the IL-6 inhibition induced by IL-1β (Figure 4A). However, the cotreatment of Δ^9-THCA-A and T0070907 only resulted in increased COX-2 expression, but no iNOS, while the cotreatment with SR141716 did not reversed the Δ^9-THCA-A activity on COX-2 and iNOS genes. (Figure 4B and 4C). These results suggest that Δ^9-THCA-A inhibits pro-inflammatory factor expression not only through PPARγ and CB_1 pathways but also by other pathways.
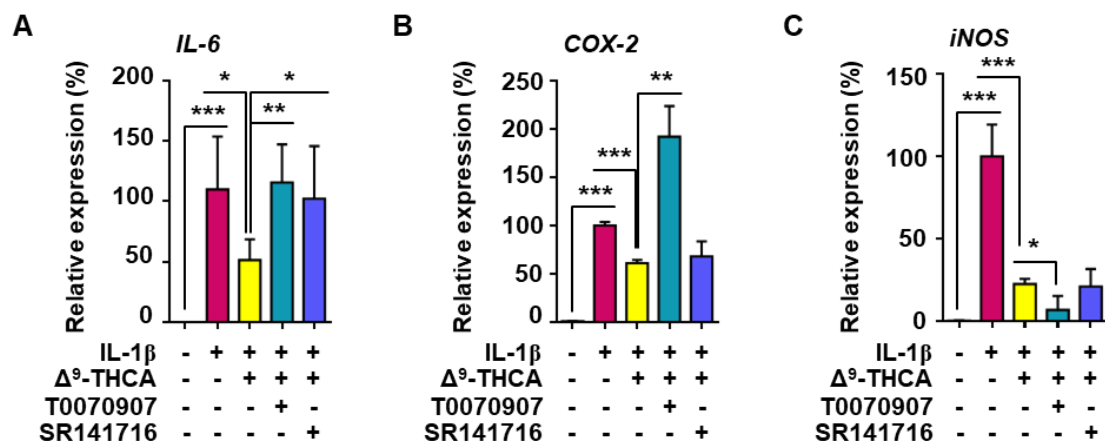
Figure 4. Chondroprotective effects in primary human chondrocytes treated with Δ⁹-THCA-A. Cells were pre-treated with T0070907 (5 µM) or SR141716 (1 µM) before Δ⁹-THCA-A (5µM) treatment. Then, cells were stimulated with IL-1β (10ng/mL) for 48 h. Gene expression of **(A)** IL-6, **(B)** COX-2 and **(C)** iNOS was measured by qRT-PCR. Bar graphs represent mean ± SD from five experiments. Statistics: *$p < 0.05$, **$p < 0.01$ and ***$p < 0.001$

3.4. Δ⁹-THCA-A prevents CIA-induced inflammation *in vivo*

It has been suggested that pharmacological manipulation of ECS as well as PPARγ agonists may represent new therapeutic options for the management of inflammatory diseases including rheumatoid arthritis [98, 128, 130]. To study the therapeutic potential of Δ⁹-THCA-A on arthritis we used the murine CIA model (Fig. 5A), which is the most widely used model for preclinical evaluation of anti-arthritis drug candidates [184]. CIA induction resulted in a significant reduction in BW as well as an increase in arthritis score compared to control mice (Figure 5B, 5C). Δ⁹-THCA-A treatment on day 21 prevented the weight loss (Figure 5B) and severe arthritis development (Figure 5C). In addition, paw inflammation measured with a plethysmometer and a caliper at the end of treatment revealed the potent antiinflammatory activity of Δ⁹-THCA-A (Fig 5D and 5E), which was significantly prevented when the animals were cotreated with Δ⁹-THCA-A in the presence of either SR141716 or T0070907.
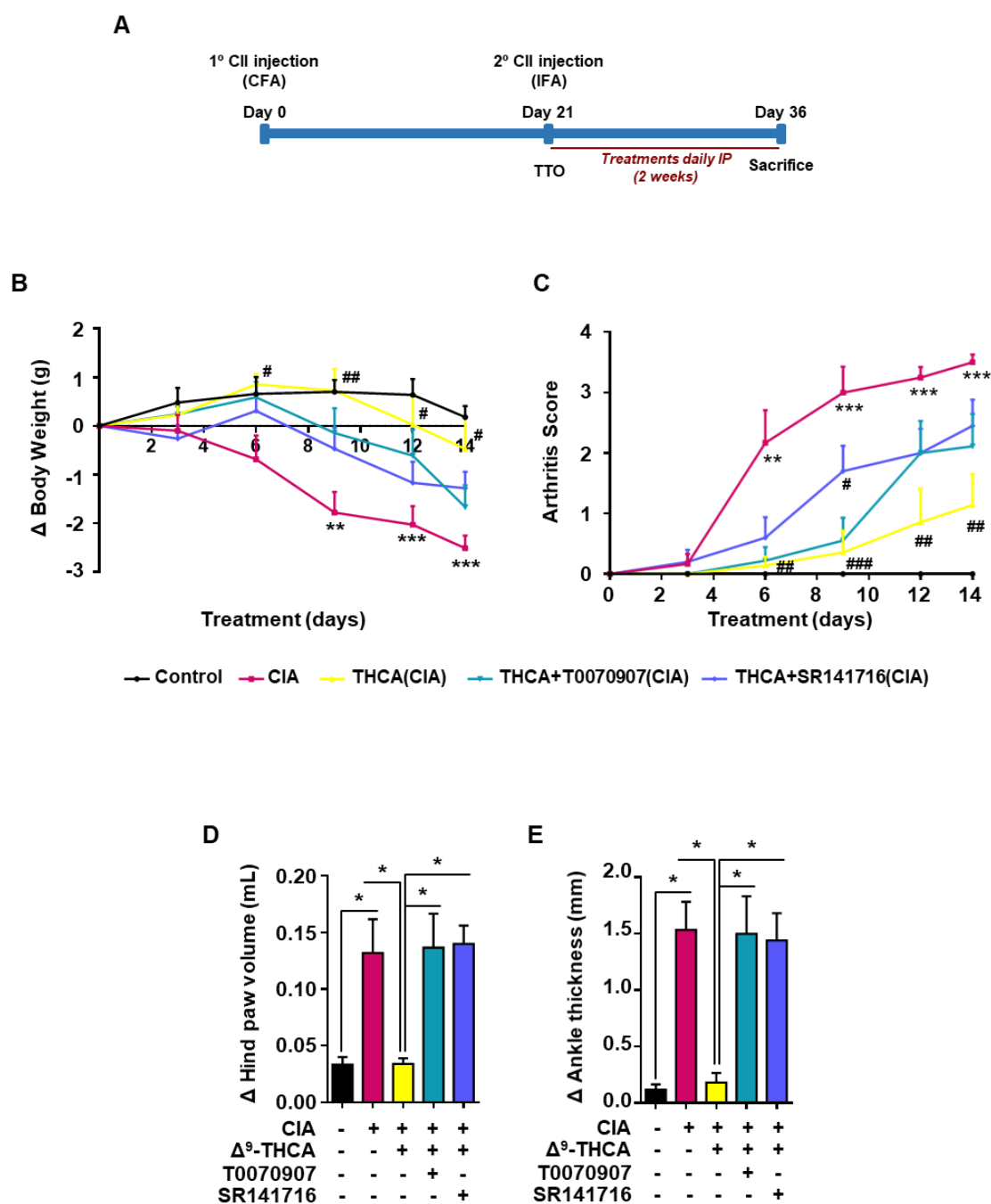
Figure 5. Effect of administration of Δ^9-THCA-A in a model of collagen-induced arthritis. (A) Timeline of treatments experiment in the CIA model. **(B)** Cumulative body weight change and **(C)** clinical scores in control mice, CIA-induced mice and treated mice during the treatment; values are referenced at the beginning of treatment (taken as 0). Measurement of paw swelling using a **(D)** plethysmometer and a **(E)** caliper at the end of the two-week treatment period. Data are means ± SEM (n= 9 mice per group). Statistics: For (B, C) **p<0.01 and ***p < 0.001 CIA mice vs. control mice; #p<0.05, ##p<0.01 and ###p<0.001 vehicle- or Δ^9-THCA-A+SR141716-treated CIA mice vs. Δ^9-THCA-A-treated CIA mice. For (D, E) *p<0.05, **p<0.01 and ***p<0.001.

The magnitude of joint inflammation and cartilage damage were examined by H&E and safranin O and toluidine blue staining, respectively. Knee histological analysis

showed that Δ^9-THCA-A prevented the pathological manifestations of RA that includes infiltration of inflammatory cells, synovial hyperplasia, pannus (H&E staining), and articular cartilage and proteoglycan loss (Safranin O and Toluidine blue staining) in comparison to the untreated CIA group (Figure 6A). In fact, the score for quantification of inflammation (H&E staining) and cartilage damage (Safranin O and Toluidine blue staining) reflected that the treatment with Δ^9-THCA-A presented evident anti-inflammatory (Figure 6B) and chondroprotective properties (Figure 6C). Again, the cotreatment with either T0070907 or SR141716 blocked the therapeutic effect of Δ^9-THCA-A. Altogether these results confirm that Δ^9-THCA-A is signalling through both CB_1 and PPARγ *in vivo*.

Next, to determine local inflammatory and catabolic changes, mRNA levels of specific cytokines, chemokines and immune markers (TNF-α, IL-1β, IL-6, IL-17, CXCL16, MCP-1, ICAM-1), proinflammatory mediators (COX-2, and iNOS) and catabolic markers (MMP-13 and ADAMTS5) linked to arthritis pathogenesis were assessed in the knee joints at the end of treatment. As depicted in Figure 7 the mRNA levels of TNF-α, IL-1β, IL-6, IL-17, CXCL16, MCP-1, ICAM-1, RANKL COX-2, iNOS and ADAMTS5 were significantly higher in the CIA group compared to control group. Moreover, levels of MMP-13 trended to increase in CIA mice, being all these results consistent with the joint damage associated to arthritis. Δ^9-THCA-A treatment resulted in a significant reduction of the upregulation of all the genes analyzed (Figure 7). However, this inhibitory activity of Δ^9-THCA-A on proinflammatory gene expression was clearly blocked by SR141716 treatment but not by T0070907 treatment, thus suggesting that CB_1 is the predominant target for Δ^9-THCA-A at articular level.

3.5. Effect of Δ^9-THCA-A on plasmatic biomarkers in CIA

CIA is an autoimmune disease and peripheral markers also correlate with disease severity. Thus, we studied the plasmatic levels and the presence of circulating anti-collagen antibodies at the end of treatment. The administration of CII caused a significant increase of IL-6 (Figure 8A), TNF-α (Figure 8B), IFNγ (Figure 8C) and IL-10 levels (Figure 8D), together with a weak elevation of IL-17 levels (Figure 8E). Δ^9-THCA-A treatment fully normalized IL-6 and TNF-α levels and partially reduced IFNγ, IL-17 and IL-10 concentrations. Notably, co-administration of T0070907 to Δ^9-THCA-A-treated CIA mice significantly increased IL-6, TNF-α, IFNγ and IL-10 levels. On the contrary,

SR141716 only trended to increase the levels of TNF-α. To further confirm the anti-arthritic activity of Δ^9-THCA-A, we analyzed the generation of anti-type II collagen antibody production, which plays a pathogenic role in CIA [185]. As shown in figure 8F, Δ^9-THCA-A treatment significantly reduced plasmatic levels of type II collagen IgG relative to those in CIA group, whereas the treatment with T0070907 and SR141716 prevented that reduction, although to a different extent.
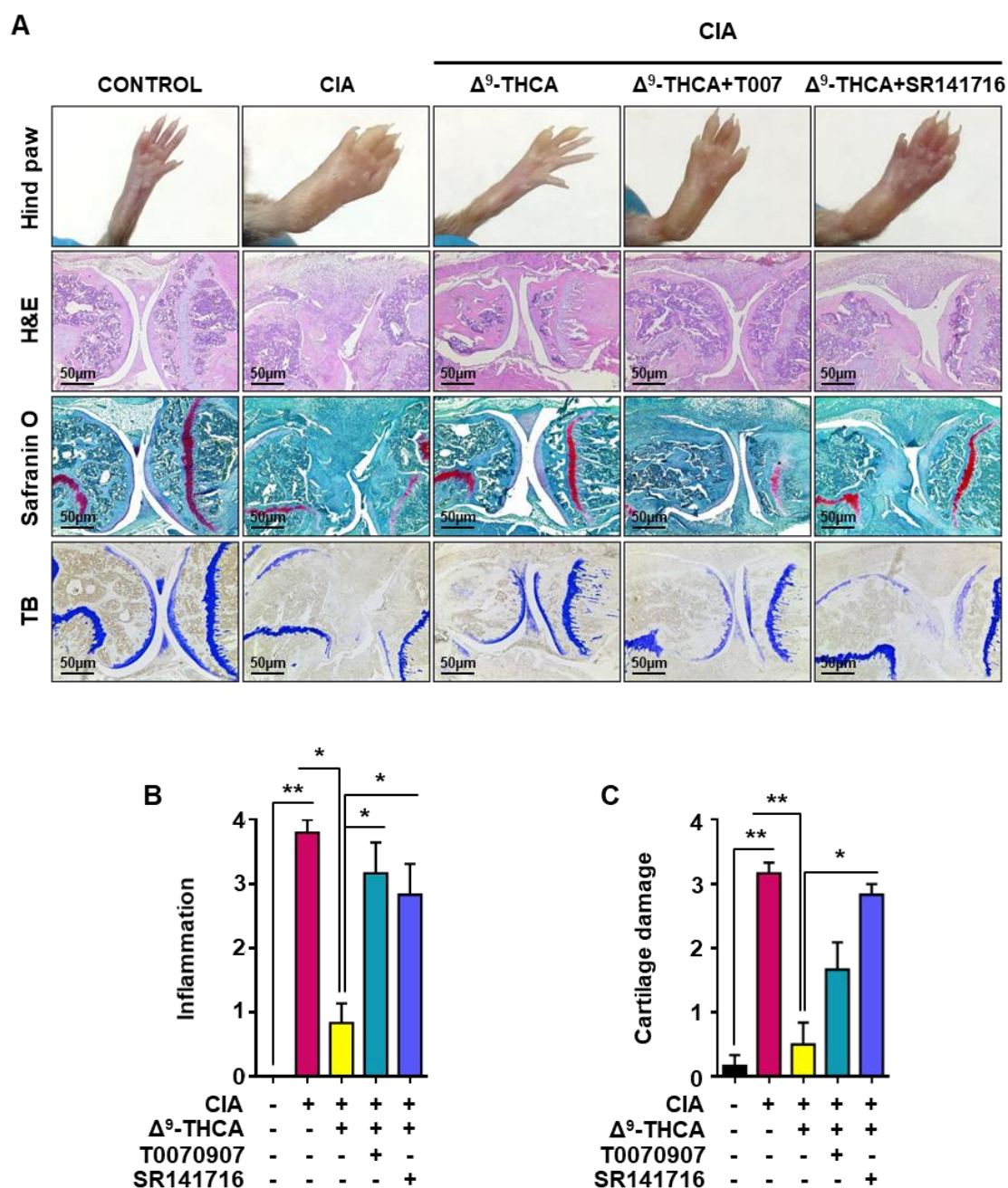
Figure 6. Effect of Δ^9-THCA-A on knee joints of the hind limbs in CIA mice. (A) Representative hind paw images and joint sections with hematoxylin and eosin (H&E), safranin O and toluidine blue staining (Original magnification 40X). (B) Scoring of histological inflammation was determined using the criteria described in material and methods. (C) Cartilage damage was evaluated based on safranin O and toluidine

blue staining according to the criteria described in materials and methods. Data are presented as mean ± SEM (n=9). Statistics: *p<0.05 and **p<0.01.
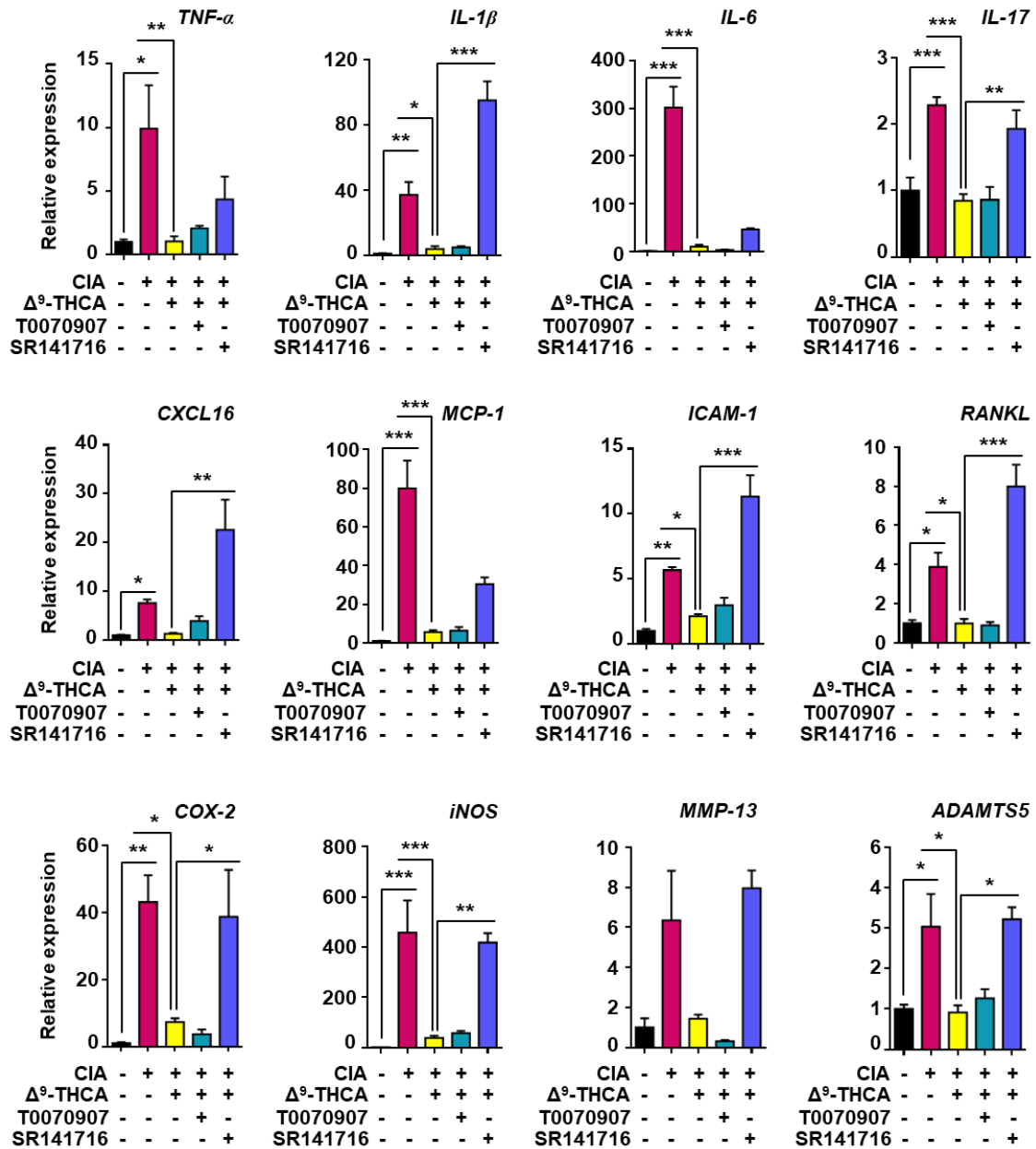
Figure 7. Effect of Δ⁹-THCA-A on the gene expression of inflammatory/catabolic markers in knee joints. qPCR analysis of cytokines, proinflammatory mediators and catabolic markers was performed on knee joints at the end of treatments. Results were obtained from nine mice per group and expressed as the mean ± SEM. Statistics: *p<0.05, **p<0.01 and ***p<0.001.
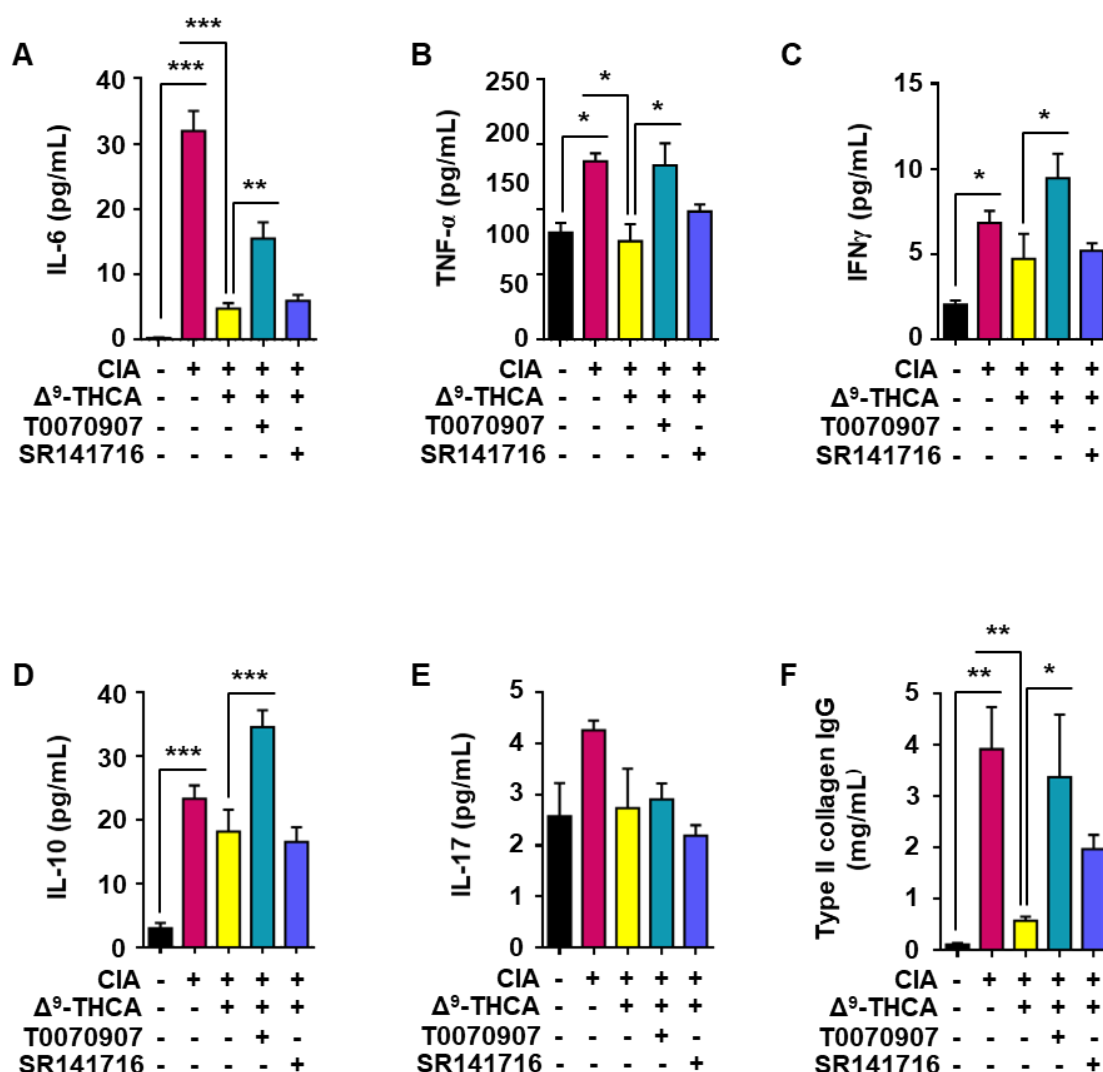
Figure 8. Effect of Δ⁹-THCA-A on circulating profile of immunomodulatory cytokines in a mouse model of collagen-induced arthritis. A panel of cytokines were assayed in control and CIA mice by multiplex immunoassay at the end of the period of treatment. The cytokines assayed were: **(A)** IL-6; **(B)** TNF-α; **(C)** IFNγ; **(D)** IL-10; **(E)** IL-17. In addition, **(F)** determination of total Ig antibodies against Type II Collagen by ELISA are shown for the five experimental groups. Values correspond to means ± SEM of nine mice per group. Statistics: *p<0.05, **p<0.01 and ***p<0.001.

Finally, we investigated the plasmatic proteomic profile in mice to identify disease biomarkers that can be modified by Δ⁹-THCA-A treatment. The analysis was performed by shotgun nLC-MS/MS followed by relative quantification by SWATH. As a result, 346 proteins were identified and quantified. Comparisons of data from different conditions against controls revealed an interesting profile where, from the 28 proteins altered by CIA, 27 normalized their levels in response to the Δ⁹-THCA-A treatment (adjusted P < 0.1 and absolute fold change > 2). Furthermore, the combination of the Δ⁹-THCA-A treatment with the antagonists of PPARγ or CB₁ produced again changes in 59 and 50

115

proteins, respectively, suggesting that the plasma proteomic profile is sensitive to the activity of both molecular targets (Figure 9A, 9B).
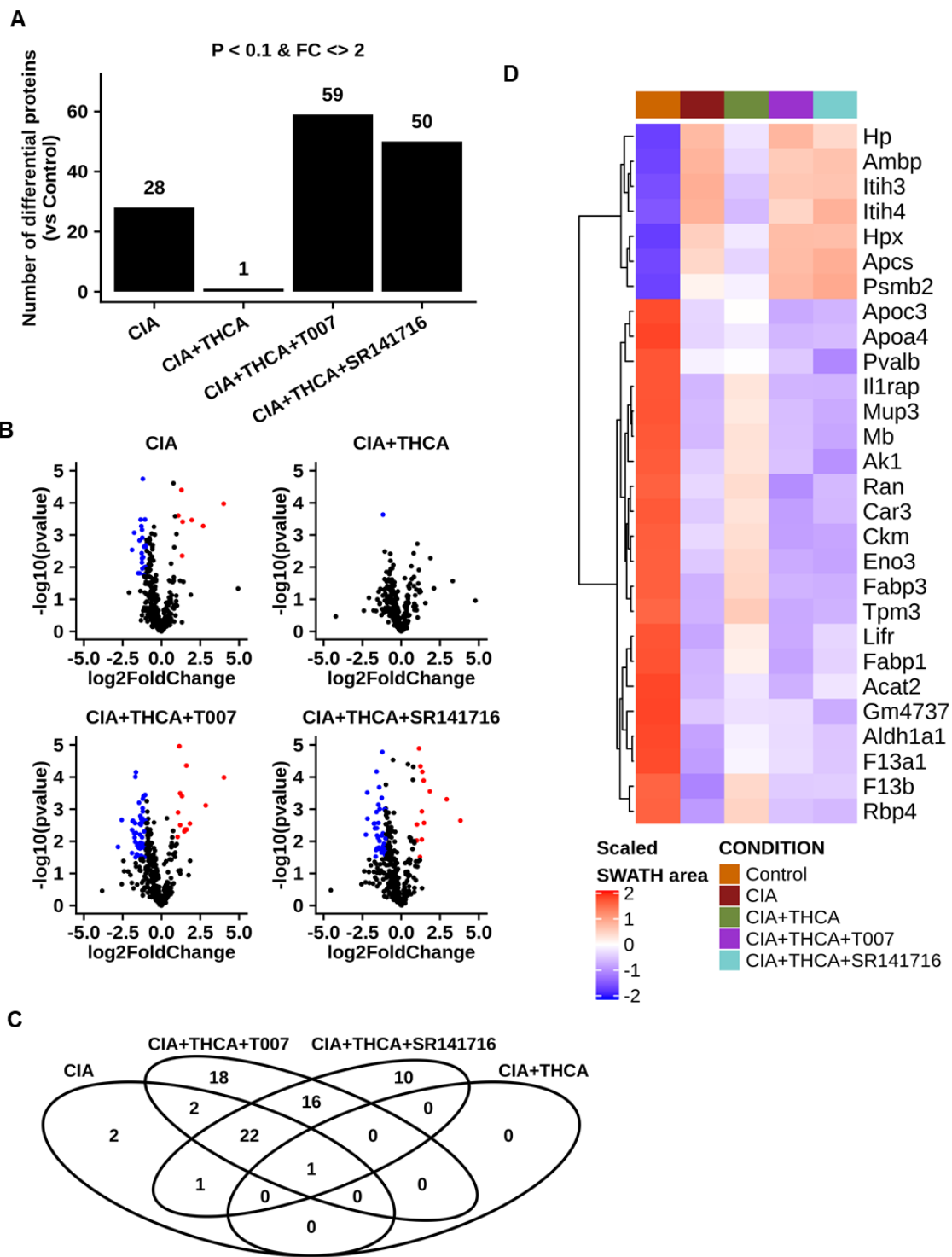
Figure 9. Proteomic analysis of Δ⁹-THCA-A effects in plasma of CIA mice. (**A**) Bar plot reflecting the number of proteins that surpass the cut-off of an adjusted P value < 0.1 and an absolute Fold Change > 2 in every comparison. (**B**) Volcano plots showing the magnitude and significance of the changes by comparison. Each point represents a protein and the colour indicate whether it is up (red) or down (blue) regulated, using the previously mentioned cut-off. (**C**) Venn diagram indicating the overlap between the

groups of altered proteins. The red box highlights the 22 common for CIA, CIA+THCA+T0070907 and CIA+THCA+SR141716. **(D)** Heatmap depicting the abundance of the 28 significantly altered proteins in the CIA versus control comparison. The colour reflects the scaled normalized SWATH areas mean by group. Representative data from six mice per group are shown.

Interestingly, from the 28 proteins mobilized by CIA, 22 were also altered when the Δ^9-THCA-A treatment was combined with any of the antagonists (Figure 9C). In this subset of 28 proteins which levels are depicted in the figure 9D heatmap, we could find some proteins related with the PPARγ signaling activity as the fatty acid binding proteins 1 and 3 (Fabp1 and Fabp3) and the apolipoproteins a1 and c3 (Apoa1 and Apoc3). Finally, a group of inter-alpha-trypsin inhibitors (Itih3, Itih4, Ambp) increased their levels in CIA and reduced them with the Δ^9-THCA-A treatment. The effect of Δ^9-THCA-A was also prevented in the presence of PPARγ or CB$_1$ antagonists.

3.6. Supplementary information
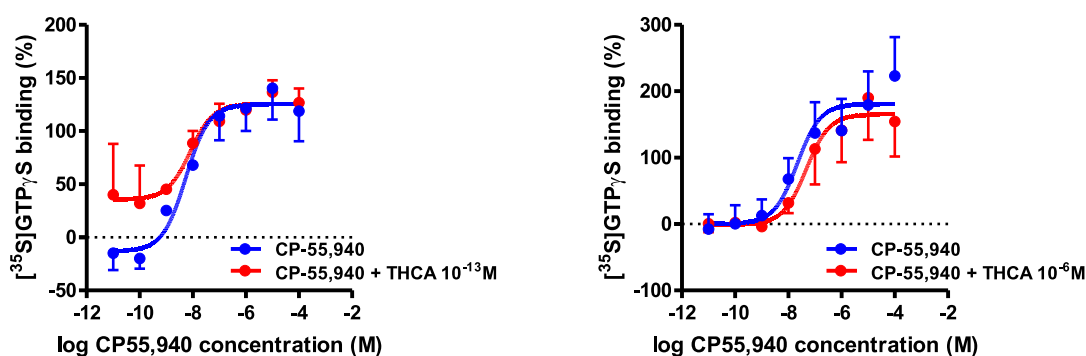
Figure S1. [^{35}S]-GTPγS binding stimulated by CP-55,940 (10^{-4}, 10^{-11} M) in the absence or presence of Δ^9-THCA-A (10^{-13} or 10^{-6} M). Data were expressed as mean ± SEM of at least five experiments performed in triplicate for each point, and were assessed by a two-way ANOVA followed by Bonferroni's posthoc test to compare CP-55,940 + Δ^9-THCA-A vs. CP-55,940 alone
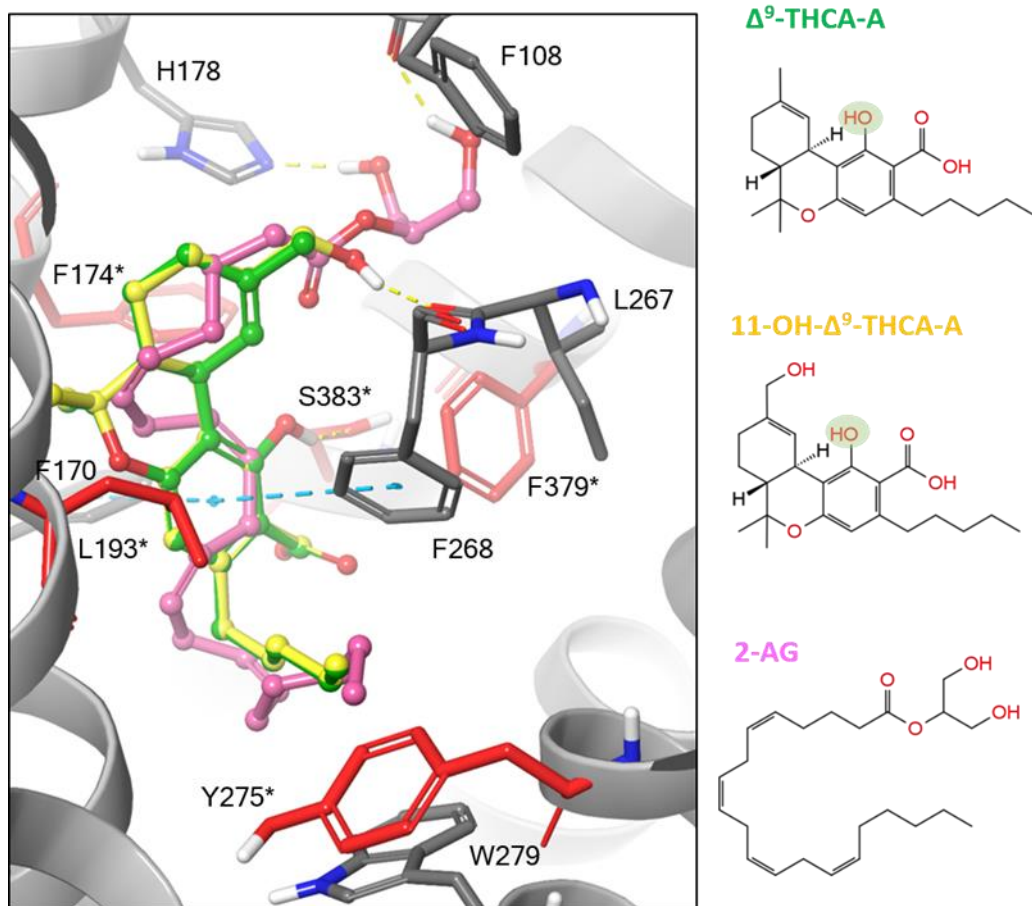
Figure S2. **Rigid (receptor) top docking results of Δ⁹-THC, 11-OH-Δ⁹-THC and 2-AG to the orthosteric site of CB₁ X-RAY structure PDB 5XR8.** Residues interacting with ligands are shown and important residues identified by mutagenesis experiments are depicted in red sticks and labeled with an asterisk. Color coding for Δ⁹-THCA-A, 11-OH-Δ⁹-THCA-A and 2-AG are in green, yellow and pink, respectively.

Discussion

Throughout its long history, the medicinal use of cannabis has been widely documented for the treatment of different diseases [2]. Currently, due to the successful research and the therapeutic properties of the cannabinoids there are several commercialized cannabinoid drugs containing synthetic or natural cannabinoids such as Cesamet, Sativex and Epidiolex that are used for the treatment of nauseas or neurophatic pain in cancer, spasticity in multiple sclerosis and epilepsies juveniles refractarias, respectively [186].

Cannabinoids, as exemplified by Δ^9-THC and CBD, are well known and clinically validated multi-target agents, whose biological profile can be modulated by structural modifications. Thus, CBD is a poor PPARγ agonist, unable to bind CB_2 and to activate the HIF pathway, but oxidation of its resorcinol core increases PPARγ binding, and the introduction of an additional nitrogen substituent beneficially affects chemical stability and induces CB_2 binding and PHDs inhibitory activity [60, 62]. A comprehensive investigation on the biological profile of these compounds (cannabinoid aminoquinones) showed that they could bind to both the canonical and the alternative sites of PPARγ, but also that PPARγ alone was unable to fully recap their biological profile, in accordance with their polypharmacology [67]. Eventually, the benzylamino adduct of the quinone form of CBD (VCE-004.8) emerged from these studies as a potential candidate for pleiotropic pharmacological interventions, and we present compelling evidence that VCE-004.8 has potential for the management of obesity and MetS, being capable to positively affect all the main manifestations of the disease.

On the other hand, Δ^9-THC is a partial agonist with a high affinity at CB_1 and CB_2 receptors and, in addition, it shows a weak affinity at PPARγ. We provide evidence that, contrary to Δ^9-THC, Δ^9-THCA-A is at least 20-fold more potent than Δ^9-THC to activate PPARγ and may exert its PPARγ activity by acting at both canonical and alternative binding sites of the PPARγ LBD [13]. However, in FRET assays we found that Δ^9-THCA-A does not affect PPARγ co-regulators interaction. Nevertheless, it has been shown that others partial agonists such as INT131 and BVT-13 do not induce significant binding or displacement of PPARγ co-regulators indicating that recruitment co-activators is not essential for the signalling pathways activated partial PPARγ agonists such as Δ^9-THCA-A as opposite to full PPARγ agonists [187-189].

Thus, our *in vitro* and *in vivo* data strongly suggest that the binding of Δ^9-THCA-A to the PPARγ orthosteric site accounts for most of its effects via this nuclear receptor. However, signaling through the alternative site or other pathways could also be of biological relevance; in lean mice, 317 genes were modified by Δ^9-THCA-A but unaffected by T0070907. Whether this pathway is linked or not to the PPARγ alternative site or to other pathways, such as CB1 signaling, remains to be investigated.

Moreover, *in silico* and *in vitro* results demonstrated for the first time that Δ^9-THCA-A can act as a functional orthosteric and also as a PAM of CB_1. For instance, Δ^9-THCA-A induced ERK 1/2 phosphorylation with the same potency than CP-55,940 and this activity is blocked in the presence of SR141716. However, Δ^9-THCA-A did not activate the cAMP pathway nor induced β-arrestin recruitment but increased these activities induced by CP-55,940 confirming the PAM nature of Δ^9-THCA-A. In this sense, Δ^9-THCA-A may bind to the CB_1 allosteric sites when the orthosteric site is occupied by the endogenous CB_1 ligand 2-Arachidonoyl Glycerol (2-AG) (supplemental Figure 2). Although docking experiments strongly suggest that THCA-A may bind to specific allosteric sites further experiments will be required to validate this finding. Our working hypothesis is that Δ^9-THCA-A, as well as its metabolite 11-OH-Δ^9-THCA-A (supplemental Figure 2), could bind to the orthosteric site of CB_1 with lower affinity than full CB_1 agonists and then can be displaced to the allosteric sites when full agonists such as CP-55,940 and 2-AG are occupying the orthosteric site

In the *in vivo* animal experiments, Δ^9-THCA-A successfully show a potential therapeutic effect in inflammatory diseases as we have observed in a model of diet-induced obesity, ameliorating adiposity and reversed the metabolic and inflammatory complications associated to metabolic syndrome (MetS) and in a model of collagen-induced arthritis, preventing joint swelling and avoiding cartilage damage.

1. Therapeutic potential of VCE-004.8 and Δ^9-THCA-A in obesity

Obesity and MetS are reaching pandemic proportions worldwide, and their associated co-morbidities represent an enormous medical and economic burden for our society [190]. The recognition of the multi-factor nature of these diseases and the involvement of numerous deregulated signalling systems in their insurgence have prompted the search of strategies based on poly-pharmaceutical agents that simultaneously target various key pharmacological end-points [191, 192]. This

polyvalent approach is less prone to the complications associated to multi-drug therapies and has the potential to alleviate the combined deregulation of different factors (food intake, glucose metabolism, energy expenditure) associated to the insurgence of MetS and its complications.

Glitazones, such as RGZ, are synthetic full PPARγ agonists that have been used for decades for the treatment of type-2 diabetes. However, the use of glitazones in diabetic patients has dropped significantly over the past years due to a series of adverse side effects that include bone loss and osteoporosis, as well as fluid retention. Bone loss could be bound to the effect of glitazones on the lineage commitment of MSC towards osteoblasts and adipocytes, as RGZ has been shown to suppress osteoblastogenesis and induce adipocyte differentiation [36]. The development of more balanced, partial PPARγ agonists, devoid of the side effects showed by the currently marketed PPARγ full agonists, is considered a major challenge for drug discovery [37]. We demonstrate that both VCE-004.8 and Δ^9-THCA-A are partial PPARγ agonists with a lower adipogenic capacity than glitazones that do not inhibit osteoblastogenesis. In fact, Δ^9-THCA-A even showed osteoblastogenesis-enhancing properties.

Conclusive evidence for the optimal profile of VCE-004.8 and Δ^9-THCA-A in the management of metabolic disease came from our pharmacological studies in a validated murine model of HFD-induced obesity and its associated complications. Indeed, male mice fed on HFD for up to 15-weeks displayed all cardinal manifestations of obesity and its major complications, including increased BW, increased calorie intake, increased fat mass, adipocyte area and adiposity index, hepatic steatosis, elevated serum triglycerides, increased basal glucose and insulin levels, as well as perturbed glucose tolerance and insulin resistance. Chronic treatment with a single daily dose of VCE-004.8 and Δ^9-THCA-A for three weeks was sufficient to revert nearly all of these adverse metabolic alterations, causing a marked suppression of body weight gain, fat mass and adiposity, significantly lowering basal glucose and insulin levels, and significantly improving HFD-induced glucose intolerance and insulin resistance. Moreover, circulating triglyceride levels were normalized and steatosis scores were substantially reduced by 3-wk VCE-004.8 and Δ^9-THCA-A treatment in HFD mice, substantially reversing the metabolic phenotype caused by the high fat content diet and defining an ideal profile for the design of novel pharmacological treatments based on both VCE-004.8 or its derivatives and Δ^9-THCA-A.

A beneficial impact on additional hormonal alterations associated to MetS was also observed in the HFD rodent model of obesity and MetS. In the first model, in addition to basal hyperinsulinemia, mice fed HFD for 15 weeks showed significantly increased leptin and PAI-1 levels, together with lower circulating concentrations of adiponectin, ghrelin and glucagon. While some of these endocrine perturbations might be compensatory, others, such as the enhanced leptin and reduced adiponectin levels, could potentially contribute to the metabolic alterations associated to obesity [193, 194]. Notably, repeated administration of VCE-004.8 to HFD mice decreased leptin and increased adiponectin levels; with an overall change in the leptin-to-adiponectin ratio that could rationalize the observation of an improved glycemic profile [194]. Furthermore, VCE-004.8 could also lower resistin levels in HFD mice, further contributing to the decrease of insulin resistance. Interestingly, the body weight loss caused by VCE-004.8 in HFD mice, was not associated to an elevation of serum levels of ghrelin, thus preventing ghrelin-induced compensatory hyperphagic responses, and a worsening of insulin resistance [195, 196]. On the other hand, the effect of VCE-004.8 on PAI-1 levels is striking and may reflect the effect of this cannabidiol aminoquinone on the HIF pathway activation [197]. Although this observation cannot be underestimated in terms of future clinical development, neither micro-vascular thrombosis episodes nor coagulation alterations have been reported for other PHDs inhibitors in preclinical models or Phase 2/3 clinical trials [147, 198].

In the second model, the major hormonal and cytokine alterations caused by HFD were reversed by Δ^9-THCA-A, with a significant decrease in circulating leptin and glucagon, and a significant increase in serum GLP-1 and adiponectin levels. Such a switch towards an anti-inflammatory state was also detected by our adipo-/cytokine arrays, which confirmed the reversal of most of the pro-inflammatory humoral alterations caused by HFD. Linking obesity and inflammation, Δ^9-THCA-A showed a very potent anti-inflammatory profile in HFD mice. Activation of innate and adaptive immune response has been observed in the fat tissue of obese individuals [199-201], and we identified 70 upregulated genes linked to NF-κB and cytokine-cytokine-receptor signaling, whose expression was largely prevented by treatment with Δ^9-THCA-A. Within them, T- and B cell markers, as well as macrophage-derived cytokines and chemokines, were identified, showing that both the innate and the adaptive immune responses account for the inflammatory status in the fat tissue of HFD mice. There is strong evidence that PPARγ

inhibits NF-κB activation through several mechanisms, repressing NF-κB-mediated transcription of pro-inflammatory cytokines in immune and non-immune cells [202]. Thus, Δ^9-THCA-A could dampen inflammation mainly through the PPARγ pathway, opening the possibility of the use of this phytocannabinoid in other chronic or acute inflammatory diseases.

Interestingly, the beneficial effects of VCE-004.8 and Δ^9-THCA-A were not only observed in HFD conditions, but also, albeit to a lesser extent, in lean animals fed a control diet, in which 3-wk treatment with VCE-004.8 and Δ^9-THCA-A was capable to reduce body weight and adiposity, as well as basal glucose and insulin, together with a significant enhancement of glucose tolerance and insulin sensitivity in the absence of obesogenic challenges. In addition, Δ^9-THCA-A also reduced triglyceride levels. All these features define an optimal pharmacological profile of VCE-004.8 and Δ^9-THCA-A for globally handling the metabolic syndrome linked to obesity.

The beneficial effects of Δ^9-THCA-A on body weight and metabolic status are somewhat at odds with the reported orexigenic and lipogenic activity of cannabinoids [80, 203]. In our studies, Δ^9-THCA-A failed to cause any detectable change in food intake, supporting a distinct pharmacological profile compared to Δ^9-THC, whose feeding-promoting effects underlie its use in the management of cachexia [204]. The lack of orexigenic effect together with the substantial body weight loss induced by Δ^9-THCA-A suggests a potential use of this compound to induce adaptive thermogenesis. Indeed, chronic treatment with Δ^9-THCA-A caused the upregulation of a large set of genes belonging of the thermogenesis pathway, with a prominent increase in the UCP-1 content in iWAT form lean and HFD mice. Altogether, these findings suggest that, acting at least partially via PPARγ, Δ^9-THCA-A causes browning of the white adipose tissue, and this activity could mechanistically underlie at least some of its beneficial effects on energy and metabolic homeostasis. Notwithstanding, it cannot be excluded that the 11-carboxylic metabolites of Δ^9-THCA-A, known to be produced in vivo [10], may mediate at least part of the metabolic effect of Δ^9-THCA-A administration in our obese, HFD mice.

We also observed an enhanced thermogenesis after the administration of VCE-004.8 to lean mice with an increased UCP-1 expression in iWAT as well as an elevation of incretin (GIP and GLP-1) levels. Similar to Δ^9-THCA-A, these beneficial effects on the metabolic profile took place in the absence of detectable changes in calorie intake,

suggesting the induction of mechanisms for body weight loss and metabolic improvement independent on feeding. The direct and indirect insulinotropic activity of VCE-004.8 is of special interest and warrants further investigation. In this context, it is worth considering that HIF-1α stabilization mediates insulin secretion by pancreatic β cells [205] and accordingly we found that VCE-004.8 induced HIF-1α and insulin secretion in the pancreatic acinar-derived AR42J cells. Moreover, GIP and GLP-1 have been target of pleiotropic strategies to improve the management of metabolic syndrome [191, 192]. Since the stimulatory effects of VCE-004.8 on GIP and GLP-1 were lost in obese animals, a state of resistance to its incretin-secretagogue actions might be associated to obesity, and the elusive mechanistic bases for this effect are worth further investigation.

Our studies also unveiled that VCE-004.8 influences the gene expression and circulating levels of FGF21, as putative mechanism for some of its metabolic effects. In recent years, FGF21 has emerged as master regulator of body weight, glucose homeostasis and insulin sensitivity [206, 207], being produced in various key metabolic tissues, including the liver and BAT. Our data document the ability of VCE-004.8 to induce FGF21 expression in BAT and iWAT of lean mice in vivo, and to enhance FGF21 mRNA levels in a murine BAT cell line in vitro. These findings are in line with previous reports showing that PPARγ ligands can enhance FGF21 expression in adipose tissues [178, 206]. Notably, in lean individuals, FGF21 has been shown to increase insulin sensitivity [207]. Thus, the above stimulatory responses may contribute to the improved glycemic profile of lean mice treated with VCE-004.8. Intriguingly, while fasting is known to potently enhance FGF21 levels, as major mechanisms to coordinate adaptive responses to starvation [208], obesity has been shown to cause also an enhancement of FGF21 levels in rodents and humans [176, 177], suggesting a state of "FGF21 resistance", defined by elevated FGF21 levels and impaired FGF21 receptor function [209], which might contribute to the aggravation of metabolic state in conditions of obesity. In good agreement, in our studies, HFD caused an elevation of FGF21 levels, associated to increased FGF21 mRNA expression in liver and WAT, while VCE-004.8 administration normalized serum FGF21 concentrations and iWAT FGF21 gene expression; the latter is compatible with an alleviation of the state of FGF21 resistance linked to obesity. Admittedly, however, the effects of VCE-004.8 on FGF21 appear to be tissue-specific, since it did not enhance FGF21 expression in the liver and eWAT of lean mice nor did it normalize FGF21 mRNA levels in these tissues in HFD animals.

Altogether, our findings establish that VCE-004.8 and Δ^9-THCA-A mainly through specific targeting of PPARγ, as well as other, including CB_1, CB_2 and HIF pathway, could represent a potential therapeutic approach to obesity and metabolic diseases, without the harmful effects on adipogenesis and osteoblastogenesis associated with PPARγ full agonists.

2. Therapeutic potential of Δ^9-THCA-A in arthritis

RA has become a prototype of inflammatory autoimmune disease in which an early diagnosis and treatment, well-known as "therapeutic window of opportunity", trigger favourable outcomes [210, 211]. Following CIA immunization, the mice develop an immunologic hypersensitivity to type II collagen, preceding an immune reaction in lymph nodes to the development of synovial inflammation and joint damage [212]. We have reported previously that Δ^9-THCA-A binds and activates PPARγ and exerted potent antiinflammatory activities in the CNS and in peripherical inflammatory conditions. [13, 213]. However, the biological activity of Δ^9-THCA-A through CB_1 receptor has been poorly investigated *in vivo*. Nevertheless, it has been shown that the anti-emetic activity of Δ^9-THCA-A in shrews is prevented by coadministration of SR141716 [18]. Our results showed the efficacy of the non-psychotropic cannabinoid Δ^9-THCA-A as anti-arthritic treatment in mice through CB_1 and PPARγ dependent pathways.

Regarding our docking studies, Δ^9-THCA-A can act as PAM for CB_1 in disease conditions where 2-AG levels are elevated. In this sense elevated levels of 2-AG have been found in the synovial liquid of arthritis patients and in animal models [101, 214]. Accordingly, our data suggest that Δ^9-THCA-A could be maintaining the balance between the catabolic activities of matrix metalloproteinases and its inhibitors by acting as a PAM for CB_1 and increasing the effect of endocannabinoids such as 2-AG [215]. For instance the inhibition of inflammatory cytokines such as IL-1β and TNF-α may prevent the expression of MMPs and ADAMPs by chondrocytes and inflammatory cell infiltrated in the synovium [215]. Although most of Δ^9-THCA-A action mechanism in joint inflammation and degeneration seems to be mediated through a CB_1 dependent pathway, we also found that Δ^9-THCA-A also has anti-arthritis activity by acting through PPARγ. Herein we demonstrated that Δ^9-THCA-A showed a pattern of systemic protection, reducing the circulation of pro-inflammatory cytokines as well as the generation of anti-CII antibodies in CIA mice. These results suggest a potential peripheral role for Δ^9-

THCA-A in regulating B and T cell response in lymph nodes that can be mediated through a PPARγ dependent pathway.

Several studies have identified some potential plasmatic biomarkers as reflect of pathological processes in RA patients [216]. Furthermore, these biomarkers may be used for prediction of response to therapy and disease prognosis. Notably, one of the strengths of this study is the use of SWATH-MS as a tool for predicting Δ^9-THCA-A response in mice and perhaps in patients [217]. We identified 27 plasmatic proteins in CIA mice whose levels where totally reverted with Δ^9-THCA-A treatment through PPARγ and CB$_1$ activation. Interestingly, our study revealed a preventive effect over inter-alpha-trypsin inhibitor heavy chain H3/4 (Itih3/Itih4) and proteasome subunit beta type-2 (Pmbs2) whose increased concentration in sera of patients with RA were associated with disease activity and used as specific biomarkers [218, 219]. In addition, Δ^9-THCA-A treatment also prevented the secretion of acute-phase proteins, including hemopexin (Hpx) and haptoglobin (Hp), synthesized in response to a proinflammatory milieu [220, 221]. These proteins as well as alpha-1-microglobulin/bikunin precursor (Ambp) are directly involved in the regulation of heme/iron metabolism [222, 223], which has been found to be frequently dysregulated in chronic inflammatory diseases such as RA [224] [225]. Δ^9-THCA-Atreatment also normalized the plasmatic levels of serum amyloid P component (Apcs) in CIA mice and elevated levels of Apcs have been also found in RA patients and in those who have amyloidosis associated with a rheumatic disease [226].

Finally, taken together these results demonstrate that Δ^9-THCA-A is acting peripherally through CB$_1$ and PPARγ signaling pathways. The lack of psychotropic activity of Δ^9-THCA-A may be explained by its binding mode to CB$_1$ and the low CNS penetration of acidic cannabinoids [227]. Altogether, these features add to our current efforts to identify pharmacological agents capable to have anti-arthritis without undesired side effects and suggest that Δ^9-THCA-A, as well as non-decarboxylated *Cannabis sativa* extracts, are worth of consideration for the management of rheumatic diseases and perhaps other inflammatory and autoimmune diseases.

Conclusions

1. The cannabidiol derivative VCE-004.8 and Δ^9-THCA-A are selective partial PPARγ agonists capable to interact with the orthosteric and allosteric PPARγ LBD binding sites.

2. VCE-004.8 and Δ^9-THCA-A are lower adipogenic than full ligand PPARγ agonists.

3. Δ^9-THCA-A enhances osteoblastogenesis *in vitro*.

4. Δ^9-THCA-A modulates CB_1 receptor through the orthosteric and allosteric binding sites.

5. VCE-004.8 and Δ^9-THCA-A alleviates metabolic perturbations and inflammatory parameters associated to obesity in a murine model of high-fat diet-induced obesity.

6. Δ^9-THCA-A exerts chondroprotective and anti-inflammatory activities in a murine model of collagen induced arthritis.

References

1. Russo, E.B., et al., *Phytochemical and genetic analyses of ancient cannabis from Central Asia.* J Exp Bot, 2008. **59**(15): p. 4171-82.

2. Brill, H., *Marihuana: The First Twelve Thousand Years.* J Psychoactive Drugs, 1981. **13**(4): p. 397-398.

3. Jeong, M., et al., *Hempseed oil induces reactive oxygen species- and C/EBP homologous protein-mediated apoptosis in MH7A human rheumatoid arthritis fibroblast-like synovial cells.* J Ethnopharmacol, 2014. **154**(3): p. 745-52.

4. Bonini, S.A., et al., *Cortical Structure Alterations and Social Behavior Impairment in p50-Deficient Mice.* Cereb Cortex, 2016. **26**(6): p. 2832-49.

5. Bastola, K.P., A. Hazekamp, and R. Verpoorte, *Synthesis and spectroscopic characterization of cannabinolic acid.* Planta Med, 2007. **73**(3): p. 273-5.

6. Andre, C.M., J.F. Hausman, and G. Guerriero, *Cannabis sativa: The Plant of the Thousand and One Molecules.* Front Plant Sci, 2016. **7**: p. 19.

7. Degenhardt, F., F. Stehle, and O. Kayser, *The Biosynthesis of Cannabinoids.* Handbook of Cannabis and Related Pathologies, ed. V. Preedy. 2017.

8. Hartsel, J.A., et al., *Cannabis sativa and Hemp.* Nutraceuticals. 2016.

9. Wang, M., et al., *Decarboxylation Study of Acidic Cannabinoids: A Novel Approach Using Ultra-High-Performance Supercritical Fluid Chromatography/Photodiode Array-Mass Spectrometry.* Cannabis Cannabinoid Res, 2016. **1**(1): p. 262-271.

10. Moreno-Sanz, G., *Can You Pass the Acid Test? Critical Review and Novel Therapeutic Perspectives of Delta(9)-Tetrahydrocannabinolic Acid A.* Cannabis Cannabinoid Res, 2016. **1**(1): p. 124-130.

11. Raikos, N., et al., *Determination of Delta9-tetrahydrocannabinolic acid A (Delta9-THCA-A) in whole blood and plasma by LC-MS/MS and application in authentic samples from drivers suspected of driving under the influence of cannabis.* Forensic Sci Int, 2014. **243**: p. 130-6.

12. Ibrahim, E.A., et al., *Determination of Acid and Neutral Cannabinoids in Extracts of Different Strains of Cannabis sativa Using GC-FID.* Planta Med, 2018. **84**(4): p. 250-259.

13. Nadal, X., et al., *Tetrahydrocannabinolic acid is a potent PPARgamma agonist with neuroprotective activity.* Br J Pharmacol, 2017. **174**(23): p. 4263-4276.

14. Ruhaak, L.R., et al., *Evaluation of the cyclooxygenase inhibiting effects of six major cannabinoids isolated from Cannabis sativa.* Biol Pharm Bull, 2011. **34**(5): p. 774-8.

15. Verhoeckx, K.C., et al., *Unheated Cannabis sativa extracts and its major compound THC-acid have potential immuno-modulating properties not mediated by CB1 and CB2 receptor coupled pathways.* Int Immunopharmacol, 2006. **6**(4): p. 656-65.

16. Moldzio, R., et al., *Effects of cannabinoids Delta(9)-tetrahydrocannabinol, Delta(9)-tetrahydrocannabinolic acid and cannabidiol in MPP+ affected murine mesencephalic cultures.* Phytomedicine, 2012. **19**(8-9): p. 819-24.

17. Ligresti, A., et al., *Antitumor activity of plant cannabinoids with emphasis on the effect of cannabidiol on human breast carcinoma.* J Pharmacol Exp Ther, 2006. **318**(3): p. 1375-87.

18. Rock, E.M., et al., *Tetrahydrocannabinolic acid reduces nausea-induced conditioned gaping in rats and vomiting in Suncus murinus.* Br J Pharmacol, 2013. **170**(3): p. 641-8.

19. Ligresti, A., L. De Petrocellis, and V. Di Marzo, *From Phytocannabinoids to Cannabinoid Receptors and Endocannabinoids: Pleiotropic Physiological and Pathological Roles Through Complex Pharmacology.* Physiol Rev, 2016. **96**(4): p. 1593-659.

20. Rock, E.M., et al., *A comparison of cannabidiolic acid with other treatments for anticipatory nausea using a rat model of contextually elicited conditioned gaping.* Psychopharmacology (Berl), 2014. **231**(16): p. 3207-15.

21. Rock, E.M., C.L. Limebeer, and L.A. Parker, *Effect of combined doses of Delta(9)-tetrahydrocannabinol (THC) and cannabidiolic acid (CBDA) on acute*

and anticipatory nausea using rat (Sprague- Dawley) models of conditioned gaping. Psychopharmacology (Berl), 2015. **232**(24): p. 4445-54.

22.   Izzo, A.A., et al., *Non-psychotropic plant cannabinoids: new therapeutic opportunities from an ancient herb.* Trends Pharmacol Sci, 2009. **30**(10): p. 515-27.

23.   Navarro, G., et al., *Cannabigerol Action at Cannabinoid CB1 and CB2 Receptors and at CB1-CB2 Heteroreceptor Complexes.* Front Pharmacol, 2018. **9**: p. 632.

24.   Vemuri, V.K. and A. Makriyannis, *Medicinal chemistry of cannabinoids.* Clin Pharmacol Ther, 2015. **97**(6): p. 553-8.

25.   Pertwee, R.G., *Cannabinoid pharmacology: the first 66 years.* Br J Pharmacol, 2006. **147 Suppl 1**: p. S163-71.

26.   Howlett, A.C., et al., *International Union of Pharmacology. XXVII. Classification of cannabinoid receptors.* Pharmacol Rev, 2002. **54**(2): p. 161-202.

27.   Ibsen, M.S., M. Connor, and M. Glass, *Cannabinoid CB1 and CB2 Receptor Signaling and Bias.* Cannabis Cannabinoid Res, 2017. **2**(1): p. 48-60.

28.   Zou, S. and U. Kumar, *Cannabinoid Receptors and the Endocannabinoid System: Signaling and Function in the Central Nervous System.* Int J Mol Sci, 2018. **19**(3).

29.   Mechoulam, R. and L.A. Parker, *The endocannabinoid system and the brain.* Annu Rev Psychol, 2013. **64**: p. 21-47.

30.   Mackie, K., *Distribution of cannabinoid receptors in the central and peripheral nervous system.* Handb Exp Pharmacol, 2005(168): p. 299-325.

31.   Maccarrone, M., et al., *Endocannabinoid signaling at the periphery: 50 years after THC.* Trends Pharmacol Sci, 2015. **36**(5): p. 277-96.

32.   Montecucco, F. and V. Di Marzo, *At the heart of the matter: the endocannabinoid system in cardiovascular function and dysfunction.* Trends Pharmacol Sci, 2012. **33**(6): p. 331-40.

33.   Devane, W.A., et al., *Isolation and structure of a brain constituent that binds to the cannabinoid receptor.* Science, 1992. **258**(5090): p. 1946-9.

34.   Mechoulam, R., et al., *Identification of an endogenous 2-monoglyceride, present in canine gut, that binds to cannabinoid receptors.* Biochem Pharmacol, 1995. **50**(1): p. 83-90.

35.   Lu, H.C. and K. Mackie, *An Introduction to the Endogenous Cannabinoid System.* Biol Psychiatry, 2016. **79**(7): p. 516-25.

36.   Morales, P. and P.H. Reggio, *An Update on Non-CB1, Non-CB2 Cannabinoid Related G-Protein-Coupled Receptors.* Cannabis Cannabinoid Res, 2017. **2**(1): p. 265-273.

37.   Dutertre, S., C.M. Becker, and H. Betz, *Inhibitory glycine receptors: an update.* J Biol Chem, 2012. **287**(48): p. 40216-23.

38.   Ahrens, J., et al., *The nonpsychotropic cannabinoid cannabidiol modulates and directly activates alpha-1 and alpha-1-Beta glycine receptor function.* Pharmacology, 2009. **83**(4): p. 217-22.

39.   Xiong, W., et al., *Cannabinoid potentiation of glycine receptors contributes to cannabis-induced analgesia.* Nat Chem Biol, 2011. **7**(5): p. 296-303.

40.   Xiong, W., et al., *Cannabinoids suppress inflammatory and neuropathic pain by targeting alpha3 glycine receptors.* J Exp Med, 2012. **209**(6): p. 1121-34.

41.   Caterina, M.J., *TRP channel cannabinoid receptors in skin sensation, homeostasis, and inflammation.* ACS Chem Neurosci, 2014. **5**(11): p. 1107-16.

42.   De Petrocellis, L., et al., *Effects of cannabinoids and cannabinoid-enriched Cannabis extracts on TRP channels and endocannabinoid metabolic enzymes.* Br J Pharmacol, 2011. **163**(7): p. 1479-94.

43.   De Petrocellis, L., et al., *Actions and Regulation of Ionotropic Cannabinoid Receptors.* Adv Pharmacol, 2017. **80**: p. 249-289.

44.   Qin, N., et al., *TRPV2 is activated by cannabidiol and mediates CGRP release in cultured rat dorsal root ganglion neurons.* J Neurosci, 2008. **28**(24): p. 6231-8.

45.   Nabissi, M., et al., *Triggering of the TRPV2 channel by cannabidiol sensitizes glioblastoma cells to cytotoxic chemotherapeutic agents.* Carcinogenesis, 2013. **34**(1): p. 48-57.

46.   De Petrocellis, L., et al., *Cannabinoid actions at TRPV channels: effects on TRPV3 and TRPV4 and their potential relevance to gastrointestinal inflammation.* Acta Physiol (Oxf), 2012. **204**(2): p. 255-66.

47.   O'Sullivan, S.E., *An update on PPAR activation by cannabinoids.* Br J Pharmacol, 2016. **173**(12): p. 1899-910.

48.   Pisanti, S., et al., *Cannabidiol: State of the art and new challenges for therapeutic applications.* Pharmacol Ther, 2017. **175**: p. 133-150.

49.   Hind, W.H., T.J. England, and S.E. O'Sullivan, *Cannabidiol protects an in vitro model of the blood-brain barrier from oxygen-glucose deprivation via PPARgamma and 5-HT1A receptors.* Br J Pharmacol, 2016. **173**(5): p. 815-25.

50.   Iseger, T.A. and M.G. Bossong, *A systematic review of the antipsychotic properties of cannabidiol in humans.* Schizophr Res, 2015. **162**(1-3): p. 153-61.

51.   Bergamaschi, M.M., et al., *Cannabidiol reduces the anxiety induced by simulated public speaking in treatment-naive social phobia patients.* Neuropsychopharmacology, 2011. **36**(6): p. 1219-26.

52.   Shoval, G., et al., *Prohedonic Effect of Cannabidiol in a Rat Model of Depression.* Neuropsychobiology, 2016. **73**(2): p. 123-9.

53.   Hsiao, Y.T., et al., *Effect of cannabidiol on sleep disruption induced by the repeated combination tests consisting of open field and elevated plus-maze in rats.* Neuropharmacology, 2012. **62**(1): p. 373-84.

54.   Boychuk, D.G., et al., *The effectiveness of cannabinoids in the management of chronic nonmalignant neuropathic pain: a systematic review.* J Oral Facial Pain Headache, 2015. **29**(1): p. 7-14.

55.   Rajesh, M., et al., *Cannabidiol attenuates cardiac dysfunction, oxidative stress, fibrosis, and inflammatory and cell death signaling pathways in diabetic cardiomyopathy.* J Am Coll Cardiol, 2010. **56**(25): p. 2115-25.

56.   Morales, P., P.H. Reggio, and N. Jagerovic, *An Overview on Medicinal Chemistry of Synthetic and Natural Derivatives of Cannabidiol.* Front Pharmacol, 2017. **8**: p. 422.

57. Mechoulam, R., Z. Ben-Zvi, and Y. Gaoni, *Hashish—XIII : On the nature of the beam test*. Tetrahedrom. Vol. 24. 1968. 5615-5624.

58. Kogan, N.M., et al., *Synthesis and antitumor activity of quinonoid derivatives of cannabinoids*. J Med Chem, 2004. **47**(15): p. 3800-6.

59. Bolton, J.L., et al., *Role of quinones in toxicology*. Chem Res Toxicol, 2000. **13**(3): p. 135-60.

60. del Rio, C., et al., *The cannabinoid quinol VCE-004.8 alleviates bleomycin-induced scleroderma and exerts potent antifibrotic effects through peroxisome proliferator-activated receptor-gamma and CB2 pathways*. Sci Rep, 2016. **6**: p. 21703.

61. Del Rio, C., et al., *VCE-004.3, a cannabidiol aminoquinone derivative, prevents bleomycin-induced skin fibrosis and inflammation through PPARgamma- and CB2 receptor-dependent pathways*. Br J Pharmacol, 2018. **175**(19): p. 3813-3831.

62. Navarrete, C., et al., *Hypoxia mimetic activity of VCE-004.8, a cannabidiol quinone derivative: implications for multiple sclerosis therapy*. J Neuroinflammation, 2018. **15**(1): p. 64.

63. Borrelli, F., et al., *Beneficial effect of the non-psychotropic plant cannabinoid cannabigerol on experimental inflammatory bowel disease*. Biochem Pharmacol, 2013. **85**(9): p. 1306-16.

64. Granja, A.G., et al., *A cannabigerol quinone alleviates neuroinflammation in a chronic model of multiple sclerosis*. J Neuroimmune Pharmacol, 2012. **7**(4): p. 1002-16.

65. Carrillo-Salinas, F.J., et al., *A cannabigerol derivative suppresses immune responses and protects mice from experimental autoimmune encephalomyelitis*. PLoS One, 2014. **9**(4): p. e94733.

66. Diaz-Alonso, J., et al., *VCE-003.2, a novel cannabigerol derivative, enhances neuronal progenitor cell survival and alleviates symptomatology in murine models of Huntington's disease*. Sci Rep, 2016. **6**: p. 29789.

67. Garcia, C., et al., *Benefits of VCE-003.2, a cannabigerol quinone derivative, against inflammation-driven neuronal deterioration in experimental Parkinson's*

disease: possible involvement of different binding sites at the PPARgamma receptor. J Neuroinflammation, 2018. **15**(1): p. 19.

68. Aguareles, J., et al., *Oral administration of the cannabigerol derivative VCE-003.2 promotes subventricular zone neurogenesis and protects against mutant huntingtin-induced neurodegeneration.* Transl Neurodegener, 2019. **8**: p. 9.

69. Bluher, M., *Obesity: global epidemiology and pathogenesis.* Nat Rev Endocrinol, 2019. **15**(5): p. 288-298.

70. Kaur, J., *A comprehensive review on metabolic syndrome.* Cardiol Res Pract, 2014. **2014**: p. 943162.

71. Bray, G.A., et al., *The Science of Obesity Management: An Endocrine Society Scientific Statement.* Endocr Rev, 2018. **39**(2): p. 79-132.

72. Bhaskaran, K., et al., *Body-mass index and risk of 22 specific cancers: a population-based cohort study of 5.24 million UK adults.* Lancet, 2014. **384**(9945): p. 755-65.

73. Karczewski, J., et al., *Obesity and inflammation.* Eur Cytokine Netw, 2018. **29**(3): p. 83-94.

74. Forny-Germano, L., F.G. De Felice, and M. Vieira, *The Role of Leptin and Adiponectin in Obesity-Associated Cognitive Decline and Alzheimer's Disease.* Front Neurosci, 2018. **12**: p. 1027.

75. Schwartz, M.W., et al., *Obesity Pathogenesis: An Endocrine Society Scientific Statement.* Endocr Rev, 2017. **38**(4): p. 267-296.

76. Trayhurn, P., *Brown Adipose Tissue-A Therapeutic Target in Obesity?* Front Physiol, 2018. **9**: p. 1672.

77. DiPatrizio, N.V. and D. Piomelli, *The thrifty lipids: endocannabinoids and the neural control of energy conservation.* Trends Neurosci, 2012. **35**(7): p. 403-11.

78. Mazier, W., et al., *The Endocannabinoid System: Pivotal Orchestrator of Obesity and Metabolic Disease.* Trends Endocrinol Metab, 2015. **26**(10): p. 524-537.

79. Silvestri, C. and V. Di Marzo, *The endocannabinoid system in energy homeostasis and the etiopathology of metabolic disorders.* Cell Metab, 2013. **17**(4): p. 475-90.

80. Di Marzo, V., et al., *Leptin-regulated endocannabinoids are involved in maintaining food intake.* Nature, 2001. **410**(6830): p. 822-5.

81. DiPatrizio, N.V., et al., *Endocannabinoid signal in the gut controls dietary fat intake.* Proc Natl Acad Sci U S A, 2011. **108**(31): p. 12904-8.

82. DiPatrizio, N.V., et al., *Endocannabinoid signaling in the gut mediates preference for dietary unsaturated fats.* FASEB J, 2013. **27**(6): p. 2513-20.

83. Senin, L.L., et al., *The gastric CB1 receptor modulates ghrelin production through the mTOR pathway to regulate food intake.* PLoS One, 2013. **8**(11): p. e80339.

84. Cristino, L., et al., *Obesity-driven synaptic remodeling affects endocannabinoid control of orexinergic neurons.* Proc Natl Acad Sci U S A, 2013. **110**(24): p. E2229-38.

85. Bellocchio, L., et al., *Bimodal control of stimulated food intake by the endocannabinoid system.* Nat Neurosci, 2010. **13**(3): p. 281-3.

86. Koch, M., et al., *Hypothalamic POMC neurons promote cannabinoid-induced feeding.* Nature, 2015. **519**(7541): p. 45-50.

87. Quarta, C., et al., *CB(1) signaling in forebrain and sympathetic neurons is a key determinant of endocannabinoid actions on energy balance.* Cell Metab, 2010. **11**(4): p. 273-85.

88. Bajzer, M., et al., *Cannabinoid receptor 1 (CB1) antagonism enhances glucose utilisation and activates brown adipose tissue in diet-induced obese mice.* Diabetologia, 2011. **54**(12): p. 3121-31.

89. Perwitz, N., et al., *Cannabinoid type 1 receptor blockade induces transdifferentiation towards a brown fat phenotype in white adipocytes.* Diabetes Obes Metab, 2010. **12**(2): p. 158-66.

90. Werner, B.L., et al., *Border separation for adjacent orthogonal fields.* Med Dosim, 1991. **16**(2): p. 79-84.

142

91. Jourdan, T., et al., *Activation of the Nlrp3 inflammasome in infiltrating macrophages by endocannabinoids mediates beta cell loss in type 2 diabetes.* Nat Med, 2013. **19**(9): p. 1132-40.

92. Kim, W., et al., *Cannabinoids inhibit insulin receptor signaling in pancreatic beta-cells.* Diabetes, 2011. **60**(4): p. 1198-209.

93. Kim, W., et al., *Cannabinoids induce pancreatic beta-cell death by directly inhibiting insulin receptor activation.* Sci Signal, 2012. **5**(216): p. ra23.

94. Rossi, F., et al., *Cannabinoid Receptor 2 as Antiobesity Target: Inflammation, Fat Storage, and Browning Modulation.* J Clin Endocrinol Metab, 2016. **101**(9): p. 3469-78.

95. Kadowaki, T. and T. Yamauchi, *Adiponectin and adiponectin receptors.* Endocr Rev, 2005. **26**(3): p. 439-51.

96. Pirola, L. and J.C. Ferraz, *Role of pro- and anti-inflammatory phenomena in the physiopathology of type 2 diabetes and obesity.* World J Biol Chem, 2017. **8**(2): p. 120-128.

97. Schmitz, K., et al., *Pro-inflammatory obesity in aged cannabinoid-2 receptor-deficient mice.* Int J Obes (Lond), 2016. **40**(2): p. 366-79.

98. Gui, H., et al., *The endocannabinoid system and its therapeutic implications in rheumatoid arthritis.* Int Immunopharmacol, 2015. **26**(1): p. 86-91.

99. Guo, Q., et al., *Rheumatoid arthritis: pathological mechanisms and modern pharmacologic therapies.* Bone Res, 2018. **6**: p. 15.

100. Bruni, N., et al., *Cannabinoid Delivery Systems for Pain and Inflammation Treatment.* Molecules, 2018. **23**(10).

101. Richardson, D., et al., *Characterisation of the cannabinoid receptor system in synovial tissue and fluid in patients with osteoarthritis and rheumatoid arthritis.* Arthritis Res Ther, 2008. **10**(2): p. R43.

102. Ignatowska-Jankowska, B.M., et al., *A Cannabinoid CB1 Receptor-Positive Allosteric Modulator Reduces Neuropathic Pain in the Mouse with No Psychoactive Effects.* Neuropsychopharmacology, 2015. **40**(13): p. 2948-59.

103.   Slivicki, R.A., et al., *Positive Allosteric Modulation of Cannabinoid Receptor Type 1 Suppresses Pathological Pain Without Producing Tolerance or Dependence.* Biol Psychiatry, 2018. **84**(10): p. 722-733.

104.   Lowin, T. and R.H. Straub, *Cannabinoid-based drugs targeting CB1 and TRPV1, the sympathetic nervous system, and arthritis.* Arthritis Res Ther, 2015. **17**: p. 226.

105.   Tam, J., et al., *The cannabinoid CB1 receptor regulates bone formation by modulating adrenergic signaling.* FASEB J, 2008. **22**(1): p. 285-94.

106.   Idris, A.I., et al., *Regulation of bone mass, bone loss and osteoclast activity by cannabinoid receptors.* Nat Med, 2005. **11**(7): p. 774-9.

107.   Kraus, J., *Expression and functions of mu-opioid receptors and cannabinoid receptors type 1 in T lymphocytes.* Ann N Y Acad Sci, 2012. **1261**: p. 1-6.

108.   Tan, C.K., Y. Zhuang, and W. Wahli, *Synthetic and natural Peroxisome Proliferator-Activated Receptor (PPAR) agonists as candidates for the therapy of the metabolic syndrome.* Expert Opin Ther Targets, 2017. **21**(3): p. 333-348.

109.   Berger, J.P., T.E. Akiyama, and P.T. Meinke, *PPARs: therapeutic targets for metabolic disease.* Trends Pharmacol Sci, 2005. **26**(5): p. 244-51.

110.   Ricote, M. and C.K. Glass, *PPARs and molecular mechanisms of transrepression.* Biochim Biophys Acta, 2007. **1771**(8): p. 926-35.

111.   Brunmeir, R. and F. Xu, *Functional Regulation of PPARs through Post-Translational Modifications.* Int J Mol Sci, 2018. **19**(6).

112.   Monsalve, F.A., et al., *Peroxisome proliferator-activated receptor targets for the treatment of metabolic diseases.* Mediators Inflamm, 2013. **2013**: p. 549627.

113.   Rosen, C.J., *Revisiting the rosiglitazone story--lessons learned.* N Engl J Med, 2010. **363**(9): p. 803-6.

114.   Grey, A., *Diabetes medications and bone.* Curr Osteoporos Rep, 2015. **13**(1): p. 35-40.

115. Benvenuti, S., et al., *Rosiglitazone stimulates adipogenesis and decreases osteoblastogenesis in human mesenchymal stem cells.* J Endocrinol Invest, 2007. **30**(9): p. RC26-30.

116. Bruedigam, C., et al., *A new concept underlying stem cell lineage skewing that explains the detrimental effects of thiazolidinediones on bone.* Stem Cells, 2010. **28**(5): p. 916-27.

117. Capelli, D., et al., *Structural basis for PPAR partial or full activation revealed by a novel ligand binding mode.* Sci Rep, 2016. **6**: p. 34792.

118. Mandrekar-Colucci, S., et al., *PPAR agonists as therapeutics for CNS trauma and neurological diseases.* ASN Neuro, 2013. **5**(5): p. e00129.

119. Shaul, M.E., et al., *Dynamic, M2-like remodeling phenotypes of CD11c+ adipose tissue macrophages during high-fat diet--induced obesity in mice.* Diabetes, 2010. **59**(5): p. 1171-81.

120. Wen, L., et al., *Polarization of Microglia to the M2 Phenotype in a Peroxisome Proliferator-Activated Receptor Gamma-Dependent Manner Attenuates Axonal Injury Induced by Traumatic Brain Injury in Mice.* J Neurotrauma, 2018. **35**(19): p. 2330-2340.

121. Choi, J.M. and A.L. Bothwell, *The nuclear receptor PPARs as important regulators of T-cell functions and autoimmune diseases.* Mol Cells, 2012. **33**(3): p. 217-22.

122. Arner, P., *The adipocyte in insulin resistance: key molecules and the impact of the thiazolidinediones.* Trends Endocrinol Metab, 2003. **14**(3): p. 137-45.

123. Giralt, M. and F. Villarroya, *White, brown, beige/brite: different adipose cells for different functions?* Endocrinology, 2013. **154**(9): p. 2992-3000.

124. Ikeda, K., P. Maretich, and S. Kajimura, *The Common and Distinct Features of Brown and Beige Adipocytes.* Trends Endocrinol Metab, 2018. **29**(3): p. 191-200.

125. Weidner, C., et al., *Amorfrutin B is an efficient natural peroxisome proliferator-activated receptor gamma (PPARgamma) agonist with potent glucose-lowering properties.* Diabetologia, 2013. **56**(8): p. 1802-12.

126. Rong, J.X., et al., *Rosiglitazone Induces Mitochondrial Biogenesis in Differentiated Murine 3T3-L1 and C3H/10T1/2 Adipocytes.* PPAR Res, 2011. **2011**: p. 179454.

127. Jang, J.Y., et al., *Structural Basis for the Enhanced Anti-Diabetic Efficacy of Lobeglitazone on PPARgamma.* Sci Rep, 2018. **8**(1): p. 31.

128. Koufany, M., et al., *The peroxisome proliferator-activated receptor gamma agonist pioglitazone preserves bone microarchitecture in experimental arthritis by reducing the interleukin-17-dependent osteoclastogenic pathway.* Arthritis Rheum, 2013. **65**(12): p. 3084-95.

129. Marder, W., et al., *The peroxisome proliferator activated receptor-gamma pioglitazone improves vascular function and decreases disease activity in patients with rheumatoid arthritis.* J Am Heart Assoc, 2013. **2**(6): p. e000441.

130. Fahmi, H., et al., *Peroxisome proliferator-activated receptor gamma in osteoarthritis.* Mod Rheumatol, 2011. **21**(1): p. 1-9.

131. Bartels, K., A. Grenz, and H.K. Eltzschig, *Hypoxia and inflammation are two sides of the same coin.* Proc Natl Acad Sci U S A, 2013. **110**(46): p. 18351-2.

132. Clambey, E.T., et al., *Hypoxia-inducible factor-1 alpha-dependent induction of FoxP3 drives regulatory T-cell abundance and function during inflammatory hypoxia of the mucosa.* Proc Natl Acad Sci U S A, 2012. **109**(41): p. E2784-93.

133. Rabinowitz, M.H., *Inhibition of hypoxia-inducible factor prolyl hydroxylase domain oxygen sensors: tricking the body into mounting orchestrated survival and repair responses.* J Med Chem, 2013. **56**(23): p. 9369-402.

134. Hosogai, N., et al., *Adipose tissue hypoxia in obesity and its impact on adipocytokine dysregulation.* Diabetes, 2007. **56**(4): p. 901-11.

135. Lefere, S., et al., *Hypoxia-regulated mechanisms in the pathogenesis of obesity and non-alcoholic fatty liver disease.* Cell Mol Life Sci, 2016. **73**(18): p. 3419-31.

136. Halberg, N., et al., *Hypoxia-inducible factor 1alpha induces fibrosis and insulin resistance in white adipose tissue.* Mol Cell Biol, 2009. **29**(16): p. 4467-83.

137. Jiang, C., et al., *Disruption of hypoxia-inducible factor 1 in adipocytes improves insulin sensitivity and decreases adiposity in high-fat diet-fed mice.* Diabetes, 2011. **60**(10): p. 2484-95.

138. Lee, K.Y., et al., *The differential role of Hif1beta/Arnt and the hypoxic response in adipose function, fibrosis, and inflammation.* Cell Metab, 2011. **14**(4): p. 491-503.

139. Zhang, X., et al., *Adipose tissue-specific inhibition of hypoxia-inducible factor 1{alpha} induces obesity and glucose intolerance by impeding energy expenditure in mice.* J Biol Chem, 2010. **285**(43): p. 32869-77.

140. Fujisaka, S., et al., *Adipose tissue hypoxia induces inflammatory M1 polarity of macrophages in an HIF-1alpha-dependent and HIF-1alpha-independent manner in obese mice.* Diabetologia, 2013. **56**(6): p. 1403-12.

141. Pasarica, M., et al., *Reduced adipose tissue oxygenation in human obesity: evidence for rarefaction, macrophage chemotaxis, and inflammation without an angiogenic response.* Diabetes, 2009. **58**(3): p. 718-25.

142. Westerterp, K.R. and B. Kayser, *Body mass regulation at altitude.* Eur J Gastroenterol Hepatol, 2006. **18**(1): p. 1-3.

143. Lippl, F.J., et al., *Hypobaric hypoxia causes body weight reduction in obese subjects.* Obesity (Silver Spring), 2010. **18**(4): p. 675-81.

144. Garcia-Martin, R., et al., *Adipocyte-Specific Hypoxia-Inducible Factor 2alpha Deficiency Exacerbates Obesity-Induced Brown Adipose Tissue Dysfunction and Metabolic Dysregulation.* Mol Cell Biol, 2016. **36**(3): p. 376-93.

145. Zhang, H., et al., *Hypoxia-inducible factor directs POMC gene to mediate hypothalamic glucose sensing and energy balance regulation.* PLoS Biol, 2011. **9**(7): p. e1001112.

146. Hyvarinen, J., et al., *Hearts of hypoxia-inducible factor prolyl 4-hydroxylase-2 hypomorphic mice show protection against acute ischemia-reperfusion injury.* J Biol Chem, 2010. **285**(18): p. 13646-57.

147.   Rahtu-Korpela, L., et al., *HIF prolyl 4-hydroxylase-2 inhibition improves glucose and lipid metabolism and protects against obesity and metabolic dysfunction.* Diabetes, 2014. **63**(10): p. 3324-33.

148.   Liu, Y., et al., *Nonerythropoietic Erythropoietin-Derived Peptide Suppresses Adipogenesis, Inflammation, Obesity and Insulin Resistance.* Sci Rep, 2015. **5**: p. 15134.

149.   Alnaeeli, M., et al., *Erythropoietin signaling: a novel regulator of white adipose tissue inflammation during diet-induced obesity.* Diabetes, 2014. **63**(7): p. 2415-31.

150.   Chen, R. and N. Forsyth, *Editorial: The Development of New Classes of Hypoxia Mimetic Agents for Clinical Use.* Front Cell Dev Biol, 2019. **7**: p. 120.

151.   Morris, G.M., et al., *AutoDock4 and AutoDockTools4: Automated docking with selective receptor flexibility.* J Comput Chem, 2009. **30**(16): p. 2785-91.

152.   Trott, O. and A.J. Olson, *AutoDock Vina: improving the speed and accuracy of docking with a new scoring function, efficient optimization, and multithreading.* J Comput Chem, 2010. **31**(2): p. 455-61.

153.   Baugh, E.H., et al., *Real-time PyMOL visualization for Rosetta and PyRosetta.* PLoS One, 2011. **6**(8): p. e21931.

154.   Lee, M.A., et al., *Structures of PPARgamma complexed with lobeglitazone and pioglitazone reveal key determinants for the recognition of antidiabetic drugs.* Sci Rep, 2017. **7**(1): p. 16837.

155.   Liberato, M.V., et al., *Medium chain fatty acids are selective peroxisome proliferator activated receptor (PPAR) gamma activators and pan-PPAR partial agonists.* PLoS One, 2012. **7**(5): p. e36297.

156.   Brusotti, G., et al., *Betulinic acid is a PPARgamma antagonist that improves glucose uptake, promotes osteogenesis and inhibits adipogenesis.* Sci Rep, 2017. **7**(1): p. 5777.

157.   Waku, T., et al., *The nuclear receptor PPARgamma individually responds to serotonin- and fatty acid-metabolites.* EMBO J, 2010. **29**(19): p. 3395-407.

148

158. Hughes, T.S., et al., *An alternate binding site for PPARgamma ligands.* Nat Commun, 2014. **5**: p. 3571.

159. Hua, T., et al., *Crystal structures of agonist-bound human cannabinoid receptor CB1.* Nature, 2017. **547**(7664): p. 468-471.

160. Krishna Kumar, K., et al., *Structure of a Signaling Cannabinoid Receptor 1-G Protein Complex.* Cell, 2019. **176**(3): p. 448-458 e12.

161. Shao, Z., et al., *Structure of an allosteric modulator bound to the CB1 cannabinoid receptor.* Nat Chem Biol, 2019. **15**(12): p. 1199-1205.

162. Friesner, R.A., et al., *Glide: a new approach for rapid, accurate docking and scoring. 1. Method and assessment of docking accuracy.* J Med Chem, 2004. **47**(7): p. 1739-49.

163. Friesner, R.A., et al., *Extra precision glide: docking and scoring incorporating a model of hydrophobic enclosure for protein-ligand complexes.* J Med Chem, 2006. **49**(21): p. 6177-96.

164. Grebner, C., et al., *Exploring Binding Mechanisms in Nuclear Hormone Receptors by Monte Carlo and X-ray-derived Motions.* Biophys J, 2017. **112**(6): p. 1147-1156.

165. Lecina, D., J.F. Gilabert, and V. Guallar, *Adaptive simulations, towards interactive protein-ligand modeling.* Sci Rep, 2017. **7**(1): p. 8466.

166. Atilgan, A.R., et al., *Anisotropy of fluctuation dynamics of proteins with an elastic network model.* Biophys J, 2001. **80**(1): p. 505-15.

167. Jorgensen, W.L., *OPLS Force Fields. Encyclopedia of Computational Chemistry.* Vol. 3. 1998: Wiley: New York 1986-1989.

168. Onufriev, A., D. Bashford, and D.A. Case, *Exploring protein native states and large-scale conformational changes with a modified generalized born model.* Proteins, 2004. **55**(2): p. 383-94.

169. Gomez-Canas, M., et al., *Biological characterization of PM226, a chromenoisoxazole, as a selective CB2 receptor agonist with neuroprotective profile.* Pharmacol Res, 2016. **110**: p. 205-215.

170.   Kleiner, D.E., et al., *Design and validation of a histological scoring system for nonalcoholic fatty liver disease.* Hepatology, 2005. **41**(6): p. 1313-21.

171.   Subramanian, A., et al., *Gene set enrichment analysis: a knowledge-based approach for interpreting genome-wide expression profiles.* Proc Natl Acad Sci U S A, 2005. **102**(43): p. 15545-50.

172.   Yu, G., et al., *clusterProfiler: an R package for comparing biological themes among gene clusters.* OMICS, 2012. **16**(5): p. 284-7.

173.   Zoete, V., A. Grosdidier, and O. Michielin, *Peroxisome proliferator-activated receptor structures: ligand specificity, molecular switch and interactions with regulators.* Biochim Biophys Acta, 2007. **1771**(8): p. 915-25.

174.   Lecka-Czernik, B., et al., *Divergent Effects of Selective Peroxisome Proliferator-Activated Receptor-gamma2 Ligands on Adipocyte Versus Osteoblast Differentiation.* Endocrinology, 2002. **143**(6): p. 2376-2384.

175.   Lecka-Czernik, B., *Bone loss in diabetes: use of antidiabetic thiazolidinediones and secondary osteoporosis.* Curr Osteoporos Rep, 2010. **8**(4): p. 178-84.

176.   Berti, L., et al., *Fibroblast growth factor 21 is elevated in metabolically unhealthy obesity and affects lipid deposition, adipogenesis, and adipokine secretion of human abdominal subcutaneous adipocytes.* Mol Metab, 2015. **4**(7): p. 519-27.

177.   Morrice, N., et al., *Elevated Fibroblast growth factor 21 (FGF21) in obese, insulin resistant states is normalised by the synthetic retinoid Fenretinide in mice.* Sci Rep, 2017. **7**: p. 43782.

178.   So, W.Y. and P.S. Leung, *Fibroblast Growth Factor 21 As an Emerging Therapeutic Target for Type 2 Diabetes Mellitus.* Med Res Rev, 2016. **36**(4): p. 672-704.

179.   Gregor, M.F. and G.S. Hotamisligil, *Inflammatory mechanisms in obesity.* Annu Rev Immunol, 2011. **29**: p. 415-45.

180.   Pandey, P., et al., *Structure-Based Identification of Potent Natural Product Chemotypes as Cannabinoid Receptor 1 Inverse Agonists.* Molecules, 2018. **23**(10).

181. Kapur, A., et al., *Mutation studies of Ser7.39 and Ser2.60 in the human CB1 cannabinoid receptor: evidence for a serine-induced bend in CB1 transmembrane helix 7.* Mol Pharmacol, 2007. **71**(6): p. 1512-24.

182. Shim, J.Y., A.C. Bertalovitz, and D.A. Kendall, *Identification of essential cannabinoid-binding domains: structural insights into early dynamic events in receptor activation.* J Biol Chem, 2011. **286**(38): p. 33422-35.

183. Lubberts, E. and W.B. van den Berg, *Cytokines in the pathogenesis of rheumatoid arthritis and collagen-induced arthritis.* Adv Exp Med Biol, 2003. **520**: p. 194-202.

184. Seeuws, S., et al., *A multiparameter approach to monitor disease activity in collagen-induced arthritis.* Arthritis Res Ther, 2010. **12**(4): p. R160.

185. Nandakumar, K.S., et al., *Induction of arthritis by single monoclonal IgG anti-collagen type II antibodies and enhancement of arthritis in mice lacking inhibitory FcgammaRIIB.* Eur J Immunol, 2003. **33**(8): p. 2269-77.

186. Papaseit, E., et al., *Cannabinoids: from pot to lab.* Int J Med Sci, 2018. **15**(12): p. 1286-1295.

187. Chrisman, I.M., et al., *Defining a conformational ensemble that directs activation of PPARgamma.* Nat Commun, 2018. **9**(1): p. 1794.

188. Ostberg, T., et al., *A new class of peroxisome proliferator-activated receptor agonists with a novel binding epitope shows antidiabetic effects.* J Biol Chem, 2004. **279**(39): p. 41124-30.

189. Kintscher, U. and M. Goebel, *INT-131, a PPARgamma agonist for the treatment of type 2 diabetes.* Curr Opin Investig Drugs, 2009. **10**(4): p. 381-7.

190. Wang, Y.C., et al., *Health and economic burden of the projected obesity trends in the USA and the UK.* Lancet, 2011. **378**(9793): p. 815-25.

191. Finan, B., et al., *A rationally designed monomeric peptide triagonist corrects obesity and diabetes in rodents.* Nat Med, 2015. **21**(1): p. 27-36.

192. Jall, S., et al., *Monomeric GLP-1/GIP/glucagon triagonism corrects obesity, hepatosteatosis, and dyslipidemia in female mice.* Mol Metab, 2017. **6**(5): p. 440-446.

193. Lopez-Jaramillo, P., et al., *The role of leptin/adiponectin ratio in metabolic syndrome and diabetes.* Horm Mol Biol Clin Investig, 2014. **18**(1): p. 37-45.

194. Stofkova, A., *Leptin and adiponectin: from energy and metabolic dysbalance to inflammation and autoimmunity.* Endocr Regul, 2009. **43**(4): p. 157-68.

195. Poher, A.L., M.H. Tschop, and T.D. Muller, *Ghrelin regulation of glucose metabolism.* Peptides, 2018. **100**: p. 236-242.

196. Vestergaard, E.T., et al., *Acyl Ghrelin Induces Insulin Resistance Independently of GH, Cortisol, and Free Fatty Acids.* Sci Rep, 2017. **7**: p. 42706.

197. Liao, H., et al., *Molecular regulation of the PAI-1 gene by hypoxia: contributions of Egr-1, HIF-1alpha, and C/EBPalpha.* FASEB J, 2007. **21**(3): p. 935-49.

198. Gupta, N. and J.B. Wish, *Hypoxia-Inducible Factor Prolyl Hydroxylase Inhibitors: A Potential New Treatment for Anemia in Patients With CKD.* Am J Kidney Dis, 2017. **69**(6): p. 815-826.

199. Chung, K.J., et al., *Innate immune cells in the adipose tissue.* Rev Endocr Metab Disord, 2018. **19**(4): p. 283-292.

200. Zhao, Y., et al., *CD4(+) T cells in obesity and obesity-associated diseases.* Cell Immunol, 2018. **332**: p. 1-6.

201. Reilly, S.M. and A.R. Saltiel, *Adapting to obesity with adipose tissue inflammation.* Nat Rev Endocrinol, 2017. **13**(11): p. 633-643.

202. Zhang, X. and H.A. Young, *PPAR and immune system--what do we know?* Int Immunopharmacol, 2002. **2**(8): p. 1029-44.

203. Cota, D., et al., *The endogenous cannabinoid system affects energy balance via central orexigenic drive and peripheral lipogenesis.* J Clin Invest, 2003. **112**(3): p. 423-31.

152

204. Verty, A.N., I.S. McGregor, and P.E. Mallet, *Paraventricular hypothalamic CB(1) cannabinoid receptors are involved in the feeding stimulatory effects of Delta(9)-tetrahydrocannabinol.* Neuropharmacology, 2005. **49**(8): p. 1101-9.

205. Zehetner, J., et al., *PVHL is a regulator of glucose metabolism and insulin secretion in pancreatic beta cells.* Genes Dev, 2008. **22**(22): p. 3135-46.

206. Kliewer, S.A. and D.J. Mangelsdorf, *Fibroblast growth factor 21: from pharmacology to physiology.* Am J Clin Nutr, 2010. **91**(1): p. 254S-257S.

207. Owen, B.M., D.J. Mangelsdorf, and S.A. Kliewer, *Tissue-specific actions of the metabolic hormones FGF15/19 and FGF21.* Trends Endocrinol Metab, 2015. **26**(1): p. 22-9.

208. Owen, B.M., et al., *FGF21 contributes to neuroendocrine control of female reproduction.* Nat Med, 2013. **19**(9): p. 1153-6.

209. Tanajak, P., *Letter to the Editor: Parameters, Characteristics, and Criteria for Defining the Term "FGF21 Resistance".* Endocrinology, 2017. **158**(5): p. 1523-1524.

210. Raza, K. and A. Filer, *The therapeutic window of opportunity in rheumatoid arthritis: does it ever close?* Ann Rheum Dis, 2015. **74**(5): p. 793-4.

211. Burgers, L.E., K. Raza, and A.H. van der Helm-van Mil, *Window of opportunity in rheumatoid arthritis - definitions and supporting evidence: from old to new perspectives.* RMD Open, 2019. **5**(1): p. e000870.

212. van Baarsen, L.G., et al., *The cellular composition of lymph nodes in the earliest phase of inflammatory arthritis.* Ann Rheum Dis, 2013. **72**(8): p. 1420-4.

213. Palomares, B., et al., *Tetrahydrocannabinolic acid A (THCA-A) reduces adiposity and prevents metabolic disease caused by diet-induced obesity.* Biochem Pharmacol, 2019. **171**: p. 113693.

214. Valastro, C., et al., *Characterization of endocannabinoids and related acylethanolamides in the synovial fluid of dogs with osteoarthritis: a pilot study.* BMC Vet Res, 2017. **13**(1): p. 309.

215. Dunn, S.L., et al., *Cannabinoids: novel therapies for arthritis?* Future Med Chem, 2012. **4**(6): p. 713-25.

216. Niu, X. and G. Chen, *Clinical biomarkers and pathogenic-related cytokines in rheumatoid arthritis.* J Immunol Res, 2014. **2014**: p. 698192.

217. Anjo, S.I., C. Santa, and B. Manadas, *SWATH-MS as a tool for biomarker discovery: From basic research to clinical applications.* Proteomics, 2017. **17**(3-4).

218. Kawaguchi, H., et al., *Identification of novel biomarker as citrullinated inter-alpha-trypsin inhibitor heavy chain 4, specifically increased in sera with experimental and rheumatoid arthritis.* Arthritis Res Ther, 2018. **20**(1): p. 66.

219. Liao, C.C., et al., *Comparative analysis of novel autoantibody isotypes against citrullinated-inter-alpha-trypsin inhibitor heavy chain 3 (ITIH3)(542-556) peptide in serum from Taiwanese females with rheumatoid arthritis, primary Sjogren's syndrome and secondary Sjogren's syndrome in rheumatoid arthritis.* J Proteomics, 2016. **141**: p. 1-11.

220. Park, H.J., et al., *Identification of a specific haptoglobin C-terminal fragment in arthritic synovial fluid and its effect on interleukin-6 expression.* Immunology, 2013. **140**(1): p. 133-41.

221. Baig, S., et al., *Hemopexin deficiency prevents joint injury following collagen antibody-induced arthritis.* The journal of inmunology, 2018. **200**(1 Supplement).

222. Smith, A. and R.J. McCulloh, *Hemopexin and haptoglobin: allies against heme toxicity from hemoglobin not contenders.* Front Physiol, 2015. **6**: p. 187.

223. Olsson, M.G., et al., *Pathological conditions involving extracellular hemoglobin: molecular mechanisms, clinical significance, and novel therapeutic opportunities for alpha(1)-microglobulin.* Antioxid Redox Signal, 2012. **17**(5): p. 813-46.

224. Osterholm, E.A. and M.K. Georgieff, *Chronic inflammation and iron metabolism.* J Pediatr, 2015. **166**(6): p. 1351-7 e1.

225. Baker, J.F. and A.J. Ghio, *Iron homoeostasis in rheumatic disease.* Rheumatology (Oxford), 2009. **48**(11): p. 1339-44.

226. Strachan, A.F. and P.M. Johnson, *Protein SAP (serum amyloid P-component) in Waldenstrom's macroglobulinaemia, multiple myeloma and rheumatic diseases.* J Clin Lab Immunol, 1982. **8**(3): p. 153-6.

227. Anderson, L.L., et al., *Pharmacokinetics of Phytocannabinoid Acids and Anticonvulsant Effect of Cannabidiolic Acid in a Mouse Model of Dravet Syndrome.* J Nat Prod, 2019. **82**(11): p. 3047-3055.